MICROCOPY RESOLUTION TEST CHART

NATIONAL BUREAU OF STANDARDS-1963-A

R87-917470-1

⟨12⟩

CARBON FIBER REINFORCED GLASS MATRIX COMPOSITES FOR SPACE BASED APPLICATIONS

AD-A184 355

Prepared by

W.K. Tredway
K.M. Prewo

ANNUAL REPORT

Contract N00014-85-C-0332

for

Department of the Navy
Office of Naval Research
Arlington, VA 22217

August 30, 1987

UNITED
TECHNOLOGIES
RESEARCH
CENTER
East Hartford, Connecticut 06108

87 9 8 081

REPORT DOCUMENTATION PAGE

1a. REPORT SECURITY CLASSIFICATION Unclassified	1b. RESTRICTIVE MARKINGS None
2a. SECURITY CLASSIFICATION AUTHORITY	3. DISTRIBUTION / AVAILABILITY OF REPORT
2b. DECLASSIFICATION / DOWNGRADING SCHEDULE	Unlimited

4. PERFORMING ORGANIZATION REPORT NUMBER(S) R87-917470-1	5. MONITORING ORGANIZATION REPORT NUMBER(S)	
6a. NAME OF PERFORMING ORGANIZATION United Technologies Research Center	6b. OFFICE SYMBOL (If applicable)	7a. NAME OF MONITORING ORGANIZATION Office of Naval Research
6c. ADDRESS (City, State, and ZIP Code) East Hartford, CT 06108		7b. ADDRESS (City, State, and ZIP Code) Arlington, VA 22217
8a. NAME OF FUNDING / SPONSORING ORGANIZATION Office of Naval Research	8b. OFFICE SYMBOL (If applicable)	9. PROCUREMENT INSTRUMENT IDENTIFICATION NUMBER N00014-85-C-0332

8c. ADDRESS (City, State, and ZIP Code)	10. SOURCE OF FUNDING NUMBERS			
	PROGRAM ELEMENT NO.	PROJECT NO.	TASK NO.	WORK UNIT ACCESSION NO.

11. TITLE (Include Security Classification)

CARBON FIBER REINFORCED GLASS MATRIX COMPOSITES FOR SPACE BASED APPLICATIONS

12. PERSONAL AUTHOR(S)
W. K. Tredway and K. M. Prewo

13a. TYPE OF REPORT Annual	13b. TIME COVERED FROM 7/1/86 TO 6/30/87	14. DATE OF REPORT (Year, Month, Day) 1987 Aug 31	15. PAGE COUNT 80

16. SUPPLEMENTARY NOTATION

17.	COSATI CODES		18. SUBJECT TERMS (Continue on reverse if necessary and identify by block number)
FIELD	GROUP	SUB-GROUP	Glass Matrix Composites
			Carbon Fiber Reinforced Composites
			Glass-Ceramic Matrix Composites

19. ABSTRACT (Continue on reverse if necessary and identify by block number)

High elastic modulus (HMU) carbon fibers were combined with several different glass and glass-ceramic matrix compositions. The importance of the fiber-matrix interface in the control of composite performance was central to the investigation and was evaluated by correlating mechanical properties with microstructural and microchemical analysis of the interfacial region. LAS glass-ceramic matrix composites were developed with tensile stress-strain behavior comparable to borosilicate glass matrix composites. Carbon fiber reinforced glass matrix composites of 0/90° orientation were found to be relatively notch insensitive. Lowering of the processing temperature of 7740/HMU composites was found to affect composite mechanical performance through matrix consolidation effects. Interfacial reactions between the carbon fiber and various matrix additives (Nb_2O_5, MoO_3) were found to have a profound effect on composite mechanical behavior via formation of an interfacial carbide layer which increased fiber-matrix interfacial bond strength.

20. DISTRIBUTION / AVAILABILITY OF ABSTRACT ☒ UNCLASSIFIED/UNLIMITED ☐ SAME AS RPT. ☐ DTIC USERS	21. ABSTRACT SECURITY CLASSIFICATION None	
22a. NAME OF RESPONSIBLE INDIVIDUAL Dr. S. Fishman, ONR	22b. TELEPHONE (Include Area Code) (202) 696-4401	22c. OFFICE SYMBOL ONR/1131

DD FORM 1473, 84 MAR   83 APR edition may be used until exhausted.   SECURITY CLASSIFICATION OF THIS PAGE
All other editions are obsolete.

**UNITED
TECHNOLOGIES
RESEARCH
CENTER**

East Hartford, Connecticut 06108

R87-917470-1

Carbon Fiber Reinforced Glass Matrix
Composites for Space Based Applications

ANNUAL REPORT

Contract N00014-85-C-0332

REPORTED BY *William K. Tredway*

W. K. Tredway

K. M. Prewo

K. M. Prewo

APPROVED BY *E. R. Thompson*

E. R. Thompson

DATE 8/31/87

NO. OF PAGES _____   **COPY NO.** _____

Carbon Fiber Reinforced Glass Matrix Composites
for Space Based Applications

Table Of Contents

Accesion For

NTIS CRA&I	✓
DTIC TAB	☐
Unannounced	☐
Justification	

By

Distribution /

Availability Codes

| Dist | Avail and/or Special |
| A-1 | |

I. Introduction

The carbon fiber reinforced glass matrix composite system provides a unique opportunity for the basic investigation of mechanisms controlling ceramic matrix composites behavior and at the same time develop a material eminently suited to structural space based applications. The United Technologies Research Center and Pennsylvania State University have joined in the herein reported activity to characterize, understand, and improve the performance of carbon fiber reinforced glass. Carbon fiber reinforced glass composites have been fabricated and studied by several investigators over the past years in an attempt to develop a composite having performance superior to that of carbon reinforced resins and metals. Early evidence of composite toughness [1] was followed by data demonstrating high levels of composite flexural strength and the importance of the fiber-matrix interface in the control of composite toughness [2-7]. More recent studies extended this work to include a broader range of carbon fibers and matrices and to continue the evaluation of composite performance over a wider range of test conditions [8-14]. In addition, it was recognized that composites of exceptional wear resistance [15, 16] and dimensional stability [11, 12, 17, 18] could be achieved. More recently, the roles that fiber orientation, fiber volume percent, and fiber-matrix reactions play in the control of composite stress-strain behavior have been investigated [19].

In the herein described investigation, the role of the fiber-matrix interface has been studied further and its importance in controlling composite stress-strain behavior and failure modes addressed. Specifically, this has included studies of the notch sensitivity of 0/90 reinforced composites, the effect of processing conditions on composite stress-strain behavior, and preliminary work on the evaluation of carbon fiber reinforced LAS glass-ceramic matrix composites. In addition, the role of matrix chemistry in controlling fiber-matrix reactions and the subsequent effect on composite properties has been investigated further.

The program participants are:

William K. Tredway	UTRC
Karl M. Prewo	UTRC
Carlo G. Pantano	Penn State
Paul M. Benson	Penn State
Karl E. Spear	Penn State

II. Experimental Procedure

A. Composite Fabrication

All composites were fabricated utilizing the tape winding and hot pressing procedure described in Figure II-1. The matrices were all obtained as -325 mesh size glass powders which were combined with water and an organic binder to produce slurries through which the carbon tows could be pulled. The infiltrated carbon fiber tows were then wound onto a mandrel, dried, the binder burned out in air, and the final composite densified under pressures of 5.51 to 20.67 MPa at temperatures of 900 to 1350°C.

This procedure was used to fabricate composites containing HMU carbon fiber and the several different glass matrices listed in Table II-1.

B. Mechanical Testing

Mechanical test procedures included both three point flexural testing and tensile testing, Figure II-2. The flexural tests were performed only on unidirectionally reinforced composites. Flexural specimen geometry was varied to permit the ratio of maximum flexural stress to shear stress to be altered. These stresses were calculated using the formulae for simple beam bending as follows where P is the maximum load applied to the specimen, b is the specimen width, and L and h are as shown in Figure II-2.

$$\sigma_{max} = 3/2 \, (PL/bh^2)$$

$$\tau_{max} = 3/4 \, (P/bh)$$

$$\sigma_{max}/\tau_{max} = 2 \, (L/h)$$

Tensile tests were performed using parallel sided specimens. Both uniaxially and 0/90 reinforced specimens were used. In all cases the gauge length was 2.5 cm and the loads were applied at a strain rate of 0.05 min^{-1}. In most instances strain measurements were made using glued-on strain gauges. Clip-on extensometers were used to measure strain in notched tensile specimens.

Table II-1

Materials Used in Composite Fabrication

Fiber	Density (g/cc)	Elastic Modulus (GPa)	Tensile Strength (MPa)	Fiber Dia. (μm)	Precursor
HMU	1.84	380	2760	8	PAN

Matrix	Density (g/cc)	Elastic Modulus (GPa)	CTE (ppm/°C)	
7740*	2.23	63	3.2	
LAS-I**	-	-	~3.0	(glass)
	2.5	88	~1.0	(ceramed)
PS 1***	2.25	~63	~3.2	
PS 2***	2.24	~63	~3.2	
PS 3***	2.23	~63	~3.2	

*   Corning Glass Works borosilicate glass
**   Lithium aluminosilicate (LAS) glass-ceramic
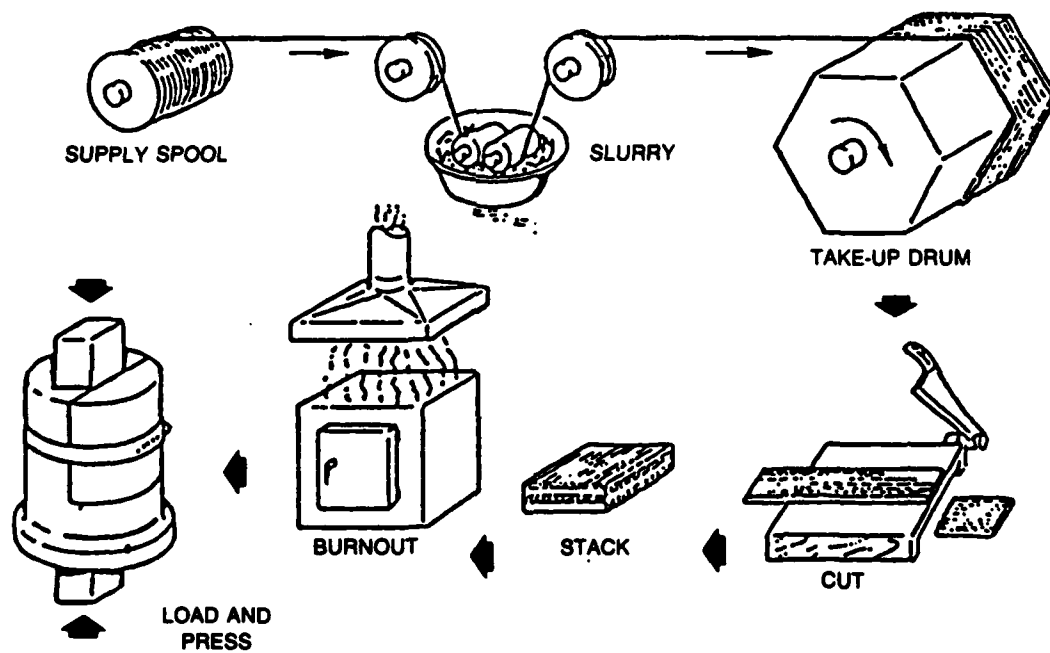*** Doped borosilicate glass; melted at Penn State University
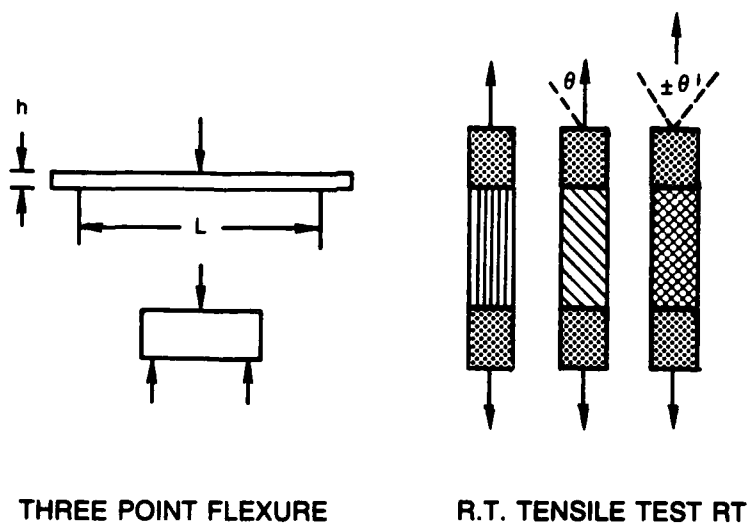
Fig. II-1. Composite Fabrication Procedure

THREE POINT FLEXURE   R.T. TENSILE TEST RT

Fig. II-2. Mechanical Test Techniques Used

III. Notch Sensitivity of 0/90° Reinforced HMU/7740 Composites

The notch sensitivity of 0/90° reinforced HMU fiber/borosilicate glass matrix (Corning Code 7740) composites was investigated in order to assess the mechanical response of the composites to localized damage in the form of circular holes. The ability of these materials to perform following perforation due to conditions such as ballistic impact would be critical for applications important to SDIO.

A. Processing

HMU/7740 composite plates were prepared using standard hot-pressing procedures. The plates were cut into tensile specimens which were then subsequently notched. The notches were in the form of circular holes of various diameter (1.6 mm, 3.1 mm, 6.4 mm) and were introduced into the tensile specimens using an ultrasonic drilling technique.

B. Mechanical Behavior

All of the notched specimens fractured at the location of the notch during tensile testing and exhibited some degree of fiber pullout during fracture, as shown in Figure III-1. The fiber pullout, along with the clean debonding between fiber and matrix in the 90° plies, is indicative of low fiber-matrix interfacial strength in the composite. The mode of fracture is not readily apparent upon inspection of the fracture surfaces. However, during testing it was observed that initial cracking of the composites occurred at the hole edges in the longitudinal direction (parallel to the direction of the applied load) followed by rapid catastrophic failure due to crack propagation in the transverse direction.

The tensile behavior of the notched composites is summarized in Tables III-1 and III-2. The d/b ratio given in the tables corresponds to the ratio of hole diameter to specimen width. Actual ultimate tensile strength (UTS) refers to strength which is calculated taking the decrease in cross-sectional area due to the hole into account. The actual UTS values were normalized to account for the different average strengths exhibited by the composites. This allowed for more meaningful direct comparison between samples cut from different composite plates. A plot of normalized actual UTS as a function of d/b is shown in Figure III-2. It is apparent from the figure that the actual strength changes very little in the presence of the notches, regardless of hole diameter. The appearance of a slightly decreasing trend in actual stress with increasing hole size is deceiving, as the scale on the ordinate is sensitive. The apparent notch insensitivity of the 0/90° reinforced composites is in agreement with fracture mechanism theory [25] which predicts that low values of interfacial shear resistance (τ_i) and high values of fiber strength should result in notch-insensitive crack growth. As discussed previously, this material fits these criteria, since the fracture behavior shown in Figure III-1 is indicative of weak fiber-matrix interfacial bonding and the strength of HMU fiber is relatively high (Table II-1).

Typical stress-strain curves for the notched composites are shown in Figure III-3. The

shape of the stress-strain curves is characteristic of those for 0/90° reinforced composites [19], with low proportional limits (the initial deviation from linearity, generally attributed to matrix microcracking) and no "plateau" region of constant stress with increasing strain. This plateau region is characteristic of unidirectional composites and is accompanied by a large, rapid increase in transverse strain that occurs when fiber tows "broom out", or expand, as a result of matrix microcracking [19, 26].

An unusual feature noted in the stress-strain behavior of the notched composite specimens was the increase in ultimate extensometer strain with increasing hole size, Figure III-4. The failure strains for the unnotched specimens were typical of those for HMU/7740 composites, ranging from 0.48% to 0.70%. With the introduction of the notches, however, the extensometer strain increased to values of 0.92% to 1.52%. These values seem high in light of the fact that the full failure strain of HMU carbon fiber is reported by the manufacturer to be 0.70%. This apparent anomalous behavior was resolved by correlating the fracture behavior with the method in which the strain data was obtained. As previously mentioned, the notched specimens initially cracked at the hole edges in the longitudinal direction (similar to the lines marking the hole diameter in the schematic diagram in Figure III-5). This allowed the sections of material above and below the hole (between the cracks) to move farther apart. Since the extensometer pins were placed in these regions of moving material, they recorded the movement as an increase in strain. Had the extensometers been placed near the edge of the specimens, so that they were not straddling the holes, strains nearer those of the unnotched samples most likely would have been recorded.

Table III-1

Mechanical Test Data for Notched 0/90° Reinforced HMU/7740 Composites

Hole Dia. (mm)	d/b	Fiber Volume %	Actual UTS (MPa)	Normalized* Actual UTS	Proportional Limit (MPa)	Ultimate Extensometer Strain (%)
Unnotched	0	39	309	1.0	43	0.48
	0	38	320	1.0	81	0.56
	0	40	341	1.0	76	0.57
1.6	0.110	39	324	1.05	121	0.92
	0.113	38	334	1.04	37	1.05
	0.112	40	330	0.97	77	0.97
3.1	0.202	39	296	0.96	16	1.08
6.4	0.431	38	297	0.93	29	1.42
	0.429	40	306	0.90	31	1.52

* Ratio of notched/unnotched tensile strength

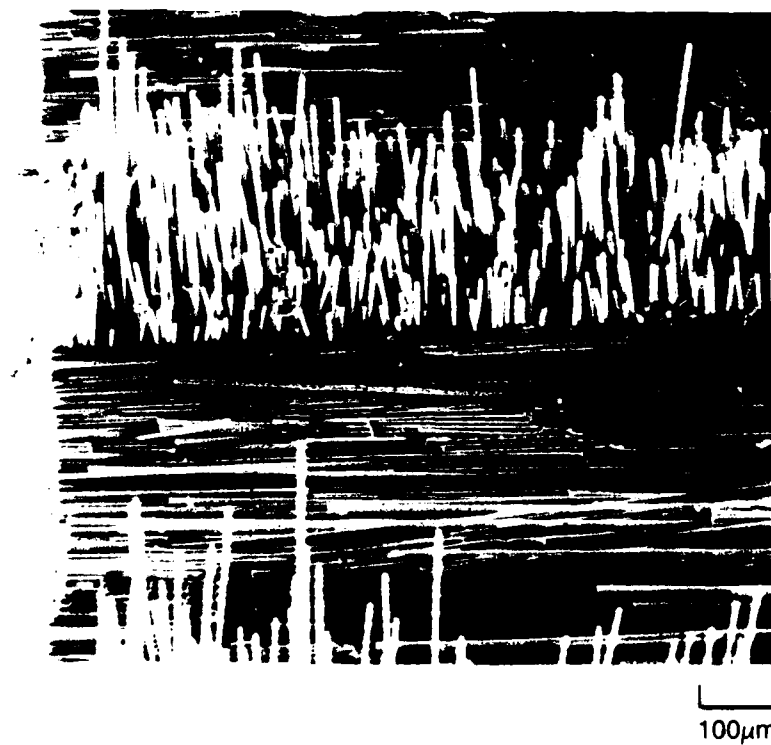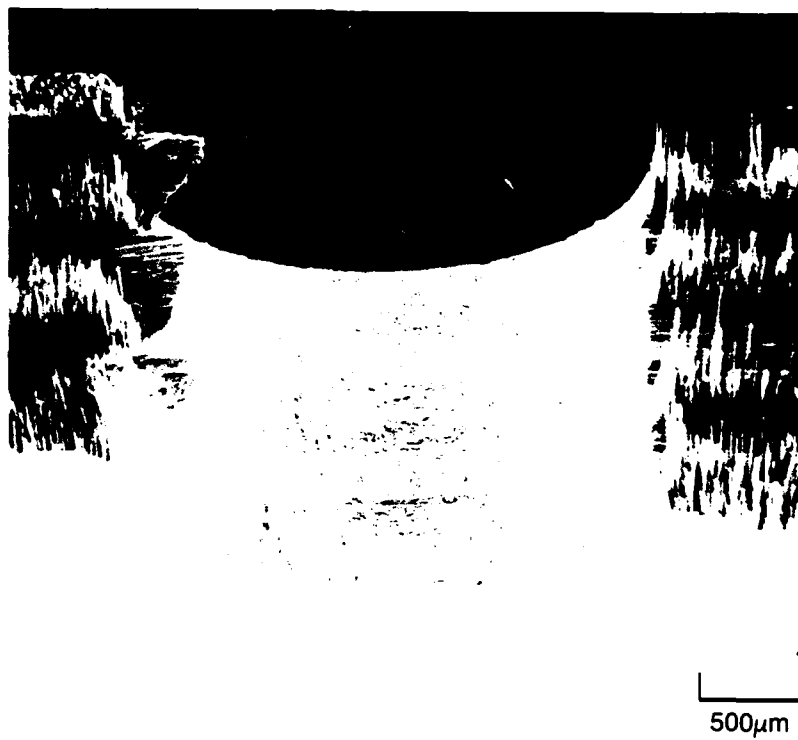**Fig. III-1 (a). Tensile Fracture Surface of 0/90° Reinforced 7740/HMU Composite with 1.6 mm Hole**

87 – 8 – 42 – 29

500μm

100μm

Fig. III-1 (b). Tensile Fracture Surface of 0/90° Reinforced 7740/HMU Composite with 3.1 mm Hole

500μm

20μm

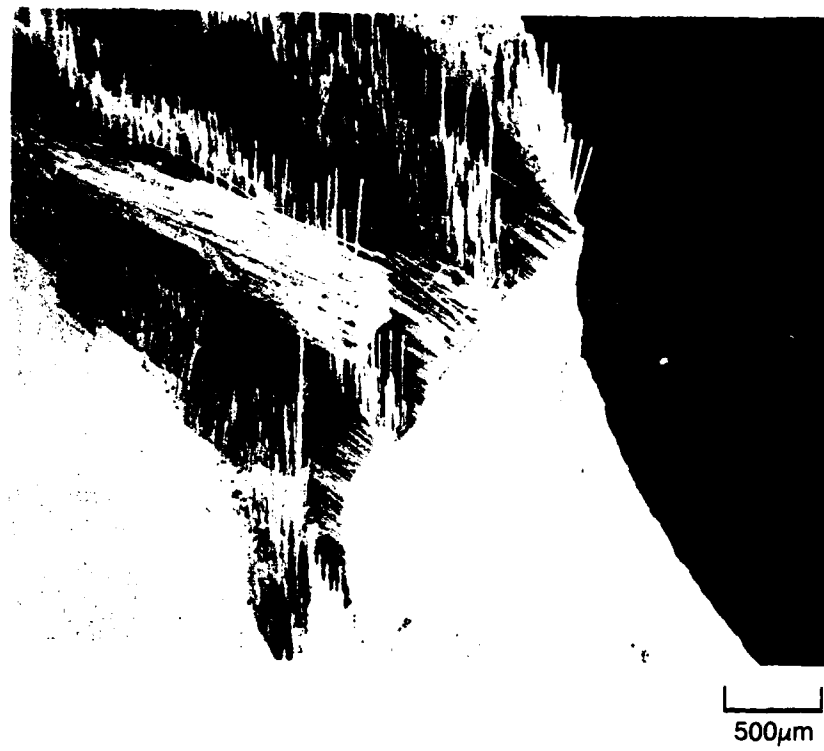**Fig. III-1 (c). Tensile Fracture Surface of 0/90° Reinforced 7740/HMU Composite with 6.4 mm Hole**

87 – 8 – 42 – 31

11

1.1

NORMALIZED ACTUAL STRESS (σ_{act})

1.0

0.9

0.8
-0.1   0   0.1   0.2   0.3   0.4   0.5

HOLE DIAMETER/SPECIMEN WIDTH (d/b)

P ← b ◯ d → P

$$\sigma_{act} = \frac{P_{max}}{(b-d) \cdot t}$$

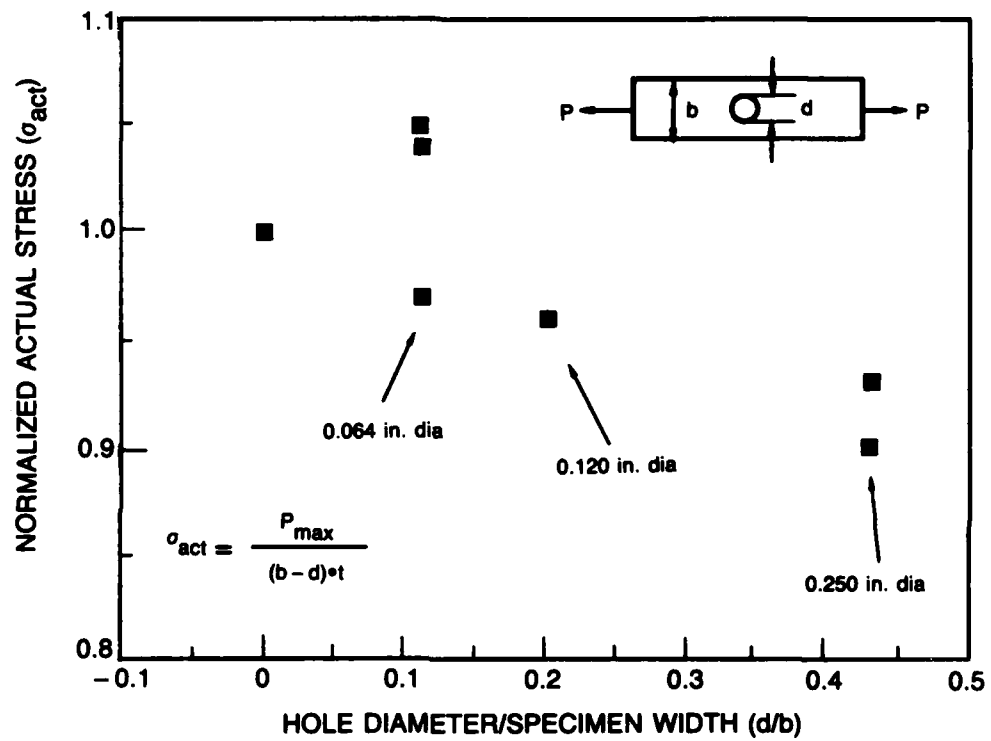0.064 in. dia

0.120 in. dia

0.250 in. dia

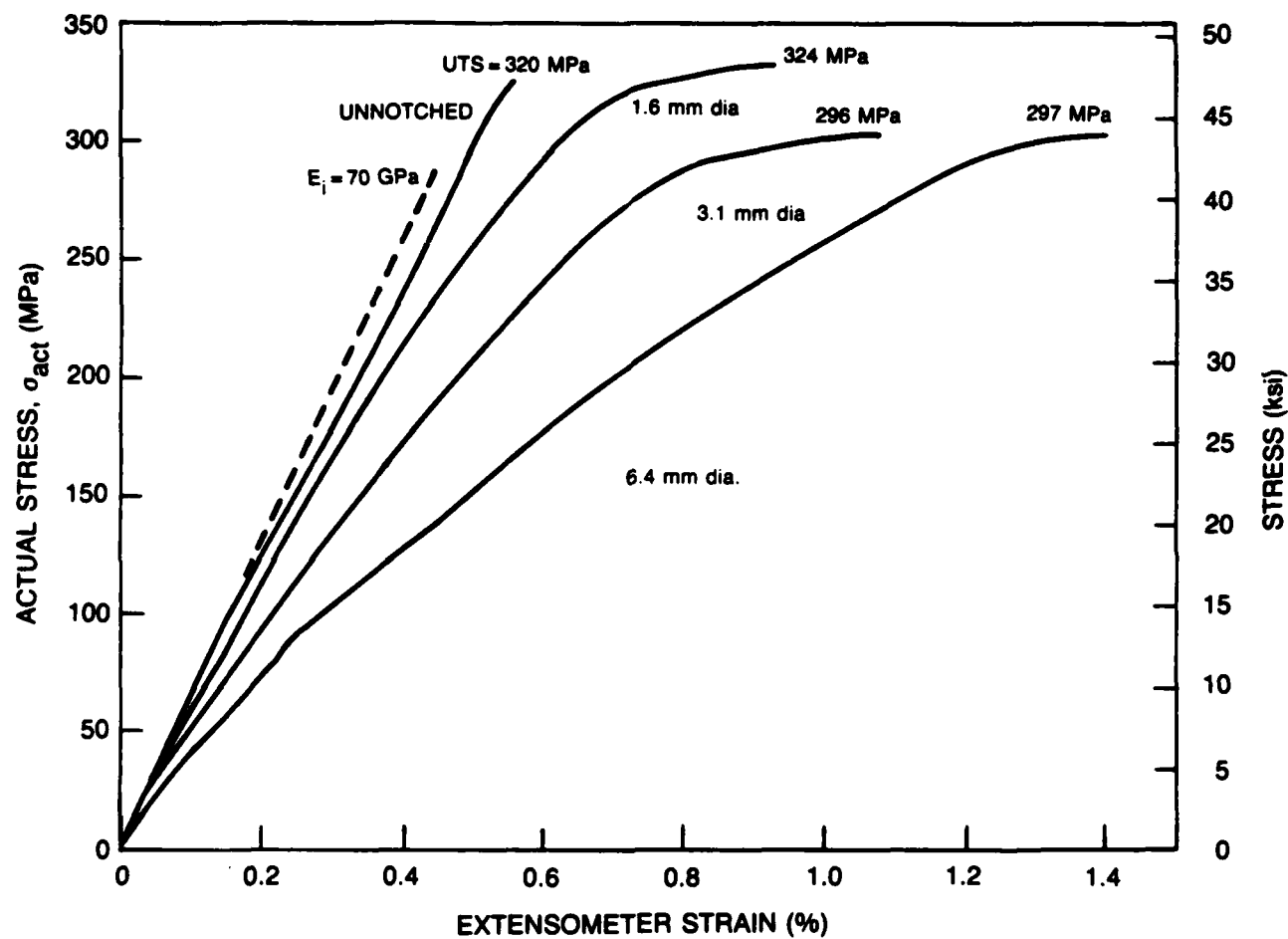**Fig. III-2. Normalized Actual Stress vs Ratio of Hole Diameter/Specimen
Width for 0/90° 7740/HMU Composites**

Fig. III-3. Tensile Stress-Strain Curves for 0/90° Reinforced 7740/HMU Composites Containing Circular Notches of Various Diameters
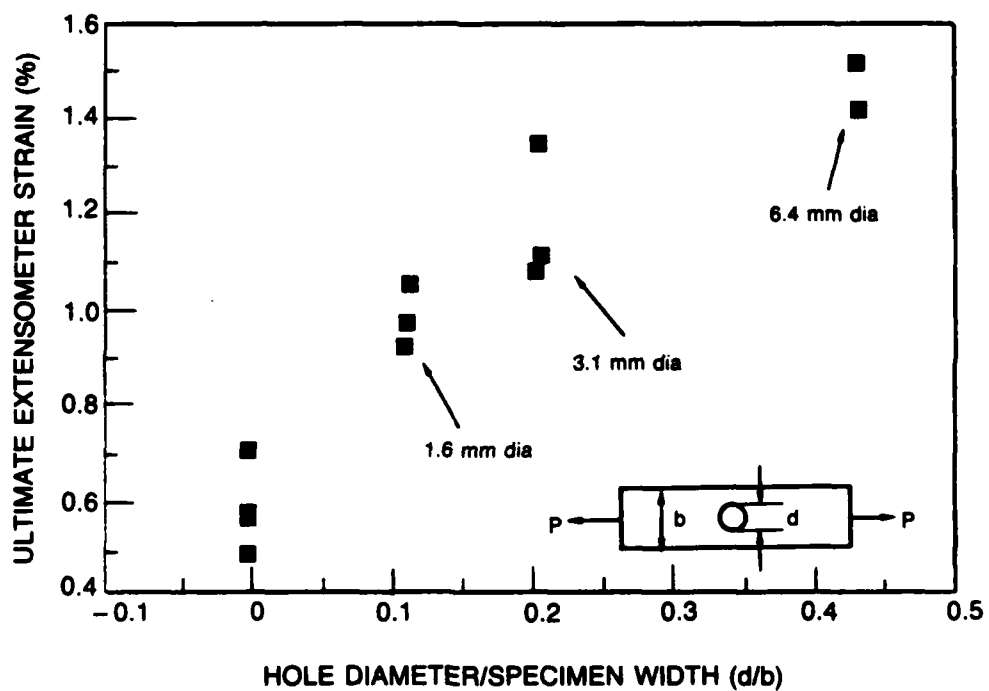
87-8-42-32

Fig. III-4. Ultimate Extensometer Strain vs Ratio of Hole Diameter/Specimen
Width for 0/90° 7740/HMU Composites

87-8-42-33

IV. LAS Matrix / HMU Carbon Fiber Composites

The purpose of this portion of the program was to develop carbon fiber reinforced composites which are more thermally stable than those with borosilicate glass matrices. Increased thermal stability would be critical to survivability of composite structures under such circumstances as a laser threat, underscoring the importance of this behavior for SDIO applications. Potential candidates for more refractory matrix materials include alkaline earth (MgO, CaO, BaO) aluminosilicate as well as lithium aluminosilicate (LAS) glasses and glass-ceramics. In addition to their high temperature capability, LAS compositions were selected for initial investigation because of their low thermal expansion behavior and UTRC's experience in fabricating LAS/Nicalon (SiC) composites.

A. Processing

Several different LAS compositions were used in attempts to fabricate carbon fiber reinforced glass-ceramic matrix composites, Table IV-1. The nucleating agent used in all the compositions was ZrO_2. Composition SP916 was the least refractory composition (due to the high B_2O_3 content) and required a hot-pressing temperature of ~1250°C. The other compositions (SP917, SP963) were much more refractory and necessitated consolidation temperatures in excess of 1350°C. A commonly encountered problem during processing of composites with SP917 or SP963 matrices was adhesion of the composite surface to the molybdenum foil used as a separating material in the graphite die. This adhesion resulted in a poor composite surface finish and was believed to be due to a reaction between the molybdenum foil and the carbon fibers. It was subsequently discovered that this adhesion was influenced by the melting (viscosity) behavior of the matrix and that it could be reduced or even eliminated through the proper selection of hot-pressing parameters.

As-pressed composites generally contained a slight amount of crystallinity in the matrix due to devitrification during cooling in the hot press. Full crystallization was induced after hot-pressing by subjecting machined composite specimens to a heat treatment designed to produce uniform nucleation and crystal growth throughout the matrix; this heat treatment will hereafter be referred to as "ceraming". Ceraming was carried out in an argon atmosphere in order to prevent degradation of the carbon fibers due to oxidation. The crystalline phase formed during ceraming was identified by x-ray diffraction as either β-quartz solid solution (LAS phase) or β-spodumene solid solution, depending on the crystallization temperature used during ceraming. SP917/HMU composites were crystallized at 900°C and contained β-quartz solid solution. This phase is not stable at temperatures above 975-1000°C, however, and transforms to β-spodumene solid solution [20]. Therefore, SP963/HMU composites, which were crystallized at 1135°C, contained β-spodumene solid solution.

B. Mechanical Properties

Three-point flexural strengths of as-pressed and ceramed composite specimens were

obtained for composites made with all three LAS compositions. Representative values of flexural strengths and the corresponding failure modes are listed in Table IV-2. As-pressed strengths were generally somewhat higher for SP963 composites than for SP917 composites, with SP916 composites proving to be significantly lower in flexural strength than either of the other two. This trend is in line with approximate liquidus temperatures of the LAS composites, with SP963 being the most refractory.

Ceramed flexural strengths were lower than as-pressed strengths in all cases, with the reduction being the most severe for SP963 composites. Strength loss for SP917 composites, on the other hand, was almost insignificant. This behavior could have been caused by a number of different factors. One factor could have been the particular ceraming schedule used in converting the composite matrices from glasses to glass-ceramics. As shown in Table IV-2, the ceraming cycle used for SP963 composites included an upper temperature which was higher and a corresponding soak time which was longer than the ceraming cycle employed for SP917 composites. This could have led to more degradation of the carbon fiber as a result of oxidation and a subsequently greater loss in strength. Even though ceraming was conducted in an argon atmosphere, the impurity level of O_2 in the argon could have been sufficient to cause oxidation of the carbon fiber. Another factor could have been that ceraming caused a redistribution of residual stresses in the composite due to such mechanisms as volume changes during the amorphous $\rightarrow$ crystalline transformation or differences in thermal expansion coefficients of the matrices. Since a different crystalline phase was precipitated in the SP917 composite (β-quartz solid solution) than in the SP963 composite (β-spodumene solid solution), this could have created different residual stresses in the composites after ceraming. Table IV-2 shows that the failure mode in the SP963 and SP916 composites switched from primarily tensile failure in the as-pressed composites to primarily compressive failure in the ceramed composites, while the SP917 composites exhibited primarily compressive failure in both cases. This provides some evidence that stresses could have been redistributed differently in the different composites during ceraming.

Tensile testing was performed only on SP917 composites after consideration of the flexural testing results, which indicated that only SP917 composites exhibited good strength in both as-pressed and ceramed condition. Tensile data are given in Table IV-3 for both unidirectional and 0/90° reinforced composites. Representative tensile stress-strain curves for SP917/HMU composites are shown in Figures IV-1 through IV-4.

The tensile data exhibited by the composites was, on the whole, very respectable compared with typical behavior of borosilicate glass matrix composites [19]. However, ultimate tensile strengths (UTS) and especially elastic moduli (E) for the unidirectional composites were somewhat lower than expected. Measured E values of ~125 GPa for the unidirectional composites were markedly lower than rule of mixtures calculations predicting elastic moduli in the range of 200 GPa. Even calculations which accounted for the apparent reduction in fiber modulus during composite processing [19] from an as-received value of 380 GPa to a "composite" value of 310 GPa predicted elastic moduli of ~175 GPa. This was surprising in light of the fact that the moduli for the 0/90° reinforced LAS composites were very similar to those for borosilicate glass matrix composites. This behavior has been at least partially reconciled by the realization that

16

the tape winding parameters used for the 0/90° composites were not the same as those used for the unidirectional composites. The 0/90° composites were made with tape which had a wider spacing between fiber tows. It is possible that the tighter spacing used in the unidirectional composite tape led to bunching or kinking of the fibers, which would drastically reduce the composite elastic modulus. At any rate, it seems likely that the UTS and moduli of unidirectional LAS composites can be improved through adjustments in processing. This will be addressed in future work.

The tensile stress-strain curves illustrated in Figures IV-1 and IV-2 indicate that the stress and strain values associated with the initial deviation from linearity, the proportional limit (PL), are quite high for both the as-pressed and ceramed unidirectional composites. In fact, these PL stresses and strains are significantly higher than those typical of borosilicate glass matrix composites that were fabricated at UTRC during the same time period, as shown in Figure IV-5, making the use of LAS/HMU composites as structural materials seem very attractive. The reduction in PL stress and strain in the ceramed composite is consistent with the idea that such processes as fiber oxidation and/or redistribution of residual stresses in the composite may be taking place during ceraming.

Table IV-3 also contains short beam shear strength (SBSS) data for the SP917 composites. The values were obtained using 3-point flexure specimens with a span/depth ratio of 4. Figure IV-6 shows the specimen orientations corresponding to interlaminar and "edge-on" SBSS values. The edge-on shear strengths are higher than the interlaminar values due to the lack of an easy shear path for fracture in the edge-on orientation. The values of SBSS for the SP917 composites are similar to those reported for borosilicate glass matrix composites [19]. The low values of interlaminar shear strength also suggest that fiber-matrix interfacial strength (τ_i) in LAS/HMU composites may be low [5]. This is supported by direct measurements of fiber-matrix interfacial debond strength (τ_{max}) in SP917/HMU composites (obtained by J. Mandell at MIT), which ranged from ~7 MPa for ceramed composites to ~10 MPa for as-pressed composites (Table IV-3). These values are somewhat lower than τ_{max} values for borosilicate glass matrix composites (~10-15 MPa), which are typically regarded as having a weak fiber-matrix interfacial bond. The high degree of fiber pullout characteristic of the tensile fracture surfaces shown in Figure IV-7 is indicative of fiber-matrix debonding occurring during fracture, suggesting that these composites possess some degree of toughness. Future work will include fracture toughness measurements using notched flexure techniques as well as Charpy impact testing.

The high temperature performance of ceramed LAS/HMU composites has not yet been fully addressed. Initial results from high temperature flexure testing indicate that a large fraction of composite strength is retained at temperatures up to 900°C in argon, although only limited data has been acquired. More testing will be necessary before conclusive results can be obtained.

C. Thermal Expansion

The thermal expansion behavior of SP917/HMU composites in as-pressed and ceramed conditions is illustrated in Figure IV-8. Figure IV-8(a) corresponds to thermal expansion in a direction parallel to the fiber direction (axial), while Figure IV-8(b) represents thermal

expansion normal to the fiber direction (transverse). It is immediately obvious that the ceramed composites possess much lower coefficients of thermal expansion (CTE) than the as-pressed composites, especially in the transverse direction. This reflects the low CTE of the ceramed matrix, which is comprised of β-quartz solid solution (LAS phase), a phase consisting of β-eucryptite ($Li_2O \cdot Al_2O_3 \cdot SiO_2$) and β-quartz (SiO_2). β-eucryptite has a negative CTE up to 1000°C, thus making it possible for the solid solution to have a negative CTE, depending on the fraction of β-eucryptite contained in the solid solution [20]. The lack of precise CTE data on HMU fiber makes it difficult to calculate a CTE for the matrix based on composite CTE behavior. From all indications, however, it appears that the ceramed matrix probably has a very low CTE (< 1 ppm/°C), possibly even slightly negative. It is also possible that some degree of preferred orientation of the β-quartz solid solution could develop during ceraming due to the presence of the aligned carbon fibers. This would make interpretation of the composite CTE data even more difficult since β-eucryptite exhibits highly anisotropic CTE behavior.

Table IV-1

LAS Compositions Used to Fabricate HMU Reinforced Composites

	Composition in Weight %		
Oxide	SP916	SP917	SP963
SiO_2	53.5	69.2	70.9
Al_2O_3	24	21.1	21.6
B_2O_3	10	-	-
Li_2O	2.5	3.1	3.2
MgO	7	1.9	2
ZnO	-	1.1	-
BaO	-	0.8	-
ZrO_2	2	1.6	1.6
As_2O_3	1	1	0.7
Other	-	< 0.5	-
		$(Na_2O + K_2O + Nd_2O_3)$	

Table IV-2

Three-Point Flexural Strength of LAS/HMU Composites

Matrix	Vol. % Fiber	Flexural Strength (MPa)				
		As-Pressed	Failure Mode	Ceramed	Failure Mode	% Strength Loss
SP916	43	862	T/S	673*	C	
		875	T/S	830*	C	
		820	T/S	___		
		852		752		11.7
SP917	42	1110	C	1040*	C/S	
		1020	C/S			
		1120	C/S	___		
		1063		1040		4.0
SP963	43	1230	T/S	700**	C/S	
		1240	T/S	719**	C/S	
		1280	T	___		
		1250		710		43.2

Ceraming Schedule

*   780°C for 2 hours; 900°C for 8 hours

**   780°C for 2 hours; 1135°C for 16 hours

Failure Mode

T = Tension

C = Compression

S = Shear

Table IV-3

Mechanical Property Data for SP917/HMU Composites

Tensile Properties

Orient.	Condition	Fiber Vol. %	UTS (MPa)	E (GPa)	Failure Strain (%)	Propor. Limit (MPa)	SBSS (MPa) Inter.	Edge-On	Average τ_{max} (MPa)
0°	As-pressed	42	646	125	0.54	556	-	-	-
	Ceramed	40	471	126	0.38	426	-	-	-
0/90°	As-pressed	40	297	79	0.44	39	-	-	-
	Ceramed	40	259	82	0.38	32	-	-	-
0°	As-pressed	40	-	-	-	-	18.6	29.6	-
	Ceramed	40	-	-	-	-	11.7	19.3	-
0°	As-pressed	42	-	-	-	-	-	-	9.9
	Ceramed	42	-	-	-	-	-	-	6.9

21
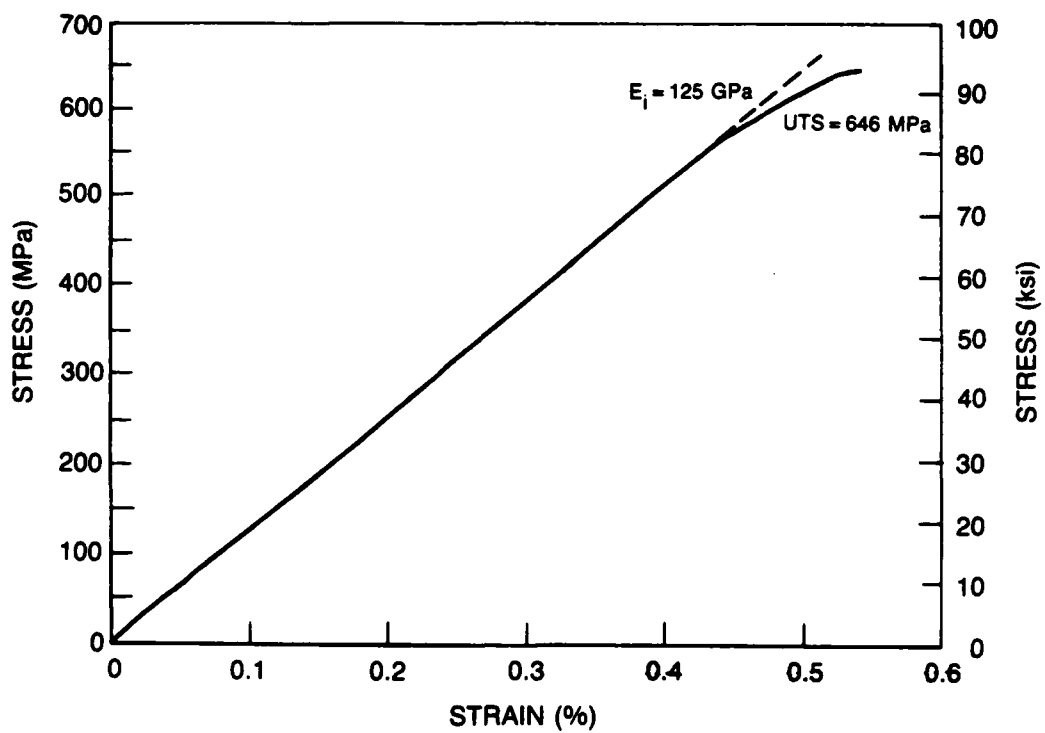
Fig. IV-1. Tensile Stress-Strain Curve for 42 v/o O° HMU/SP917, As-Pressed
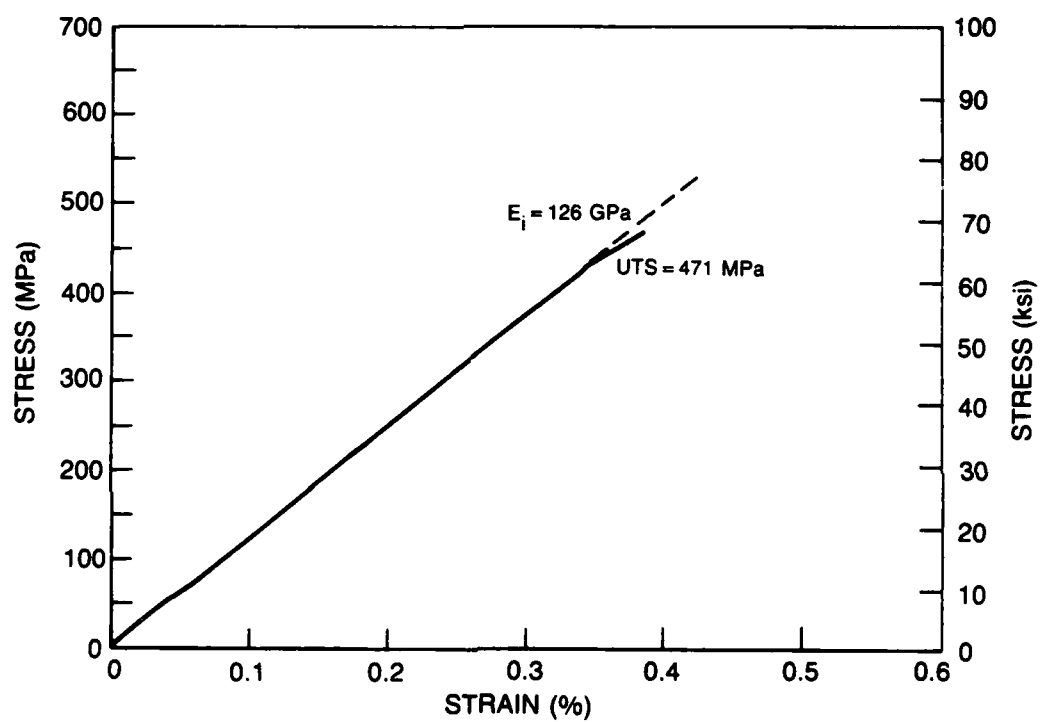
Fig. IV-2. Tensile Stress-Strain Curve for 40 v/o O° HMU/SP917, Ceramed

23
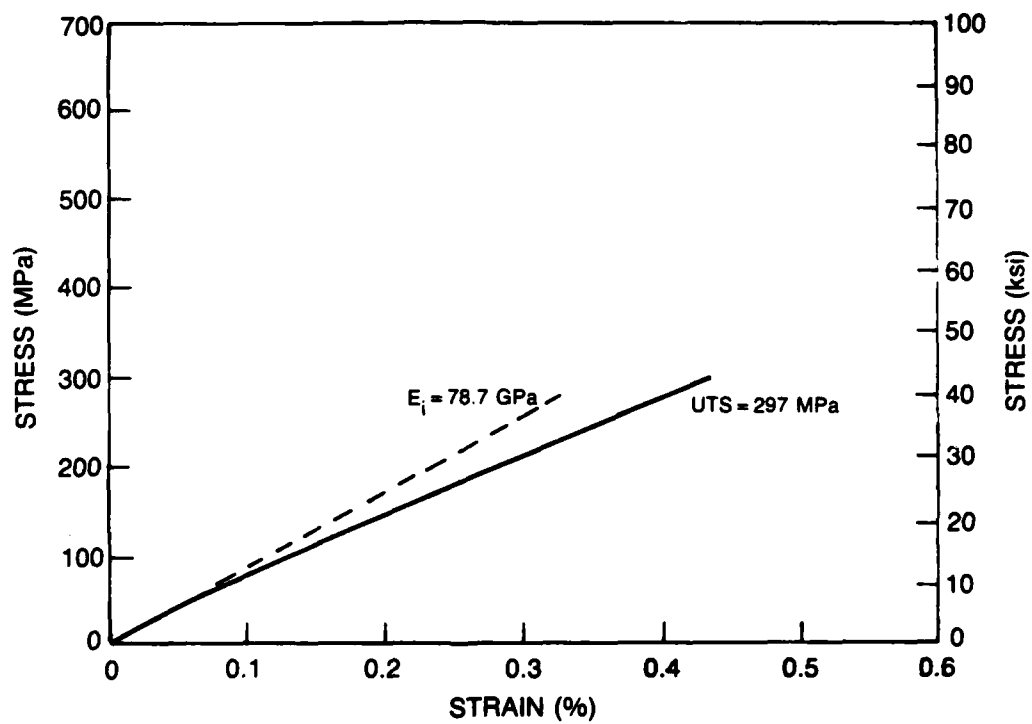
Fig. IV-3. Tensile Stress-Strain Curve for 40 v/o 0/90° HMU/SP917, As-Pressed

87 – 8 – 42 – 3
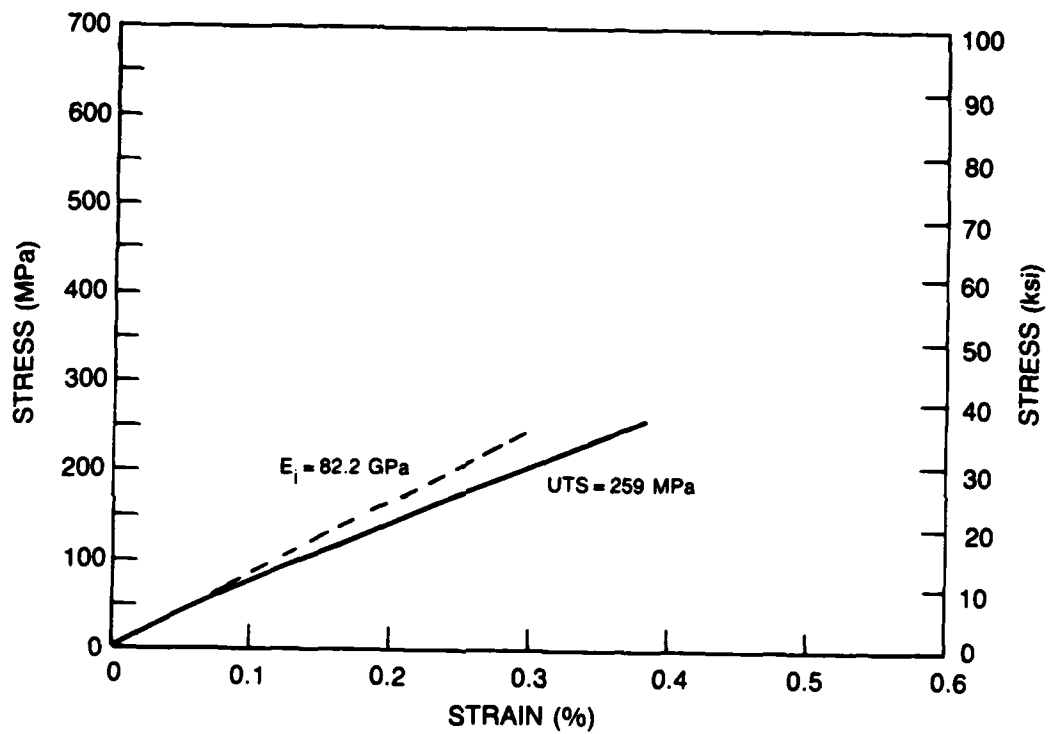
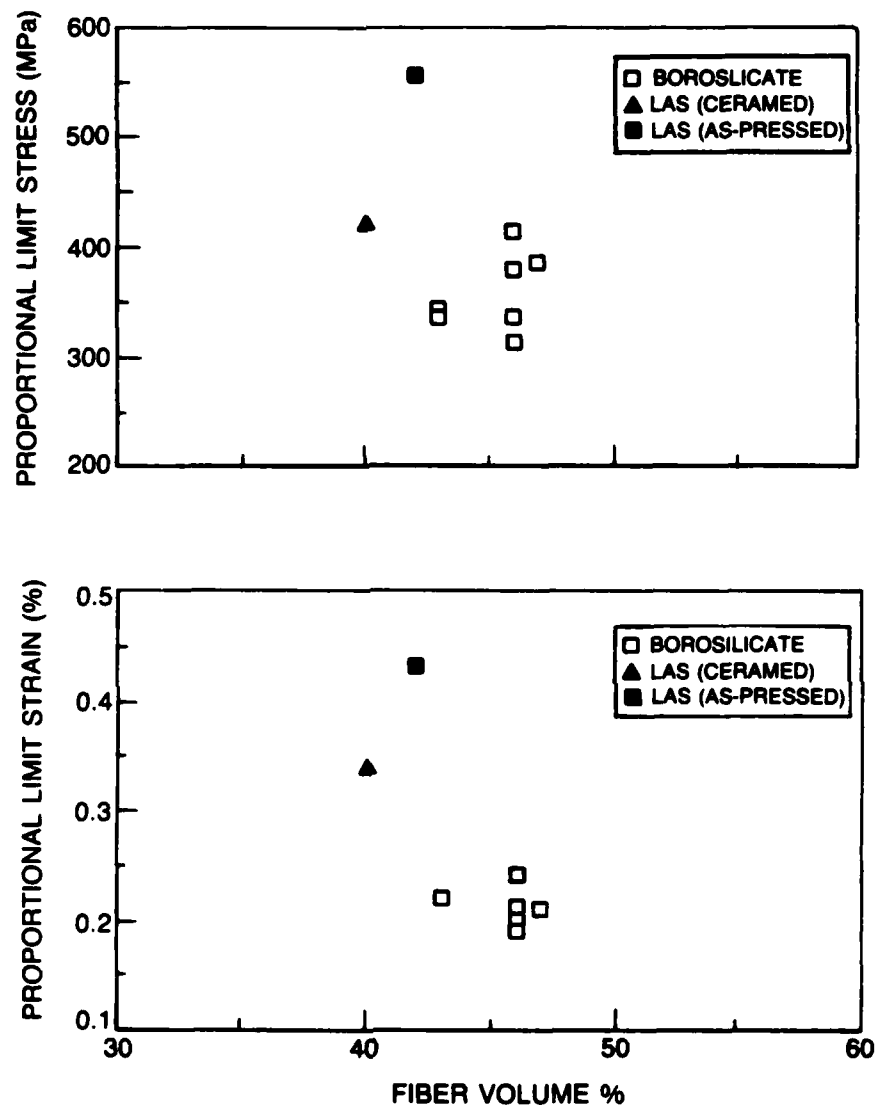Fig. IV-4. Tensile Stress-Strain Curve for 40 v/o 0/90° HMU/SP917, Ceramed

Fig. IV-5. Proportional Limit Stress and Strain vs Fiber Volume Percent for 0° HMU Reinforced LAS and Borosilicate Matrix Composites
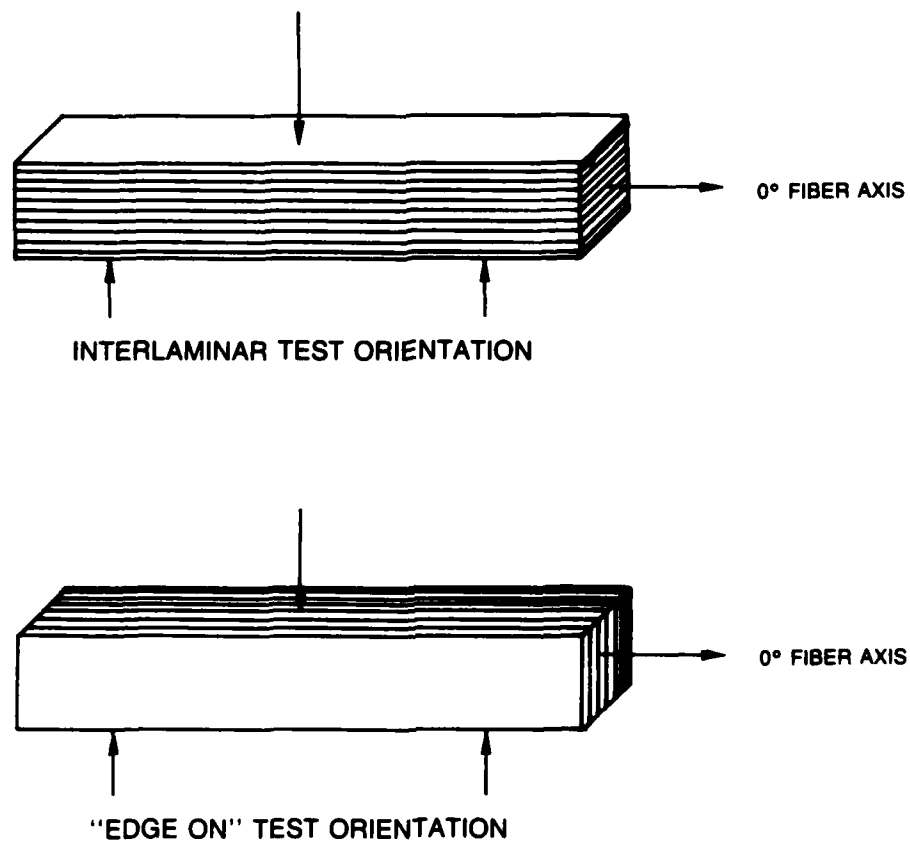
Fig. IV-6. Specimen Orientations, Showing Plys, Tested in Flexure With L/h = 4

100μm

20μm
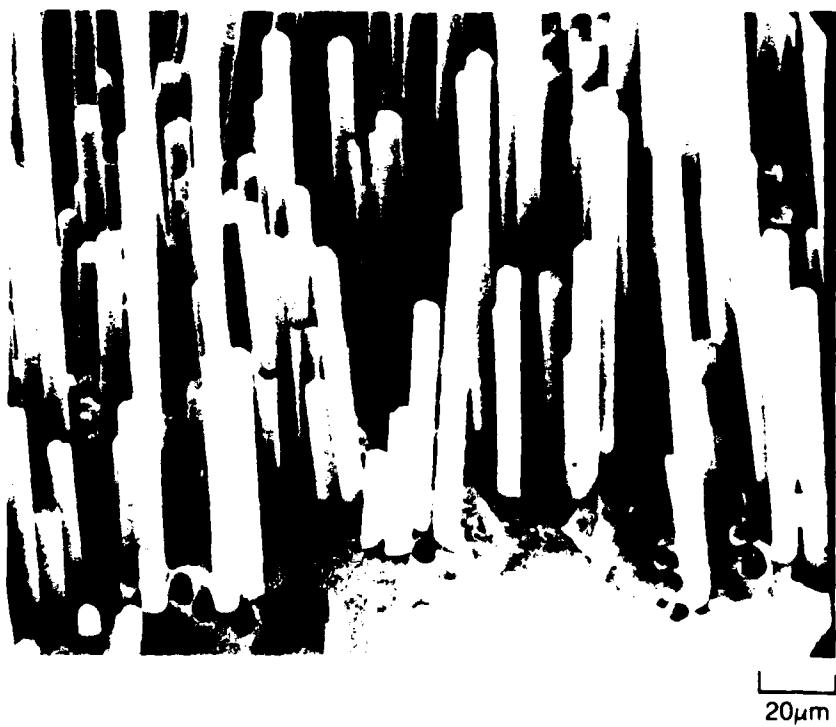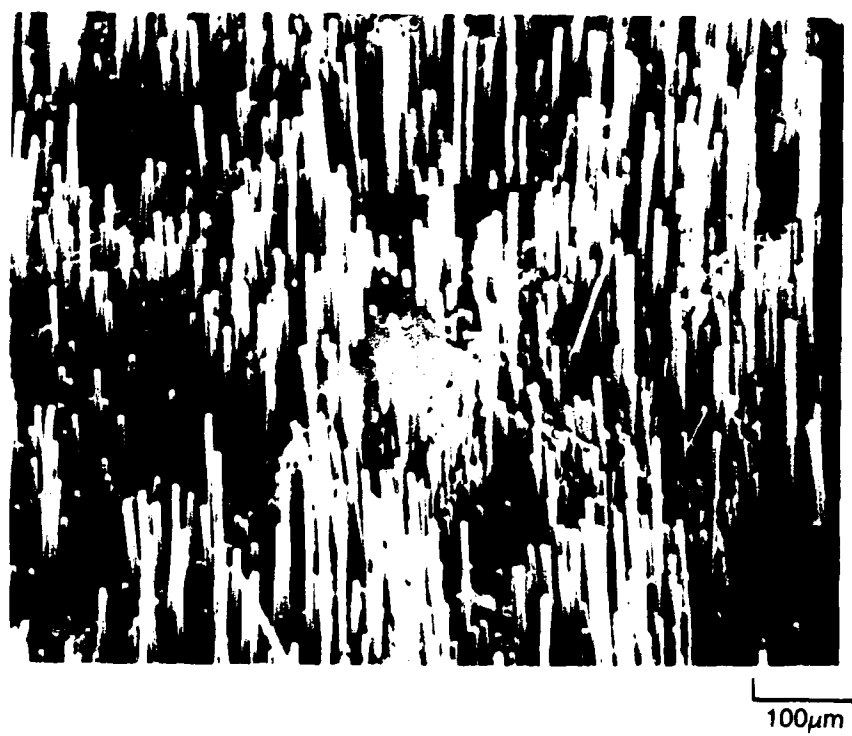
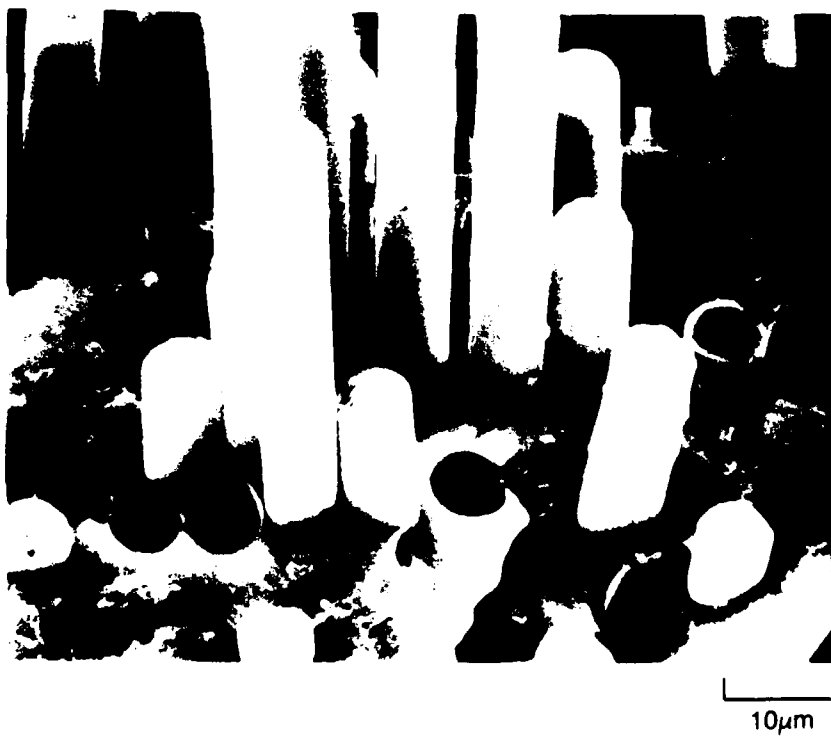Fig. IV-7 (a). Tensile Fracture Surface of 0° SP917/HMU (As-Pressed)

Fig. IV-7 (b). Tensile Fracture Surface of 0° SP917/HMU (Ceramed)

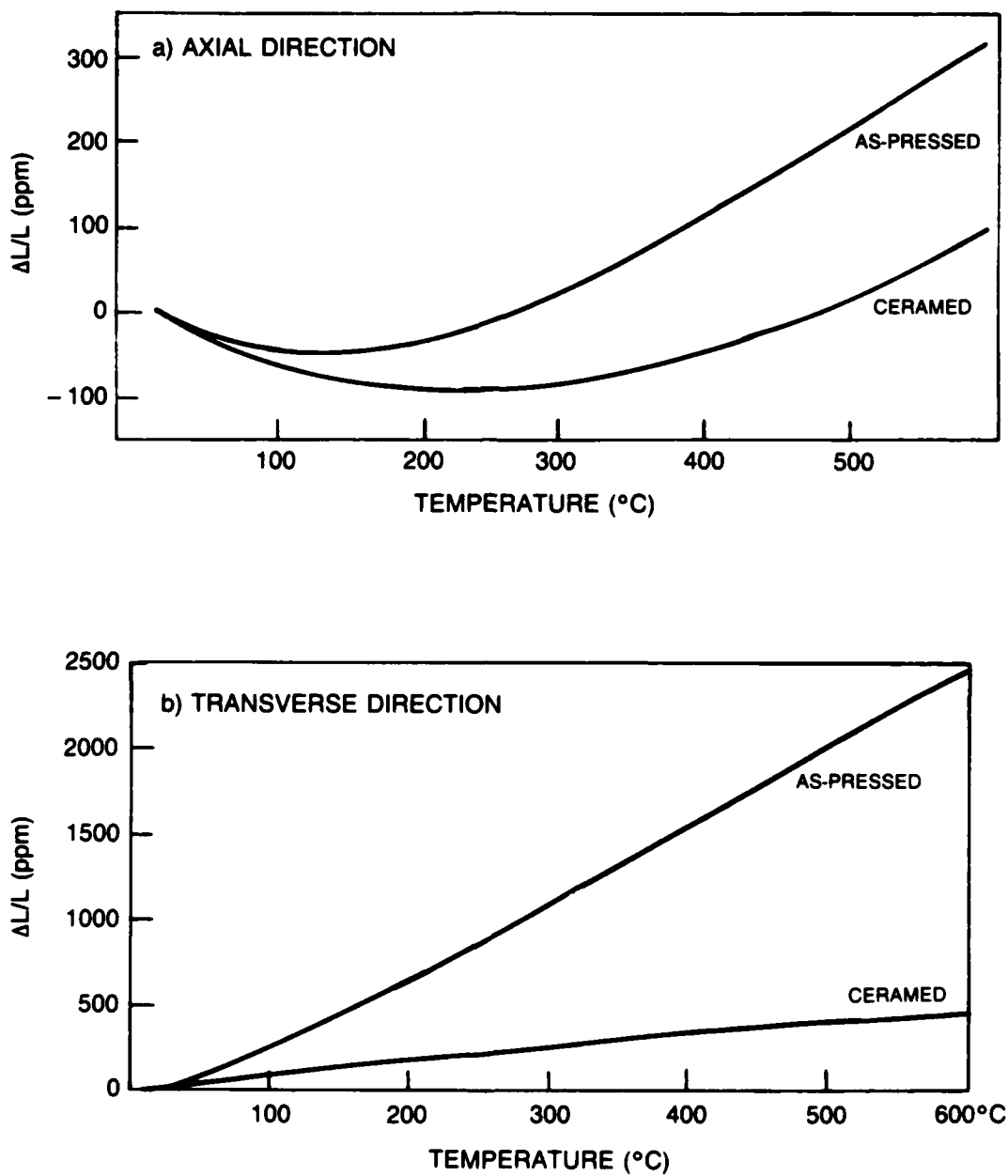**Fig. IV-8.** ΔL/L vs Temperature for 40 v/o SP917/HMU Composites: (a) Axial Direction; (b) Transverse Direction

V. Effect of Processing Conditions on Mechanical Behavior

The effect of hot-pressing temperature and pressure on the mechanical behavior of HMU reinforced borosilicate glass matrix (Corning Code 7740) composites was evaluated for the purpose of determining whether processing temperatures could be lowered without sacrificing composite performance. Such behavior has been observed in the SiC (Nicalon)/7740 composite system [24], where optimum performance was achieved using hot-pressing parameters of approximately 900°C and 6.9 MPa. Since HMU/7740 composites have in general exhibited strength and stiffness behavior below that predicted by theory after processing at temperatures in excess of 1200°C [19], it was thought that lowering of the hot-pressing temperature may lead to a similar improvement in composite properties in this system by more effectively preserving fiber strength and stiffness.

A. Processing

Unidirectional HMU/7740 composites were processed under the different sets of conditions given in Table V-1. Three different nominal hot-pressing temperatures were used: 900°C, 1100°C, and 1280°C (the latter temperature is the standard temperature normally used to process HMU/7740 composites). Temperatures in the range of 1000-1100°C were avoided because of devitrification which may occur in this temperature region. An unusually high pressure of 20.7 MPa (3000 psi) was initially used at 900°C to assist in densification of the matrix, since the glass viscosity was extremely high at that temperature. Another pressing was subsequently performed at 6.9 MPa (1000 psi) because of the concern over possible fiber damage incurred by pressing at high pressures.

Microstructures of the resulting composites are shown in Figure V-1. The two composites hot-pressed at 900°C exhibited a large degree of porosity in the matrix as a result of incomplete matrix densification. The two different pressures do not appear to have made any significant difference in the degree of porosity in the two composites, implying that matrix viscosity was high enough to resist complete flow even under 20.7 MPa ram pressure. The composites pressed at nominal temperatures of 1100°C and 1280°C did not exhibit any obvious porosity and appeared to be fully densified.

B. Mechanical Behavior

Tensile specimens of the composites hot-pressed at 900°C exhibited a fibrous fracture mode, as shown in Figures V-2 and V-3. The composites hot-pressed at 1100°C and 1280°C, however, showed very little fiber pullout and were essentially non-fibrous in fracture (Figures V-2 and V-4). This difference in degree of pullout can be attributed to the previously described microstructural differences between the composites. The incomplete matrix densification of the composites pressed at 900°C resulted in a significant fraction of fiber surface area which was weakly or incompletely bonded to the matrix; in fact, fibers residing directly next to pores had areas of completely unbonded surface. This incomplete fiber-matrix interfacial contact was

31

directly responsible for the large degree of fiber pullout observed in these composites. In direct contrast, the full matrix densification of the 1100°C and 1280°C composites resulted in complete fiber-matrix interfacial contact which in turn led to a much lower degree of fiber pullout. The almost complete lack of pullout in the dense composites was surprising in light of the fibrous fracture mode demonstrated by the 0/90° reinforced 7740/HMU composites discussed in a previous section (Section III). Both sets of composites were similar in all respects except ply orientation. Inspection of the fracture surface in Figure V-4(b) revealed that the distribution of fiber throughout the matrix did not appear to be especially uniform. Glass-rich regions exhibited little or no fiber pullout, while regions containing a larger fiber volume fraction demonstrated some degree of fiber-matrix debonding, though not to the same extent as the 0/90° reinforced composites. This behavior is not fully understood and will be studied further in subsequent investigations.

The difference in matrix densification can also be used to explain other aspects of the composite mechanical behavior. Table V-1 summarizes the tensile stress-strain behavior exhibited by the composites. It is clear that the elastic moduli of the 900°C composites (~145 GPa) are significantly lower than those of the composites pressed at 1100°C and 1280°C (~170-175 GPa). Figure V-5 shows a direct comparison between the stress-strain behavior of composites processed at 900°C, 6.9 MPa and at 1280°C. Incomplete matrix densification in the 900°C composite has led to only partial load transfer between matrix and fibers, resulting in an elastic modulus which is significantly below that of the fully dense composite pressed at 1280°C. Rule of mixtures calculations predicted composite elastic moduli in the range of 200 GPa when using the reported fiber modulus of 380 GPa, well above all of the measured composite elastic modulus values. The E values of the 1100°C and 1280°C composites are typical of those obtained in previous work on HMU reinforced borosilicate glass matrix composites [19] and suggest that the actual fiber elastic modulus in the composite may be closer to 310 GPa than to 380 GPa. One possible explanation for this apparent loss in modulus could be that diffusion of species into the fiber during processing alters the crystal structure in such a way as to reduce the elastic modulus. This subject will be addressed in future work.

Another property that appears to be somewhat microstructure dependent is the proportional limit (PL) stress. Table V-1 indicates that the PL stress is low (223 MPa) for the composite processed at 900°C, 6.9 MPa, then increases and remains relatively constant at approximately 350 MPa for the other three composites. The fact that the two dense composites exhibit higher PL stresses than the 900°C, 6.9 MPa composite is understandable in light of the difference in microstructure. However, the high PL stress displayed by the 900°C, 20.7 MPa composite is not readily understood considering the porous nature of the microstructure. One explanation for the anomalous behavior could be that the higher pressure used for the 900°C, 20.7 MPa composite created a higher fiber-matrix interfacial bond strength than in the 900°C, 6.9 MPa composite. This would lead to a higher proportional limit based on the concept that the proportional limit is directly related to the fiber-matrix interfacial bond strength. The similarity of the proportional limit of the 900°C, 20.7 MPa composite to those of the fully dense composites is probably coincidental.

The other tensile properties given in Table V-1 appear to be much less sensitive to

microstructure. Ultimate tensile strength (UTS) and failure strain seem to be related more to the press temperature, as they both show increasing trends towards maximum values for the composite pressed at 1280°C. The reason for the lower strength of the fully dense 1100°C composite is not clear, although it could be related to possible devitrification which may have occurred to a slight extent during processing. Although this was not confirmed by x-ray diffraction, 7740 glass is known to show some signs of devitrification in the temperature range of 1000-1100°C. The reasons behind the lower strength of the 1100°C composite deserve further consideration and will be more fully addressed in future work.

Table V-1

Processing Conditions and Mechanical Behavior of HMU/7740 Composites

| Vol. % Fiber	Hot-Press Temp. (°C)	Pressure (MPa)	UTS (MPa)	E (GPa)	Failure Strain (%)	PL Stress (MPa)	Fracture Behavior
43	904	6.9	420	146	0.38	267	Fibrous
			377	143	0.35	179	
			399	145	0.37	223	
44	888	20.7	502	143	0.38	371	Fibrous
			521	144	0.37	349	
			512	144	0.38	360	
44	1117	10.3	430	181	0.30	375	Non-fibrous
			577	168	0.62	371	
			504	175	0.46	373	
46	1286	8.3	695	171	0.59	312	Non-fibrous
			579	168	0.57	335	
			696	173	0.63	413	
			657	171	0.60	353	

UTS = Ultimate tensile strength
E = Elastic modulus
PL = Proportional limit
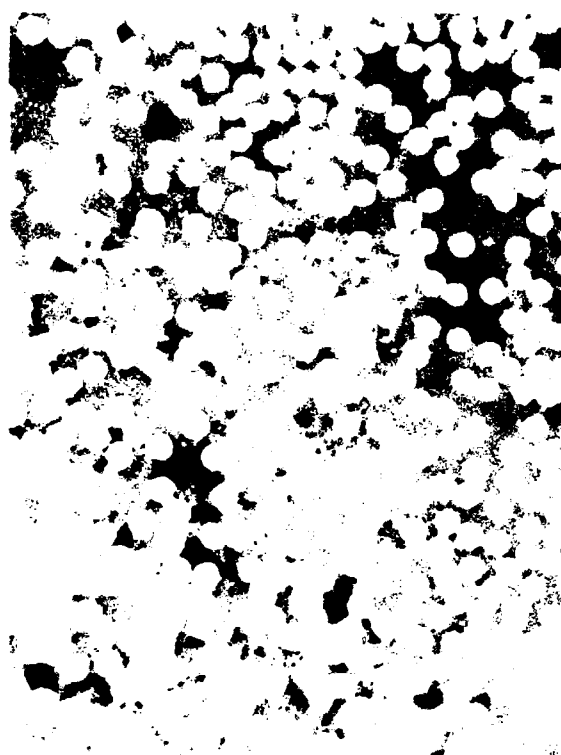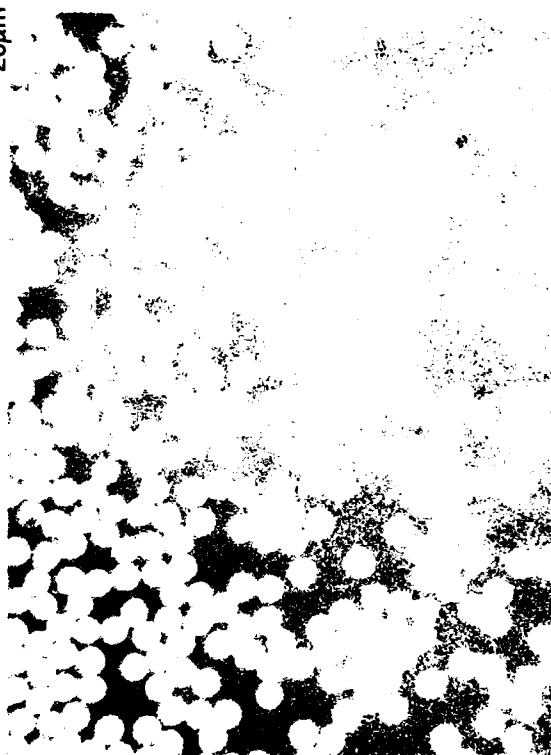
900°C, 20.7 MPa
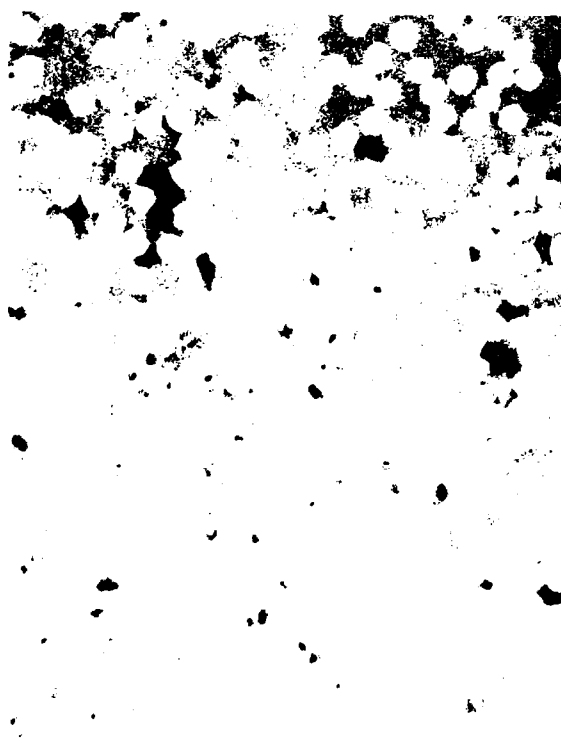
1280°C, 8.3 MPa

900°C, 6.9 MPa

1100°C, 10.3 MPa

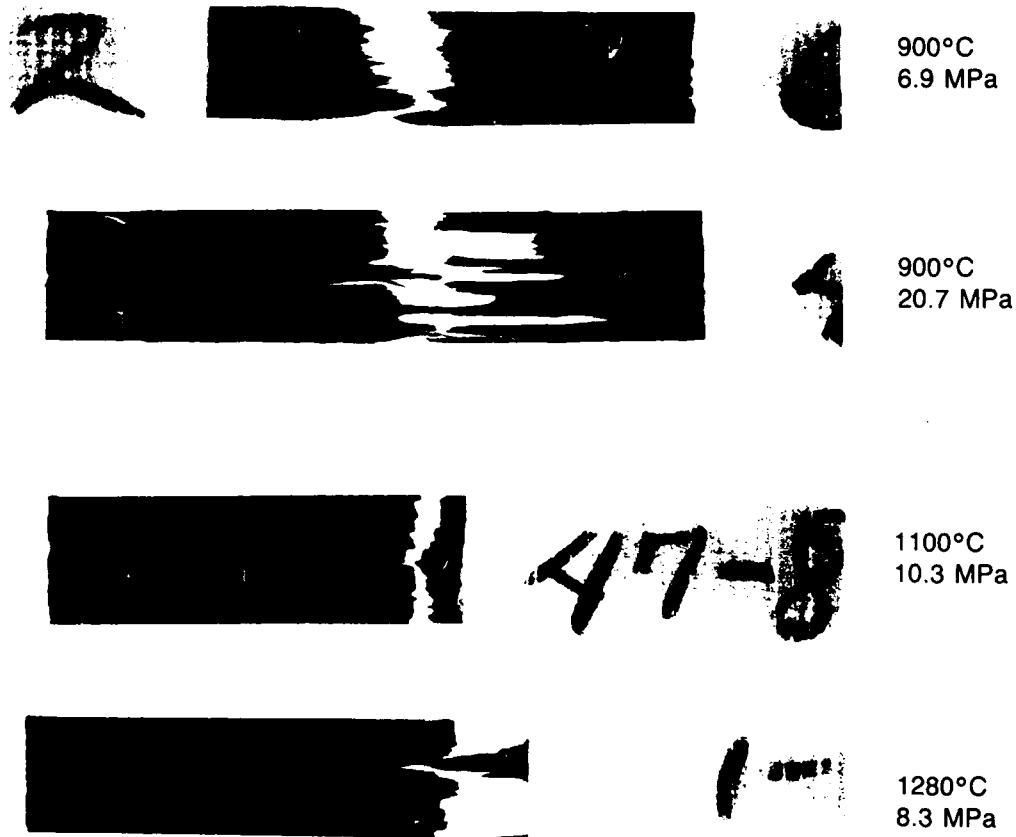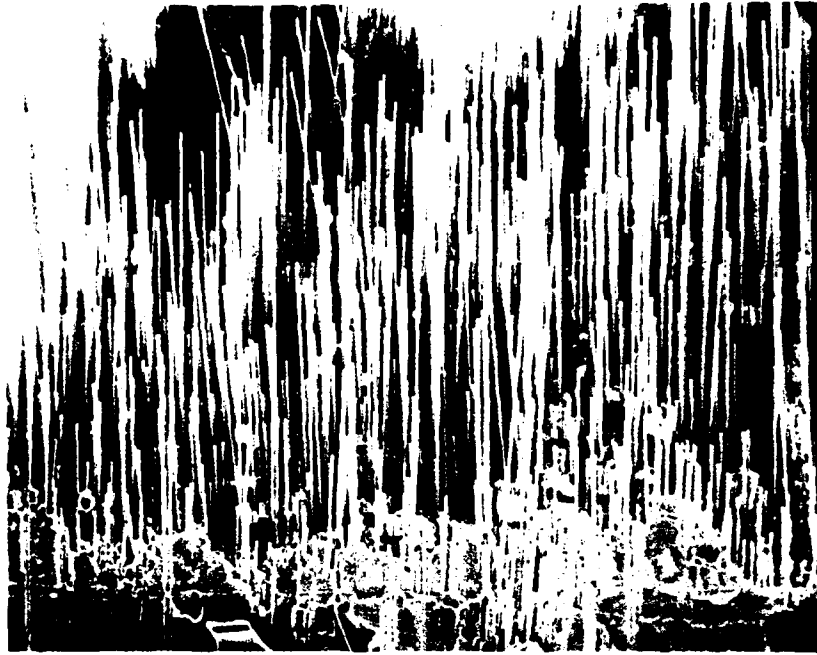**Fig. V-1. Microstructures of 0° 7740/HMU Composites Processed Under Different Conditions**

35

Fig. V-2. Fractured Tensile Specimens of 0° 7740/HMU Composites Processed Under Different Conditions

900°C
6.9 MPa

900°C
20.7 MPa

1100°C
10.3 MPa
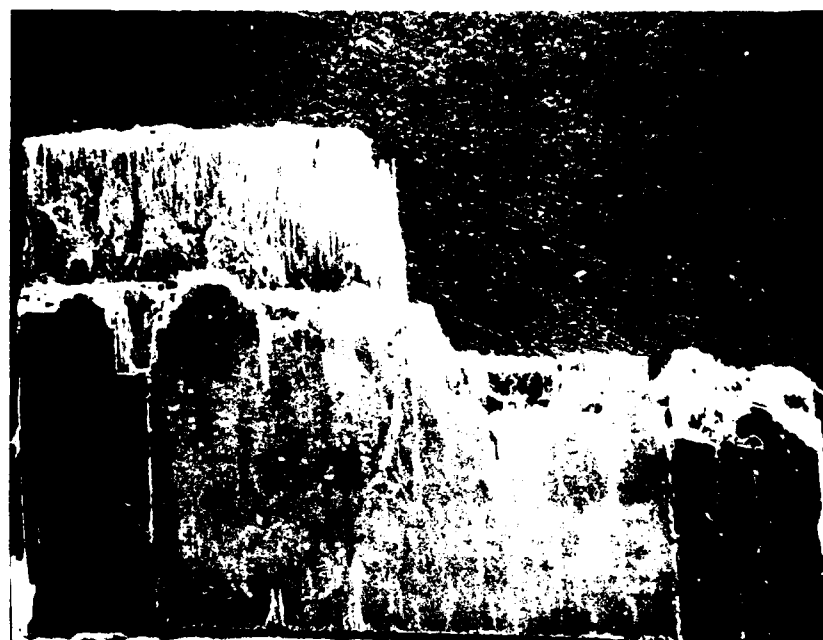
1280°C
8.3 MPa

87 – 8 – 42 – 10

900°C, 20.7 MPa

200μm

900°C, 6.9 MPa

100μm

Fig. V-3. Tensile Fracture Surfaces of 0° 7740/HMU Composites Hot-Pressed at 900°C

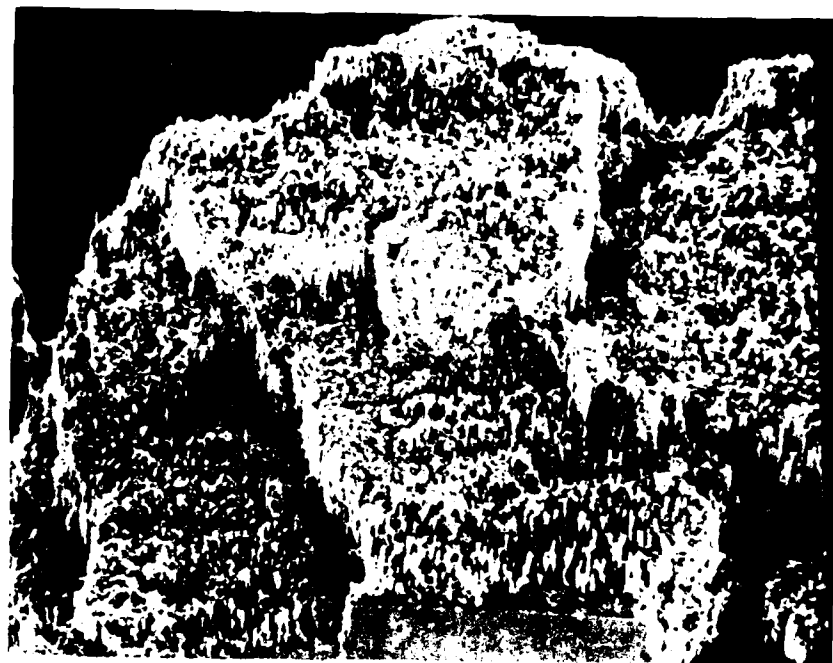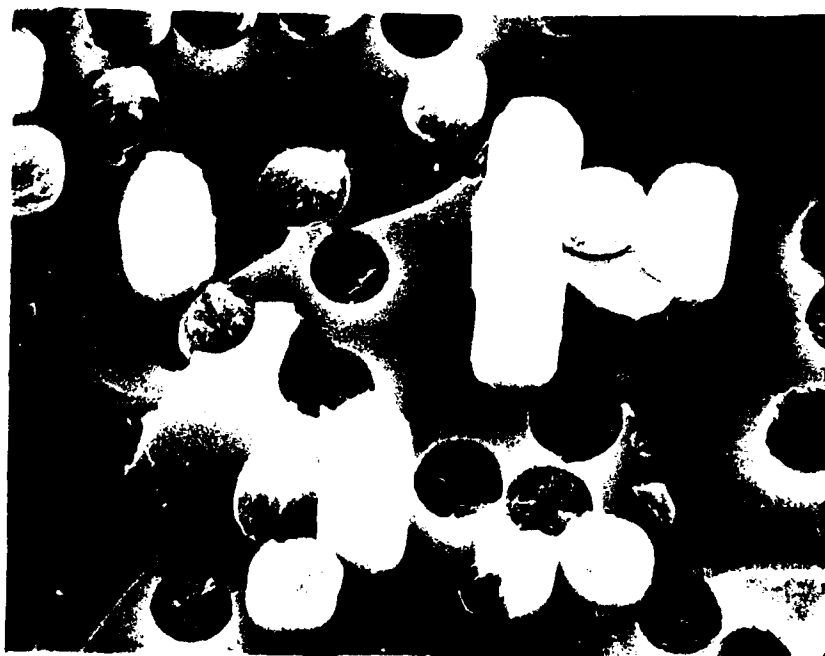**Fig. V-4 (a). Tensile Fracture Surface of 0° 7740/HMU Composite Hot-Pressed at 1100°C**

200µm

10µm

Fig. V-4 (b). Tensile Fracture Surface of 0° 7740/HMU Composite Hot-Pressed at 1280°C
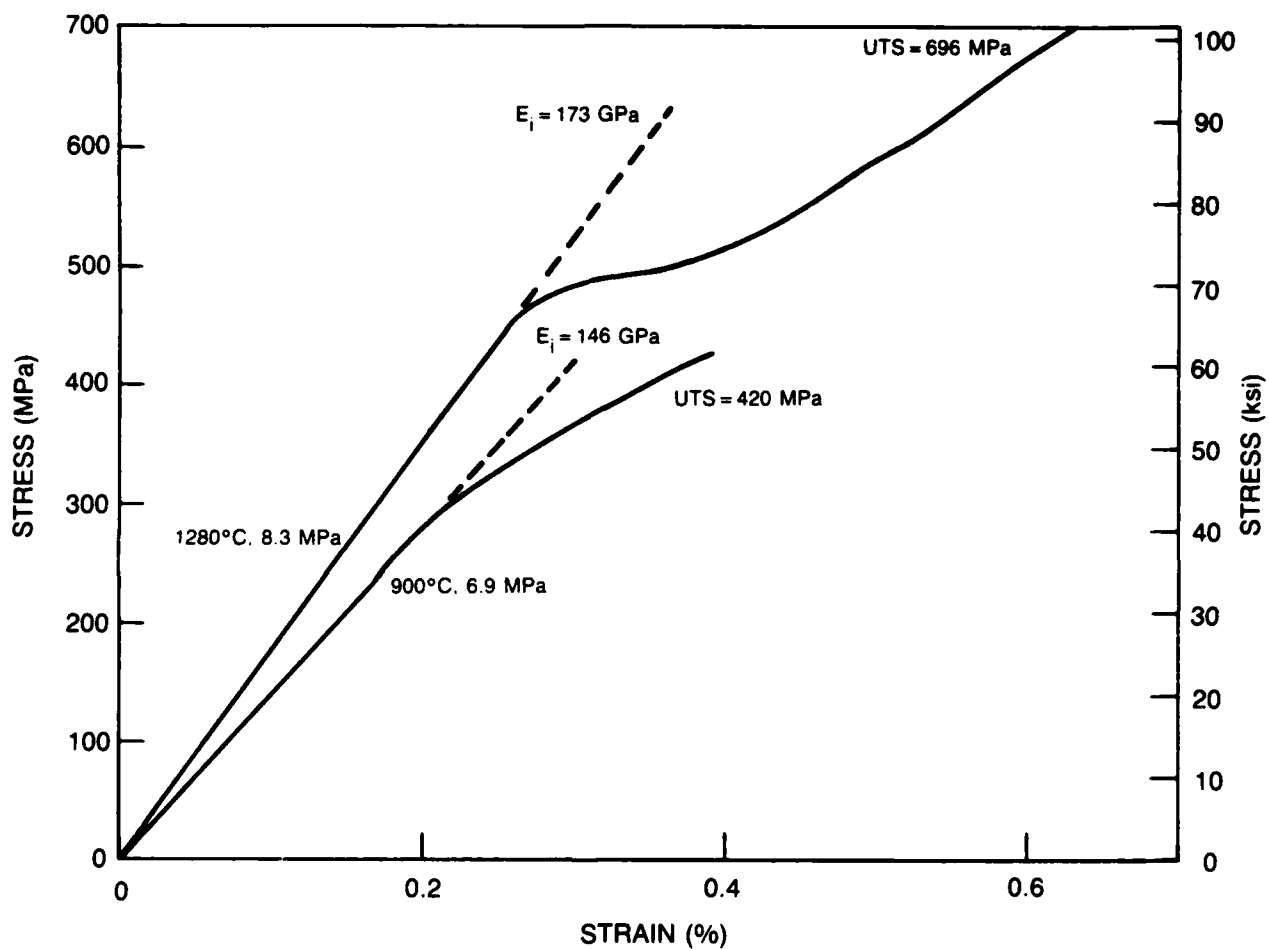
Fig. V-5. Tensile Stress-Strain Curves for Unidirectionally Reinforced 7740/HMU Composites Processed Under Different Conditions

87 – 8 – 42 – 14

VI. Effect of Interfacial Reactions on Mechanical Behavior of HMU Reinforced Borosilicate Glass Matrix Composites

Fiber-matrix interfacial strength (τ_i) is known to exert a strong influence on many composite properties [5, 25]. Two properties which demonstrate a particularly strong dependence on τ_i are composite toughness and composite interlaminar shear strength. Composites exhibiting high values of both of these properties would be very desirable; unfortunately, this is difficult to achieve due to the converse dependencies of these characteristics on τ_i. Composite toughness, which is closely related to the work of fracture (γ), is inversely proportional to τ_i, while interlaminar shear strength exhibits a direct proportionality to τ_i. This contrariety in behavior clearly poses problems for composite design if one wishes to incorporate both high toughness and high interlaminar shear strength into a composite. Ideally, it would be possible to control τ_i to some intermediate value which would allow for increased interlaminar shear strength while sacrificing very little in composite toughness.

The purpose of this portion of the program was to gain a better understanding of the role of the fiber-matrix interface in the control of composite behavior. While some experiments along this line were performed in the previous year's activity, the glasses used at that time were suspected of being very nonuniform in composition. Also, the analysis of resultant interfacial chemistry had been incomplete. Compositions of increased homogeneity were melted at Penn State University for the current stage of the investigation. In this present effort, the nature of the fiber-matrix interface was altered through reactions between the carbon fiber and various dopants in the matrix. The resultant effect of these reactions on composite mechanical behavior was observed and correlated with analysis of the fiber-matrix interface.

A. Processing

Unidirectionally reinforced HMU composites were prepared using the matrix compositions and hot-pressing parameters shown in Table VI-1. The compositions are identical except for minimal additions of Nb_2O_5 to PS 2 and MoO_3 to PS 3. These oxides were added for the specific purpose of reacting with the carbon fibers in the composite during processing so as to alter the nature of the fiber-matrix interface. They were selected based on a detailed thermodynamic analysis [19] which indicated that at elevated temperatures these oxides should react readily with carbon to produce carbides (NbC, Mo_2C) at the fiber-matrix interface. The analysis revealed that several different gaseous species (e.g., CO, SiO) are produced as result of these reactions, with the removal of these gases from the interface being a rate-limiting step in the overall interfacial reaction. Though thermodynamics is a powerful tool for predicting reactions between different chemical species, it should be understood that the influence of kinetic effects on the reactions was not considered in the analysis. The degree of mobility of Nb and Mo atoms in the borosilicate glass must be taken into account when interpreting the overall fiber-matrix interactions.

A simplified approach to assessing the relative stability of oxides in the presence of carbon

is through the use of an Ellingham diagram, Figure VI-1. Ellingham diagrams have been used successfully in the analysis of interfacial reactions in SiC/LAS composites [27]. Figure VI-1 plots the standard free energy of formation (ΔG_f°) of various oxides in units of kilocalories per mole of O_2 as a function of temperature. An oxide is relatively stable in the presence of carbon if its ΔG_f° falls below that of CO at a given temperature; however, if the ΔG_f° of the oxide lies above that of CO_2, then the oxide will tend to be readily reduced by the carbon. From Figure VI-1, it appears that MoO_3 should be readily reduced in the presence of carbon at all temperatures above 800°C. On the other hand, Nb_2O_5 should be more stable and would probably be reduced more slowly at all temperatures. In short, this simplified approach predicts that, compared with Nb_2O_5, MoO_3 should be more reactive with carbon at all temperatures covered by the range of the diagram.

B. Fiber-Matrix Interfacial Analysis

Microstructures of the composites after hot-pressing at 1150°C for 20 minutes are shown in Figure VI-2. The composite containing the base glass as a matrix shows no signs of porosity and appears to be very dense. The composites containing Nb_2O_5 and MoO_3, however, contain quite a bit of porosity, indicating that gas-evolving reactions have taken place between the matrix additives and the carbon fibers. It is believed that this porosity is due solely to gas evolution and not to such factors as incomplete matrix consolidation due to increased matrix viscosity, as discussed in a previous section (Section V). The viscosity behavior of the doped glasses should not have been altered noticeably by the minor additions of Nb_2O_5 and MoO_3. The amount of porosity in the MoO_3 composite appears to be greater than in the Nb_2O_5 composite, supporting the thermodynamic prediction that MoO_3 should be more reactive than Nb_2O_5 in the presence of carbon. The non-uniformity of the porosity in the MoO_3 composite is likely the result of somewhat inhomogeneous distribution of MoO_3 in the glass during melting.

Fracture surfaces of the composites after hot-pressing at 1150°C for 20 minutes are shown in Figure VI-3. The surfaces of the fibers give a good indication of interfacial reactions which may have taken place during processing. Fiber surfaces in the base glass composite are relatively clean, indicating that little or no reaction occurred. Examination of fibers in the Nb_2O_5 composite reveals some evidence of interfacial reaction, though not to any great extent. On the other hand, a reaction layer is obviously present on the surfaces of fibers in the MoO_3 composite, indicating that a strong interfacial reaction took place during processing.

Scanning Auger microprobe (SAM) analysis of fiber-matrix interfacial regions in the composites was conducted to establish elemental concentration profiles at the interface. Neighboring fiber and matrix trough areas were analyzed after repeatedly sputtering away very thin layers of material using an argon ion gun. A SAM concentration profile of a fiber-matrix interfacial region in the base glass composite is shown in Figure VI-4. It is evident from the figure that C diffused into the glass matrix to depths in excess of 2000Å, while O, Si, and Na were detected at similar depths into the fiber. The only element showing no propensity for diffusion was B, which could not be detected in the fiber even at a depth of only 50Å. SAM analysis of a Nb_2O_5 composite interfacial region appeared very similar to that of the base glass composite, with Nb failing to be detected in the analysis. It was subsequently determined that the primary

Auger peaks of B and Nb overlapped, so that the B peak effectively masked the presence of Nb in the spectrum. After discovering that the same situation existed for B and Mo, it was decided that SAM analysis was not particularly suited for establishing concentration gradients of Nb and Mo in these compositions.

As an alternative to SAM analysis, electron microprobe (EM) analysis was conducted to establish the concentration gradients of Nb and Mo in the interfacial regions. The spot size in the microprobe was ~1 μm in diameter, with an effective sampling area of ~3 μm diameter due to beam spreading effects. While not offering resolution on the level of the SAM, the EM was able to detect Nb and Mo in the interfacial regions, as shown by the profiles in Figure VI-5. The profiles show that the level of Nb in the Nb_2O_5 composite remains fairly constant in moving through the matrix towards the fiber. The concentration of Mo in the MoO_3 composite, however, is relatively depleted in the matrix but rises sharply in the fiber-matrix interface region. This result suggests that the reaction layer on the fiber surfaces of the MoO_3 composite (Figure VI-3) is most likely a Mo-containing compound. The lack of an increase in Nb concentration at the interface agrees well with the absence of an obvious reaction layer on the fibers.

X-ray diffraction (XRD) traces of crushed composite samples are shown in Figure VI-6. Traces of α-cristobalite are present in all three composites, with a noticeably larger amount present in the Nb_2O_5 composite. All three glass compositions were found to devitrify readily in the temperature range of 900-1100°C to form α-cristobalite. The processing temperature of 1150°C was probably close enough to this range to allow some devitrification to occur. Figure VI-6 also establishes the presence of Mo_2C in the MoO_3 composite; this undoubtedly corresponds to the reaction layer formed at the fiber-matrix interface in this composite (Figure VI-3). XRD failed to detect any NbC in the Nb_2O_5 composite, although it is possible that NbC could be present at a level too low to be detected above the background noise.

In summary of the fiber-matrix interfacial analysis, it was found that a reaction layer of Mo_2C formed at the interface in the MoO_3 composite. However, a reaction layer in the Nb_2O_5 composite was difficult to detect. The formation of Mo_2C in the MoO_3 composite along with the fact that MoO_3 reacted to a greater extent than Nb_2O_5 both agree well with the thermodynamic analysis discussed previously. The lack of an obvious reaction in the Nb_2O_5 composite to form NbC is at odds with the thermodynamic prediction, however. This conflict could be the result of kinetic influences related to the relative mobilities of Mo and Nb in the matrix. It is clear from Figure VI-5 that the mobility of Mo in the glass is high based on the concentration gradient of Mo at the fiber-matrix interface. It is possible that the mobility of Nb in the glass could be much lower. Nb_2O_5 is known to be a glass-forming oxide in some complex compositions [28] when present in small concentrations and when in the presence of other glass-forming oxides (e.g., SiO_2, B_2O_3). This could account for the observed behavior, since an atom that is part of the glass network would be much less mobile than an "interstitial" atom such as Mo.

C. Composite Behavior

The influence of fiber-matrix interfacial reactions on composite behavior was assessed by measuring fiber-matrix interfacial debond strength, mechanical properties (flexural strength,

axial tensile strength), and composite thermal expansion. Each of these areas will be discussed separately below.

1. Fiber-Matrix Interfacial Debond Strength

Direct measurements of fiber-matrix interfacial debond strength (τ_{max}) were obtained by J. Mandell at MIT using a technique which applies a load to the ends of individual fibers until debonding occurs [29]. By knowing the elastic stress field present at the initiation of debonding, it is possible to calculate a value of τ_{max} through the use of a complex finite element analysis computer program. The results, shown in Table VI-3, were obtained from composites which had been hot-pressed at 1150°C for 20 minutes. Each value of τ_{max} is an average of at least 14 separate measurements performed on individual fibers.

The results indicate that τ_{max} is higher for both the Nb_2O_5 and MoO_3 composites than for the base glass composite, with the MoO_3 composite exhibiting the highest value of τ_{max}. This implies that interfacial reactions which have occurred in the Nb_2O_5 and MoO_3 composites during processing have altered the nature of the fiber-matrix interface in such a way as to increase the fiber-matrix interfacial strength. The higher value of τ_{max} for the MoO_3 composite suggests that the degree of reactivity at the interface was higher than it was for the Nb_2O_5 composite. The increase in τ_{max} in the Nb_2O_5 composite is the first real evidence of an interfacial reaction in this composite, confirming the thermodynamic prediction discussed previously. Even though microstructural porosity had suggested gas evolution due to interfacial reaction (Figure VI-2), examination of fiber surfaces and EM analysis had failed to positively indicate that any reaction had actually taken place.

Correlation of the observed increases in τ_{max} with composite toughness and interlaminar shear strength has not yet been thoroughly completed. Measurements of interlaminar short beam shear strength (SBSS) were complicated by problems with the sample fixturing in the three-point flexure testing equipment. Previous work on similar composites indicated that SBSS increased with increasing values of τ_{max}, as expected [19]. Composite toughness will be evaluated in the next phase of the program using notched flexure testing techniques. A qualitative measure of the influence of τ_{max} on composite toughness was obtained by observing the degree of fiber pullout exhibited on composite fracture surfaces. Figure VI-7 shows that the degree of fiber pullout is relatively high for the base glass composite and decreases slightly in the Nb_2O_5 composite. In the MoO_3 composite, however, there is virtually no fiber pullout displayed, with the fracture mode being very brittle in nature. These observations are consistent with the increasingly stronger interfacial bond strengths obtained in the Nb_2O_5 and MoO_3 composites.

2. Composite Mechanical Behavior

The results of flexural testing and axial tensile testing are presented in Tables VI-2 and VI-3. Testing was conducted on composite samples that had been fabricated using the three different sets of processing conditions given previously in Table VI-1 in order to correlate interfacial reaction kinetics with mechanical behavior. The effect of temperature on the

44

kinetics was established by keeping the soak time constant at 20 minutes and varying the temperature from 1150°C to 1350°C. For the effect of interfacial reaction kinetics as a function of time, the soak time was varied from 5 minutes to 20 minutes for a soak temperature of 1350°C. Since fiber volume percent was found to vary significantly among the composites, a parameter designated as "effective fiber strength" was used to judge the effects of the different conditions. Effective fiber strength was obtained by dividing the UTS by the fiber volume fraction, which basicly attributes all of the composite strength to the fibers and allows for direct comparison of strength in composites containing different amounts of fiber. This procedure is valid since the tensile strength of the matrix is virtually insignificant compared to that of the fiber.

In general, effective fiber strength (EFS) was found to be significantly higher in the base and Nb_2O_5 composites pressed at 1350°C compared to those pressed at 1150°C (Table VI-2). This was especially surprising in the case of the base composite, since the matrix in the 1150°C composite appeared to be fully densified (Figure VI-2). Similar behavior was noted in an earlier section (Section V) which evaluated the effect of processing conditions on composite behavior. Again, no obvious explanation could be found to account for this reduction in strength at lower processing temperatures. One possibility is that it could somehow be related to the formation of α-cristobalite in the 1150°C composite. Figure VI-11 indicates that while α-cristobalite was obviously present in the 1150°C composites, it was not detected in the composites pressed at 1350°C. Table VI-2 also indicates that in all cases the effective fiber elastic modulus (E_{eff}), which was calculated using the rule of mixtures, was significantly lower than the reported as-received value of 380 GPa. For the composites pressed at 1350°C, E_{eff} ranged from ~300-315 GPa, which is consistent with previous work at UTRC on HMU reinforced borosilicate glass matrix composites [19]. The composites pressed at 1150°C exhibited somewhat lower values of E_{eff}, especially in the case of the MoO_3 composite. This behavior is similar to the trend displayed by EFS, as discussed previously. The noticeably lower value of E_{eff} in the MoO_3 composite pressed at 1150°C is an indication that degradation of the fiber structure is more severe at 1150°C than at 1350°C. This behavior can be at least partially attributed to the thermodynamic stability of MoO_3 at temperatures above 1150°C. Since MoO_3 sublimes at ~1155°C (under standard atmospheric conditions), it is possible that hot-pressing temperatures above 1150°C could allow some MoO_3 to escape from the system before reacting with the carbon fiber to form Mo_2C.

Representative axial stress-strain curves for the composites pressed at 1350°C are shown in Figures VI-8 through VI-10. These curves were selected based on the fact that the composites pressed at 1350°C exhibited strength and stiffness characteristics superior to those fabricated at 1150°C, as discussed previously. The stress-strain curves indicate that all three composites possess similar initial elastic modulus behavior. Since the fiber-matrix interfacial debond strength varies significantly among the three composites (assuming that the trend in τ_{max} in the 1350°C composites is similar to that in the 1150°C composites), this similarity in initial elastic modulus suggests the existence of a critical value of τ_{max} above which the interfacial bond strength does not further affect composite stiffness. The stress-strain curves also make it clear that the MoO_3 composites vary drastically from the base and Nb_2O_5 composites in terms of ultimate tensile strength (UTS) and toughness characteristics. The MoO_3 composite represented in Figure VI-10 demonstrated brittle failure and a very low tensile strength, in direct contrast with the base and Nb_2O_5 composites which both exhibited a proportional limit corresponding to the

onset of matrix microcracking followed by fiber-matrix debonding and a secondary linear region representative of load carried by the fibers alone. The "knee" in the curve separating the two linear regions is typical of unidirectionally reinforced glass matrix composites and corresponds to the large and sudden increase in transverse strain which occurs when fiber tows "broom out" after microcracking of the matrix [19, 26]. This extreme difference in behavior was observed for both tensile and flexural testing and was independent of the processing conditions (refer to Tables VI-2 and VI-3). The lack of a proportional limit in the MoO_3 composite is the result of cracks which begin either in the matrix or in the fiber-matrix interfacial layer (Mo_2C) and then propagate directly through the fibers due to the strong fiber-matrix interfacial bond, resulting in brittle failure of the composite.

In evaluating the effect of temperature on the interfacial reaction kinetics, it was observed that while the base and Nb_2O_5 composites possessed virtually the same EFS after processing at 1150°C for 20 minutes, the EFS of the Nb_2O_5 composite (1502 MPa) was significantly less than that of the base composite (1964 MPa) after processing at the higher temperature of 1350°C for 20 minutes. The EFS of the MoO_3 composite was essentially the same at both temperatures. These results suggest that two very different rate-limiting mechanisms exist in the Nb_2O_5 and MoO_3 composites. The interfacial reaction in the Nb_2O_5 composite appears to be rate-limited by the diffusion of Nb through the glass matrix to the interface. The diffusion of Nb was more rapid at 1350°C than at 1150°C, allowing more Nb to migrate to the interface and react with the C fiber during the 20 minute soak time. The degradation of EFS in the MoO_3 composite, on the other hand, was probably limited only by the rate of reaction between Mo and the C fiber. In other words, the mobility of Mo in the glass is so high that there was always a high concentration at the fiber-matrix interface. The extent of the reaction was limited only by the amount of Mo in the glass and the duration of the reaction. The fact that the EFS in the MoO_3 composites were the same at both temperatures after 20 minutes implies that the reaction had essentially gone to completion in both cases. Based on these descriptions of the reactions, the rate of the interfacial reaction in the Nb_2O_5 composite can be said to be "diffusion controlled", while that in the MoO_3 composite can be described as "interface controlled".

These proposed mechanisms are supported by the results of the second part of the kinetic study, where the soak time was varied while keeping the temperature constant at 1350°C. The EFS of both the Nb_2O_5 composite and the MoO_3 composite was found to to be higher after a 5 minute soak period than after a longer 20 minute hold. In the Nb_2O_5 composite, this was due to a shorter amount of time for Nb to diffuse to the interface, resulting in a lower Nb concentration which limited the extent of the fiber-matrix interfacial reaction. For the MoO_3 composite, the higher EFS corresponding to the shorter soak period was simply the result of less time for the interfacial reaction to take place. The rapid rate of the reaction in the MoO_3 composite was apparent from observing the 70% reduction in EFS (compared to the base glass composite) after only 5 minutes at 1350°C.

3. Thermal Expansion Behavior

The effect of fiber-matrix interfacial reactions on coefficient of thermal expansion (CTE) behavior of the composites processed at 1150°C for 20 minutes is shown in Figure VI-12. Axial

CTE behavior corresponds to thermal expansion in the fiber direction, while transverse CTE refers to expansion in a direction normal to the fibers. Figure VI-12(a) shows that transverse CTE behavior was virtually identical for all three composites, exhibiting no dependence on fiber-matrix interfacial reactions. Axial CTE behavior, however, did demonstrate a relationship to interfacial reactions, as seen in Figure VI-12(b). The low temperature portion of the curve for the MoO_3 composite was essentially flat from room temperature to 100°C, followed by positive expansion to 500°C. The other two composites, on the other hand, possessed identical curves which exhibited pronounced negative expansion up to ~150°C followed by positive expansion to 500°C.

This difference in low temperature CTE behavior can be accounted for by differences in the degree of reactivity exhibited by the composites. The contribution of the fibers and the matrix to composite thermal expansion depends strongly on the product of CTE and elastic modulus (αE) of each component. The negative CTE of the fibers in the low temperature regime coupled with the high elastic modulus of the fibers combine for a highly negative fiber αE which dominates the composite CTE behavior at temperatures up to ~150°C. This accounts for the negative CTE of the base and Nb_2O_5 composites in this temperature range, since the fibers in these composites possess high strength and stiffness (Table VI-2). The fibers in the MoO_3 composite, however, were strongly degraded as a result of interfacial reaction, exhibiting lower modulus and strength than fibers in the other composites. The CTE of the fibers may not even be as negative due to the degradation. These factors combined to produce a less negative αE contribution for fibers in the MoO_3 composite in the low temperature region, resulting in a less negative composite CTE.

Table VI-1

**Matrix Compositions and Hot-Pressing Parameters Used to Fabricate Composites
for Fiber-Matrix Interfacial Study**

Composition in Mole %

Oxide	PS 1 (Base)	PS 2 (Nb_2O_5)	PS 3 (MoO_3)
SiO_2	83.7	83.3	83.2
B_2O_3	12.3	12.4	12.4
Na_2O	4.0	4.0	4.0
Nb_2O_5	-	0.25	-
MoO_3	-	-	0.4

Nominal Hot-Pressing Parameters

Soak Temperature (°C)	Soak Time (mins)
1150	20
1350	20
1350	5

Table VI-2

Mechanical Property Data for HMU Composites Containing Matrix Additives

Hot-Press Temp (°C)	Soak Time (mins)	Matrix	Fiber Vol %	Average 3-Point Flexural Strength (MPa)	Average UTS (MPa)	Effective Fiber Strength (MPa)	Average Elastic Modulus (GPa)	Effective Fiber Elastic Modulus (GPa)
1150	20	Base	55	1397	699	1275	185	285
		Nb_2O_5	45	1279	575	1268	169	296
		MoO_3	44	196	107	248	134	226
1350	20	Base	47	1452	923	1964	181	313
		Nb_2O_5	45	1004	679	1502	169	297
		MoO_3	50	342	114	227	187	311
1350	5	Base	46	1390	878	1895	176	308
		Nb_2O_5	45	1171	820	1833	168	298
		MoO_3	45	280	251	558	176	314

R87-917470-1

Table VI-3

Mechanical Property Data for HMU Composites Containing Matrix Additives

Hot-Press Temp. (°C)	Soak Time (mins)	Matrix	Fiber Vol. %	Average I_{max} (MPa)	Average Failure Strain (%)	Average Prop. Limit Stress (MPa)	Average Prop. Limit Strain (%)
1150	20	Base	55	16	0.585	451	0.249
		Nb_2O_5	45	27	0.722	265	0.169
		MoO_3	44	38	0.078	–*	–*
1350	20	Base	47	-	0.644	383	0.214
		Nb_2O_5	45	-	0.561	287	0.169
		MoO_3	50	-	0.063	–*	–*
1350	5	Base	46	-	0.571	377	0.214
		Nb_2O_5	45	-	0.636	328	0.196
		MoO_3	45	-	0.145	–*	–*

* Brittle failure

50
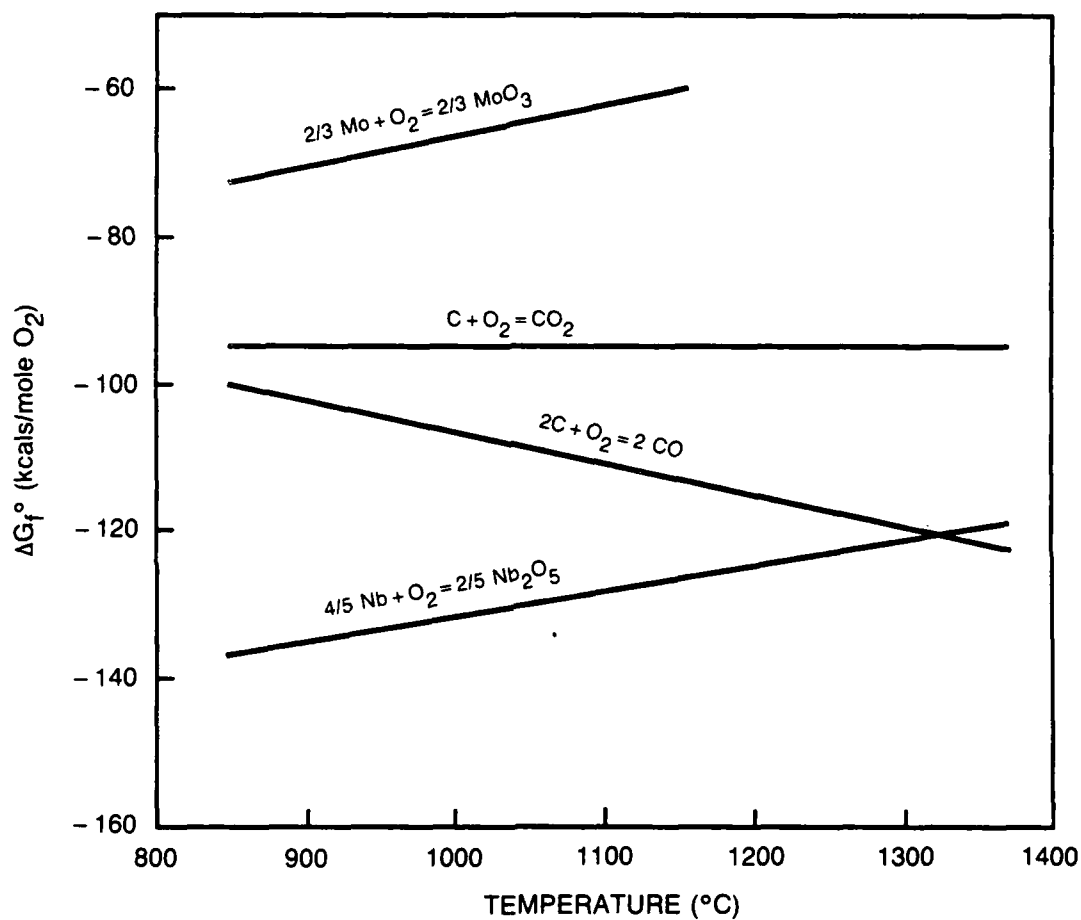
Fig. VI-1. Ellingham Diagram Representing the Relative Stability of Nb_2O_5 and MoO_3 in the Presence of Carbon

51
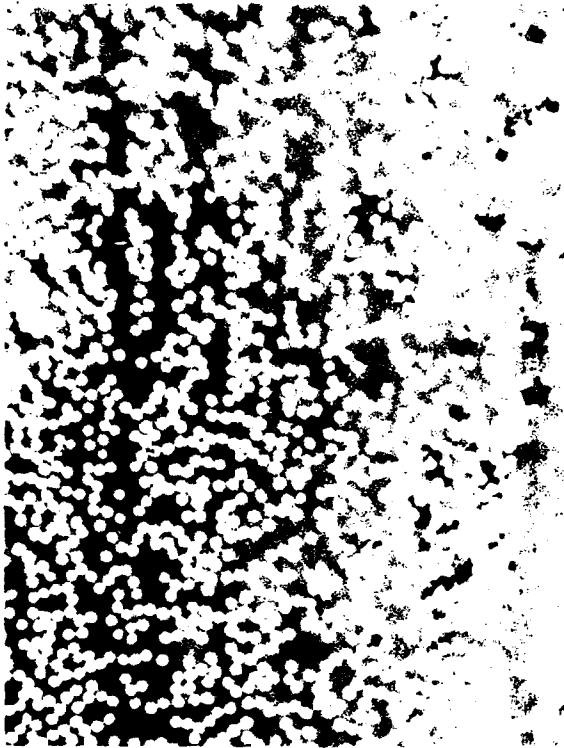
Nb₂O₅ COMPOSITE (45 v/o)
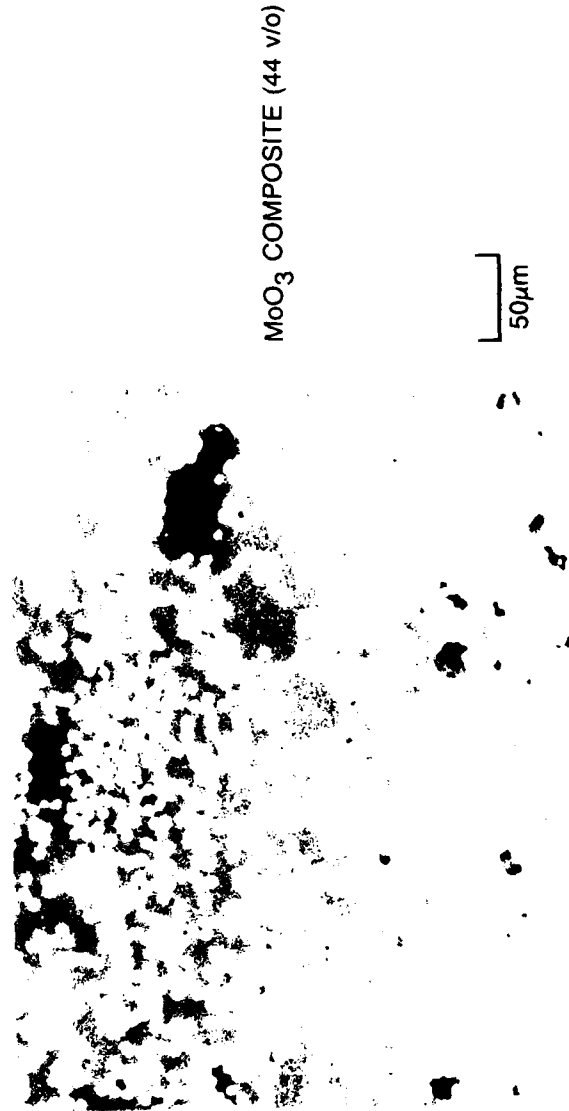
MoO₃ COMPOSITE (44 v/o)

BASE COMPOSITE (55 v/o)

Fig. VI-2. Microstructures of HMU Reinforced Composites Containing Matrix Additives

50μm

50μm

50μm

87 – 8 – 42 – 16

52

NB2O5 COMPOSITE (45 v/o)

BASE COMPOSITE (55 v/o)

MoO3 COMPOSITE (44 v/o)

5µm

5µm

Fig. VI-3. Fracture Surfaces of HMU Reinforced Composites Containing Matrix Additives Showing Reaction Layer on Fiber Surfaces

87 - 8 - 42 - 17

53
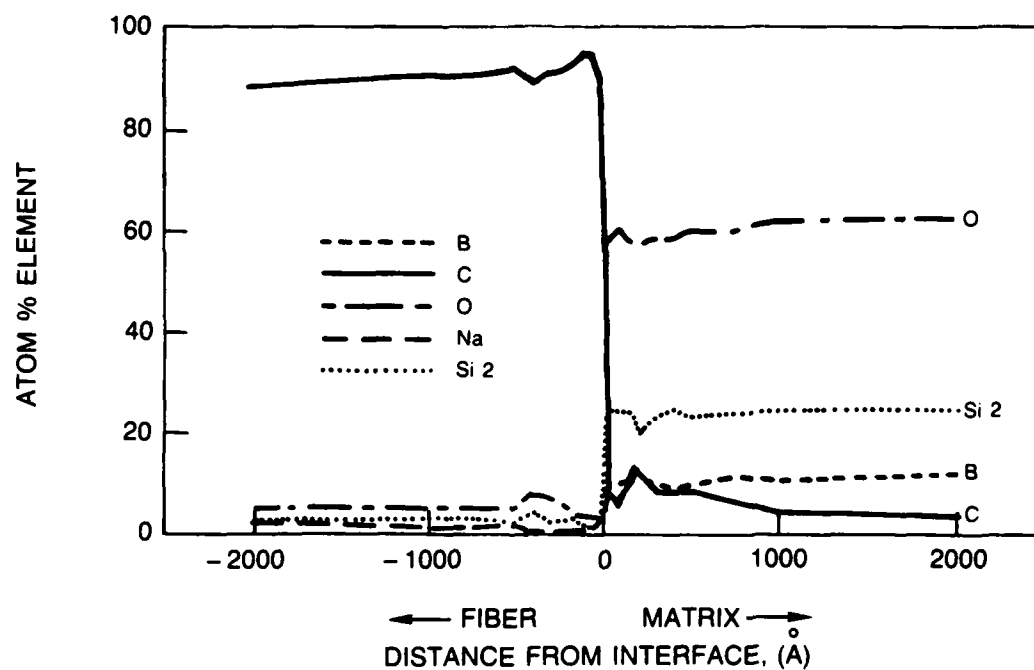
Fig. VI-4. Auger Profile for Base Composite Hot-Pressed at 1150°C

87 – 8 – 42 – 18

54
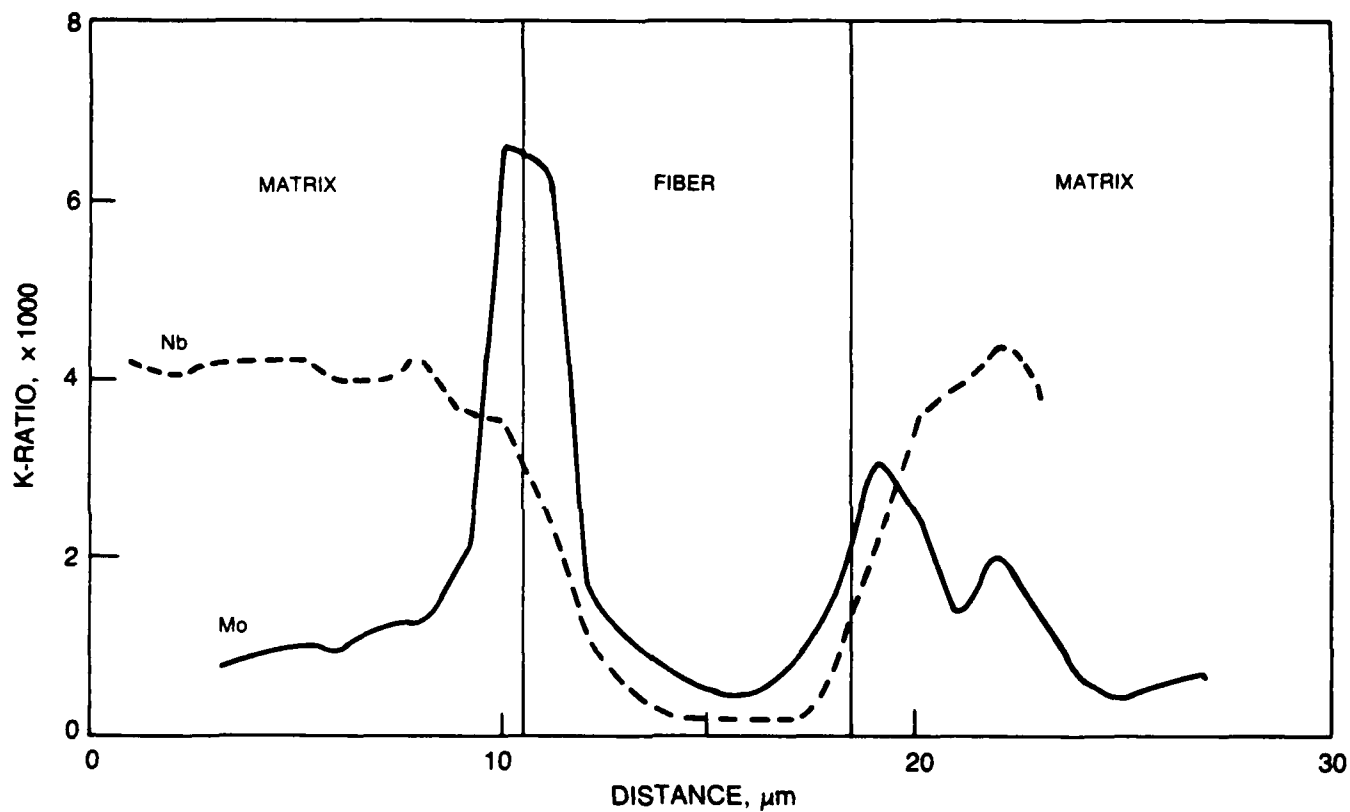
Fig. VI-5. Electron Microprobe Analysis of HMU Reinforced Composites Containing Nb_2O_5 and MoO_3
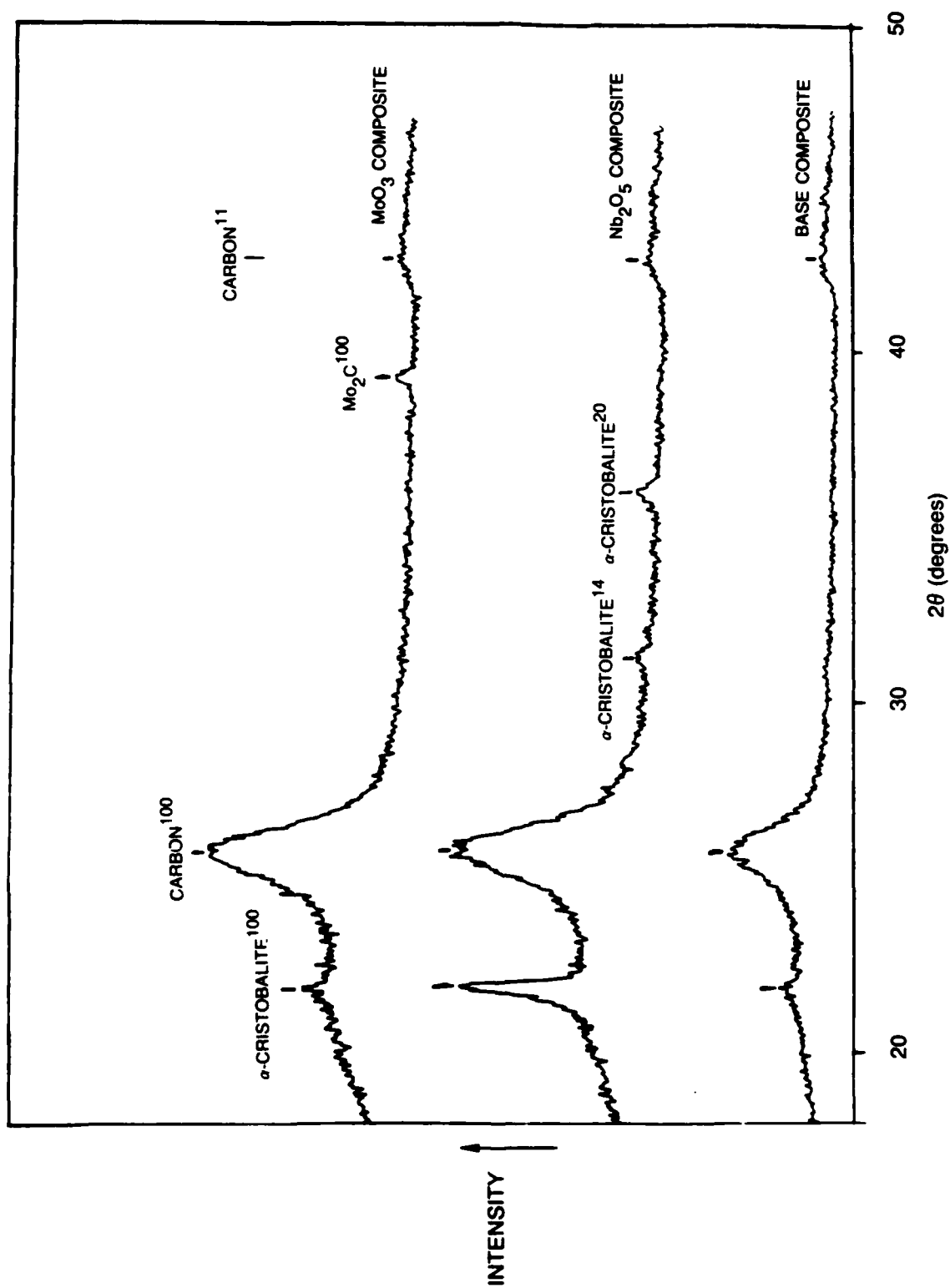
Fig. VI-6. X-ray Diffraction Traces of HMU Reinforced Composites with Matrix Additives Hot-Pressed at 1150°C for 20 min.

87 – 8 – 42 – 20

NbₒO₅ COMPOSITE (45 v/o)

MoO₃ COMPOSITE (44 v/o)

BASE COMPOSITE (55 v/o)

Fig. VI-7. Flexural Strength Fracture Surfaces of 0° HMU Reinforced Composites Containing Matrix Additives

87 – 8 – 42 – 21

57
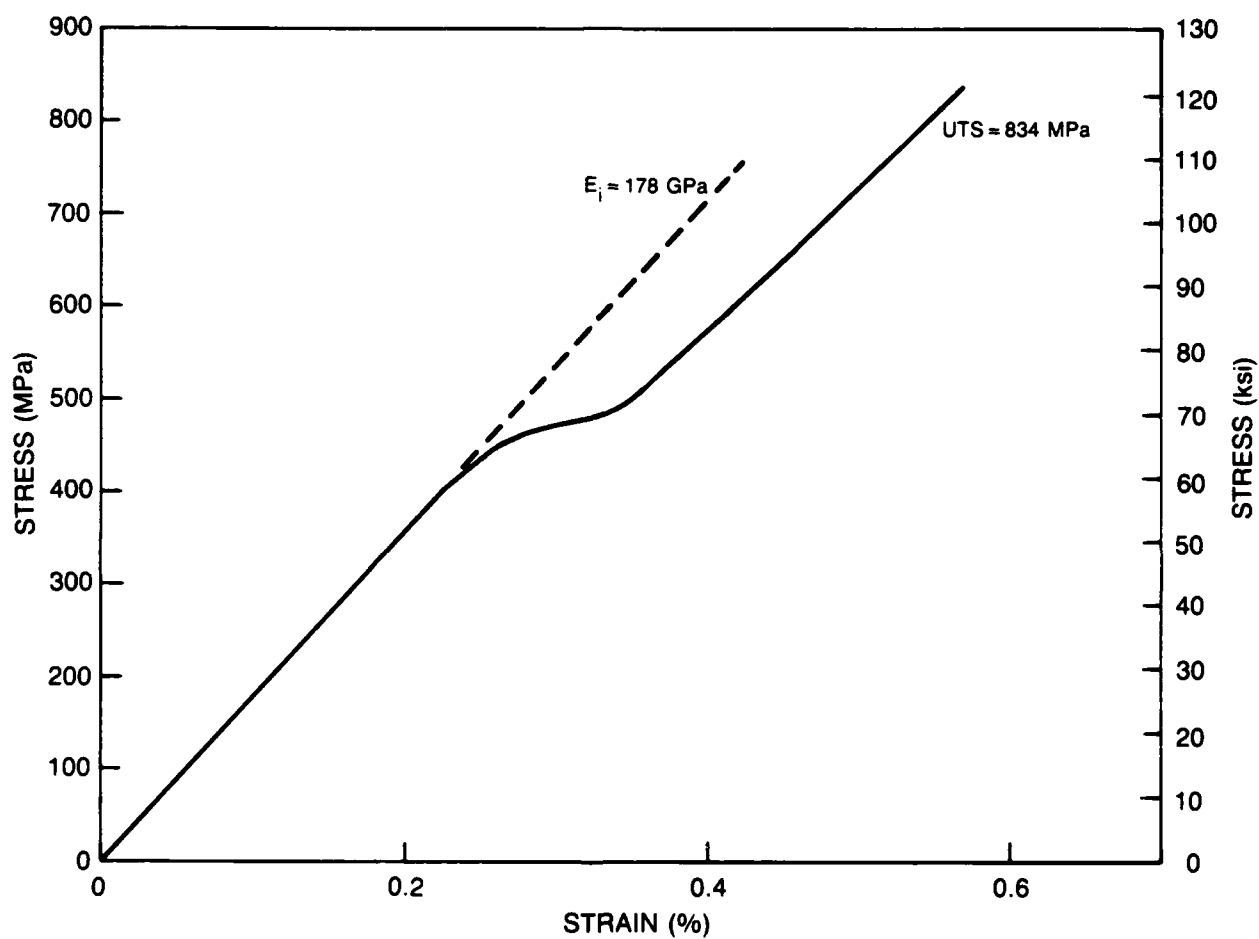
Fig. VI-8. Tensile Stress-Strain Curve for 0°-46 v/o Base Glass/HMU Composite

58
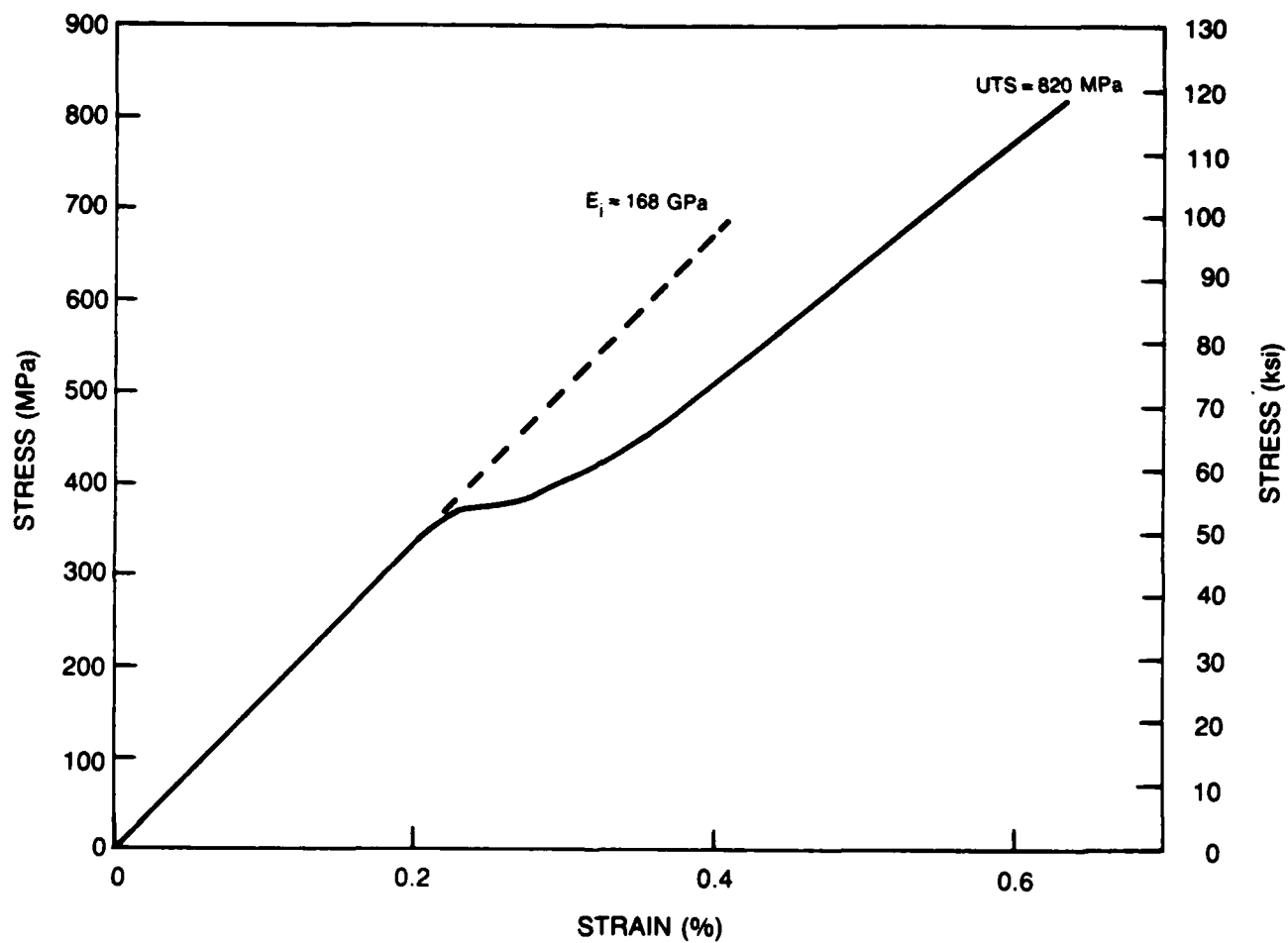
Fig. VI-9. Tensile Stress-Strain Curve for 0°-45 v/o Nb$_2$O$_5$ Glass/HMU Composite
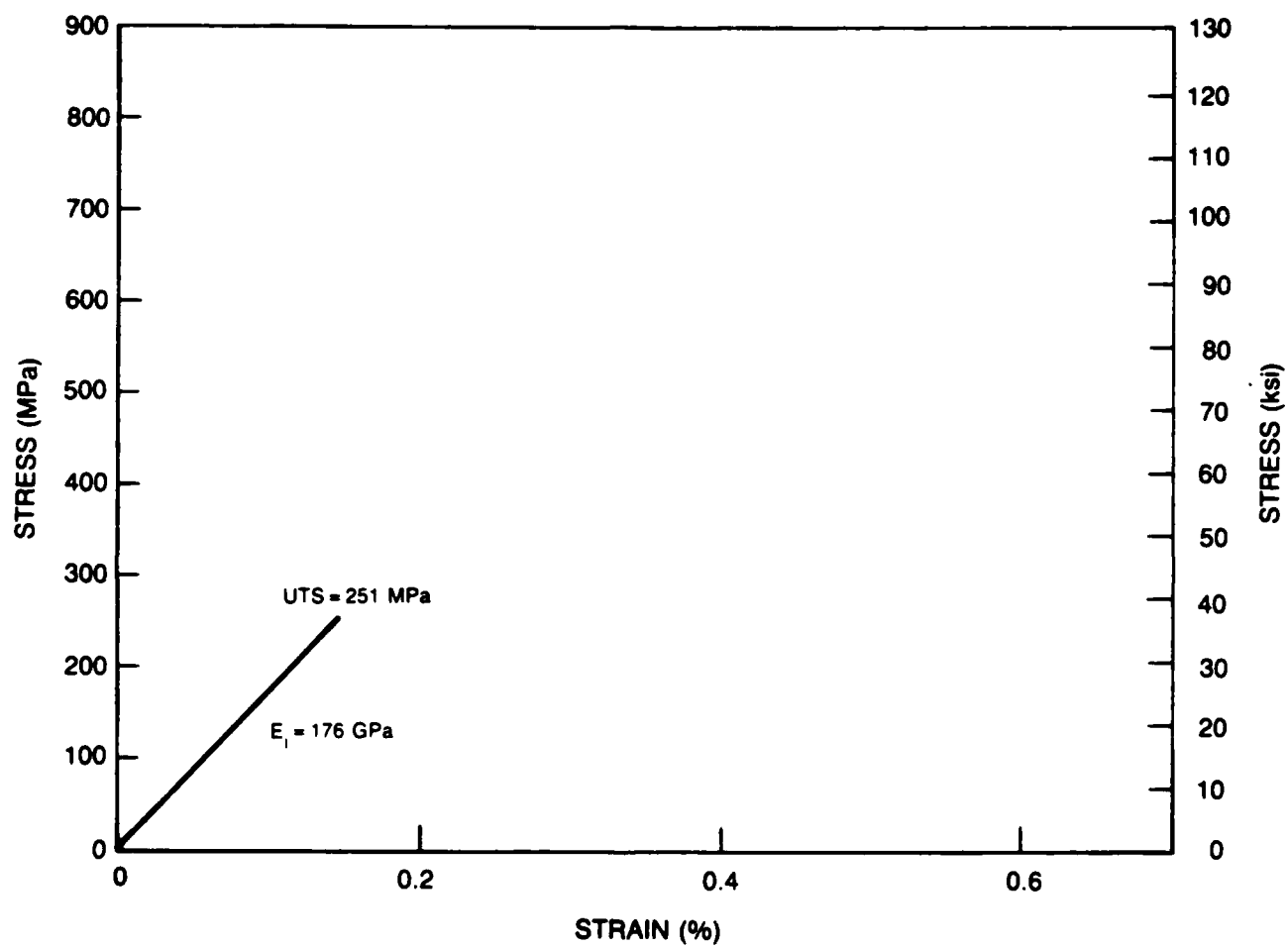
Fig. VI-10. Tensile Stress-Strain Curve for 0°-45 v/o MoO₃ Glass/HMU Composite
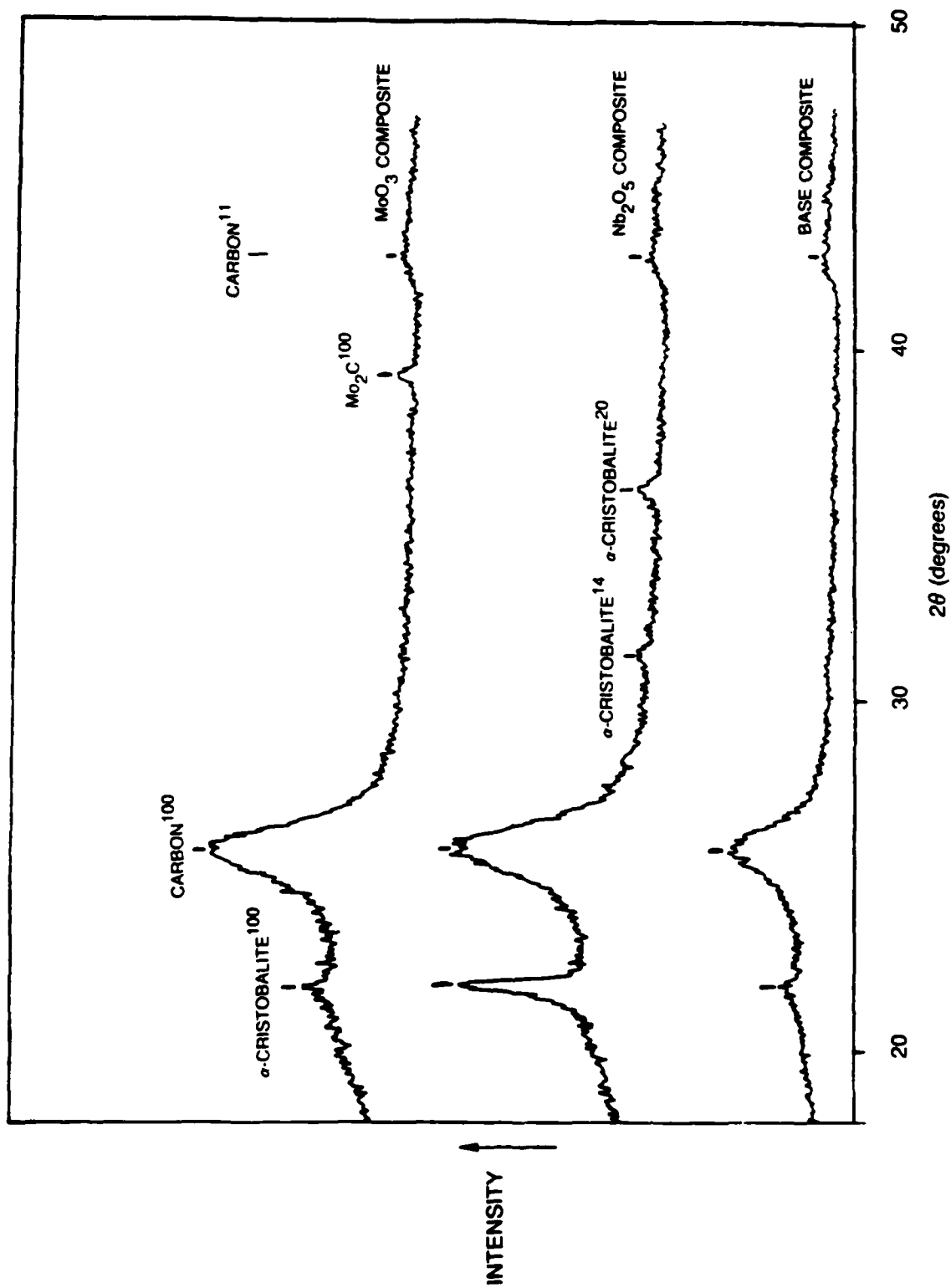
Fig. VI-11 (a). X-ray Diffraction Traces of 0° HMU Reinforced Composites with Matrix Additives Hot-Pressed at 1150°C for 20 min.

87 – 8 – 42 – 25
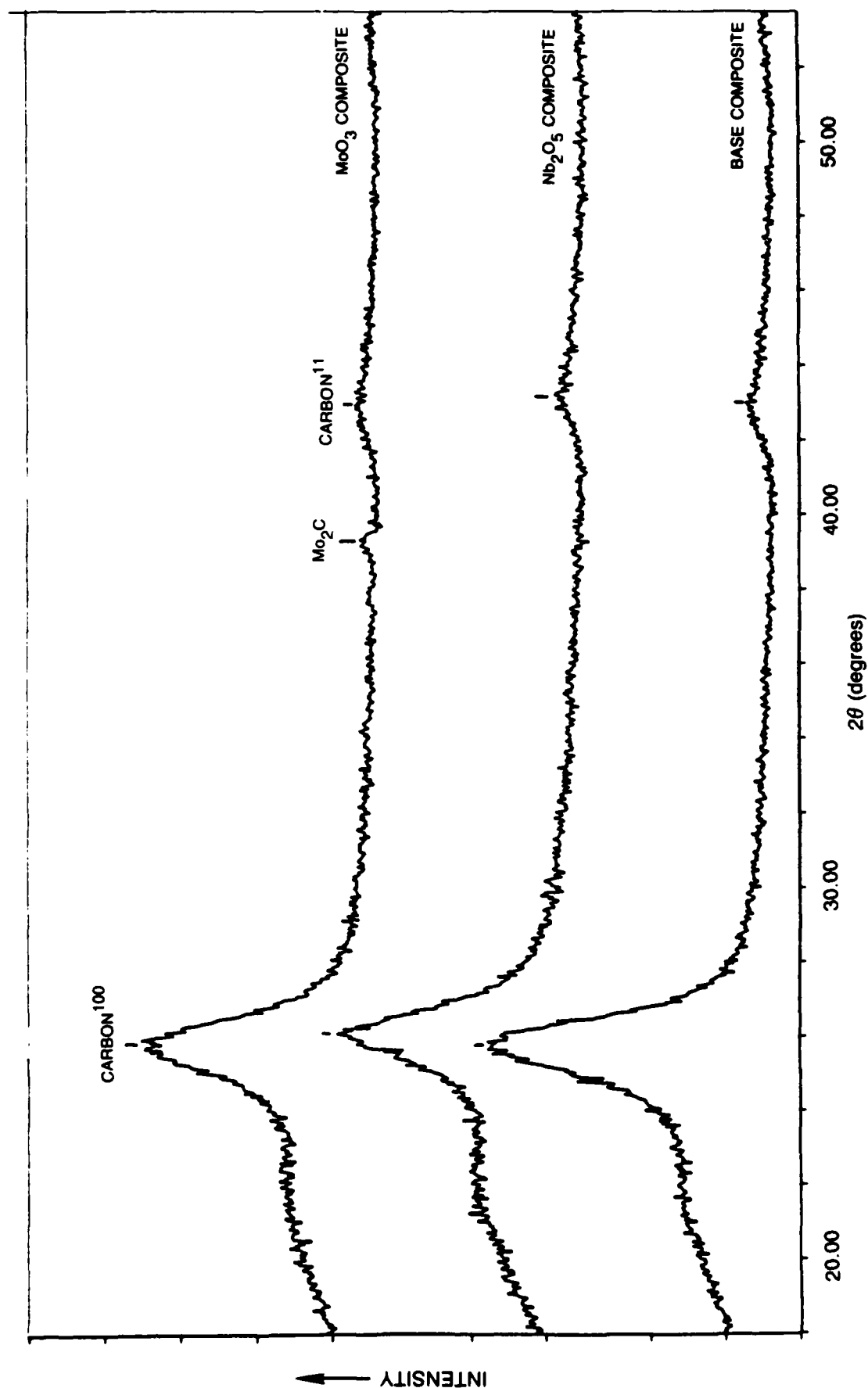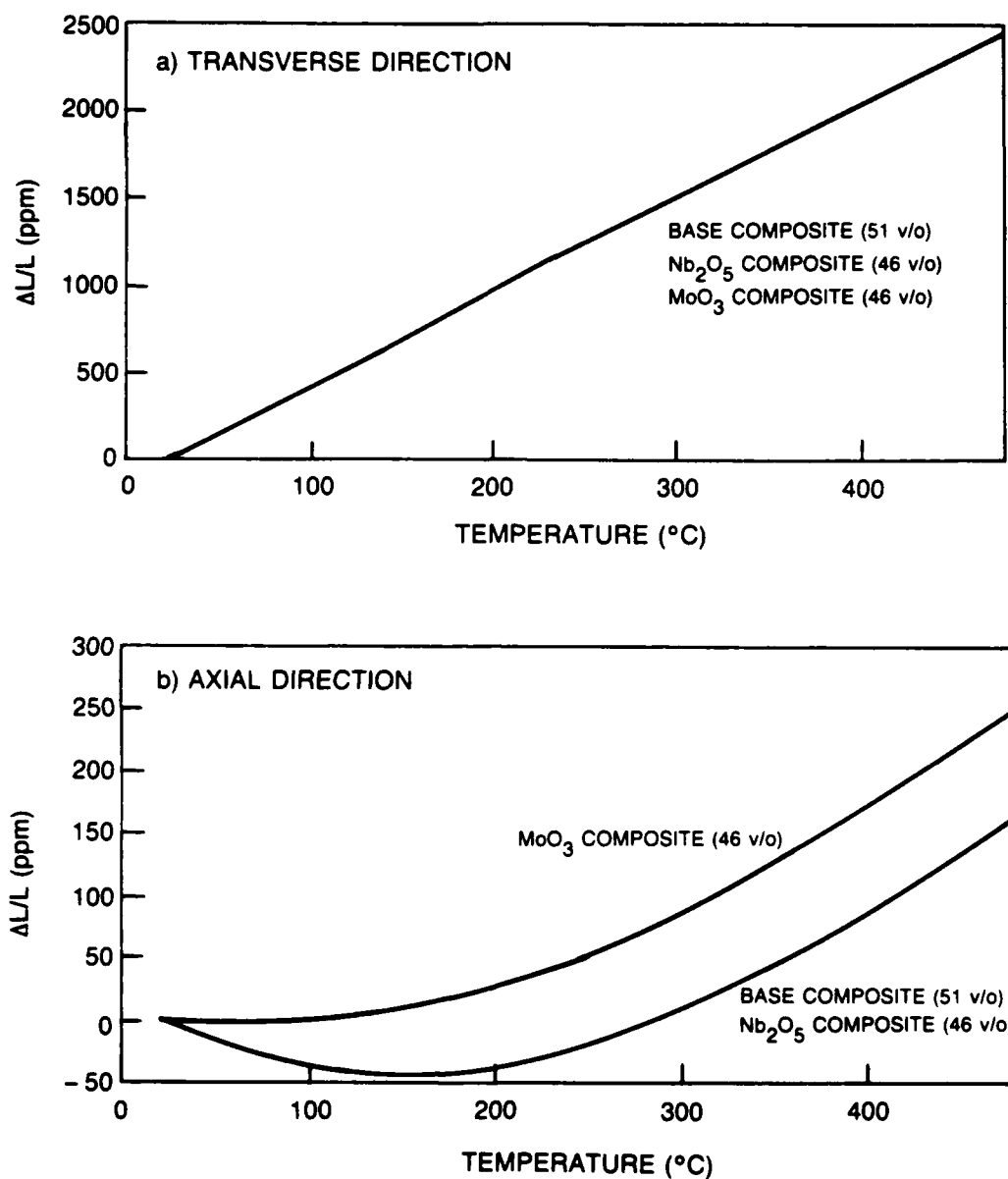
Fig. VI-11 (b). X-ray Diffraction Traces of 0° HMU Reinforced Composites with Matrix Additives Hot-Pressed at 1350°C for 5 min.

87 – 8 – 42 – 26
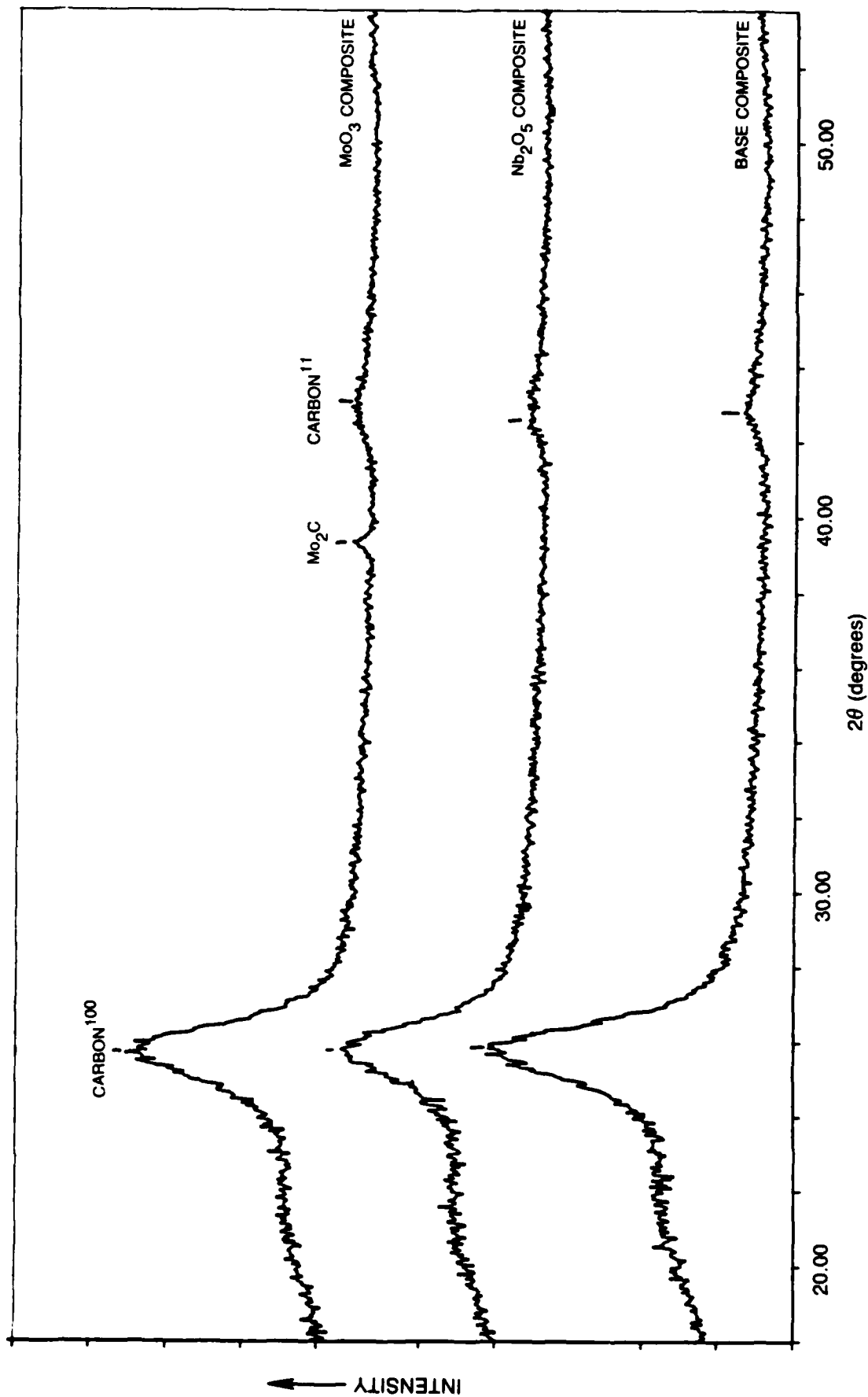
Fig. VI-11 (C). X-ray Diffraction Traces of 0° HMU Reinforced Composites with Matrix Additives Hot-Pressed at 1350°C for 20 min.

87 – 8 – 42 – 27

Fig. VI-12. ΔL/L vs Temperature for HMU Reinforced Composites with Matrix Additives: a) Transverse Direction; b) Axial Direction

64

Characterization of Interface Reactions in Carbon-Fiber
Reinforced Glass Matrix Composites

P.M. Benson, K.E. Spear, and C.G. Pantano

Department of Materials Science and Engineering
The Pennsylvania State University
University Park, PA 16802

Introduction

Several analysis techniques were used to characterize the fiber/matrix interfaces in carbon-fiber reinforced glass matrix composites. In all cases, the composites were fabricated with 30 to 50 volume percent carbon fibers, the glass matrix material was introduced in the form of frit, and the hot-pressing was carried out at approximately 1150°C. The variable introduced in the materials fabrication was the presence or absence of specific oxide dopants; namely Nb_2O_5 and MoO_3. These were added at the one weight percent level to the standard sodium-borosilicate composition. On the basis of current theory, any variations in the mechanical strength and toughness of these composites -where the matrix, fibers, and their relative concentrations have been fixed- would be attributed to changes in the strength at the fiber matrix interface due to dopants. The data presented in other sections of this report showed that the presence of these dopants influence the mechanical performance. In general, the MoO_3 had the biggest effect where excessive porosity and loss of strength and toughness were observed. The objective of this portion of the study was to identify any unique interfacial features associated with the presence of the oxide dopants.

Review of the Themochemistry

The details of thermodynamic calculations have already been reported (19). Primarily, they predict that contact between carbon fibers and silicate glass matrix materials will result in the formation of CO, CO_2, and SiO gases, and correspondingly, solid carbide or oxycarbide reaction products. The extent of this reaction is determined by a variety of factors, but the predominant one is transport of the oxygen-bearing reaction products away from the interface. Figure 1 describes two, perhaps, limiting cases. If a continuous 'interphase' of SiC forms (fig. 1a), and the external pressure is sufficient to maintain contact between the fiber and matrix, the reaction is limited by the diffusion of CO, CO_2, and/or SiO reaction products away from the reaction interface through the matrix and/or fibers and by the diffusion of C and/or SiO_2 through the SiC interphase. Equilibria is established between SiC and the glass matrix, and between SiC and the carbon fibers. The local equilibria at these interfaces can be examined by running the calculations with an excess of carbon (the SiC/fiber interface) or an excess of glass (the SiC/matrix interface). Of course, it is necessary to perform experimental studies to determine whether this model is correct, and which reaction step is rate limiting. Under these conditions, though, one would expect very adherent interfaces with high shear strength.

Alternatively, one can consider the situation where the external pressure is <u>not</u> sufficient to maintain contact between the fibers and the matrix (fig. 1b). In this case, the extent of the reaction will be dictated not only by the transport of oxygen bearing reaction products, but also by the gas phase transport of the reactant species across the gap. This situation is further complicated by the possible nucleation of bubbles due to high CO/CO_2 pressures, and/or by the intermittent bridging of glass or reaction products across the interface. In general though, one anticipates that the creation of solid 'interphase' reaction products would be greatly diminished here. In fact, the presence of carbonaceous and/or oxidizing volatiles in the composite preform may generate high CO and CO_2 pressures initially, and these would thereby preclude the formation of any carbide reaction products. Again, experimental analyses will be required to distinguish the correct model and rate controlling steps, but clearly, one would expect these interfaces to be much less adherent than those shown in figure 1a.

The calculations reveal that the generation of CO and CO_2 gas is fundamental to the carbon fiber/glass matrix interactions. The purpose of the oxide dopant additives is to modify -locally- the CO/CO_2 gas pressures. The reaction between silica and the carbon fibers can be limited by the introduction of variable valence oxides whose reduction to suboxides occurs in preference to the reduction of SiO_2 to SiC. Or oxides can be introduced whose reduction to carbides can occur at higher CO/CO_2 pressures than those required for SiC to form. It was predicted -again using the thermochemical calculations- that the presence of Nb_2O_5 or MoO_3 would generate CO/CO_2 gas pressures which are three orders of magnitude higher than the equilibrium partial pressure required for the reduction of SiO_2. Thus, the interactions between SiO_2 and C can be essentially eliminated. Moreover, the calculations revealed that NbC could form at CO pressures between .01 and .1 atm, and Mo_2C could form at CO pressure greater than .3 atm at processing temperatures (approximately 1150°C). Thus, the possible creation of interfacial carbide reaction products is greatly enhanced over the situation present with the standard borosilicate glass composition (where SiC formation requires $P_{CO} < 10^{-4}$ atm at approximately 1150°C).

Experimental Procedure

The glass matrices used in the composite fabrication were prepared by melting. Due to the small concentration of dopants, and the high viscosity of these borosilicate compositions, homogenization of the melts was a critical issue. The first set of composites (see UTRC) did show a dependence of mechanical properties upon the presence of various dopants, but there were indications that the matrix composition was not uniform throughout the composite. Thus, a new set of doped glasses were synthesized using a procedure which provided better composition homogeneity. The glasses were batched (Appendix 1), mixed, and melted in platinum crucibles at 1650°C for 24-32 hrs to insure fining and homogeneity. These glasses were then used to fabricate a second set of composites, and in addition, were used to carry-out selected sessile drop experiments. Pieces of the glass compositions were heat treated on vitreous carbon plates and analyzed ɪor contact angle, reboil, and

interfacial reactions using ion scattering spectroscopy. Appendix 2 shows selected properties of the glasses used to prepare the second set of composites along with the sessile drop experiments.

Results and Discussion

The sessile drop experiments revealed some important features associated with the carbon/glass interactions. First, the contact angles -at least macroscopically- were always greater than 90° and did not depend in any significant way on the dopant. Of more interest was the presence of a gas bubble which formed at the center of the interfacial region of each specimen (fig. 2a). This bubble is undoubtedly a response to the generation of CO and CO_2 gas at the interface, and clearly indicates the need for the application of external pressure in the manufacture of carbon/glass composites. Of course, contact was maintained between the glass and the carbon along the periphery of the drop and careful examination in the SEM revealed that (micro) wetting, some reaction and limited adhesion had occurred in this region.

The interfaces associated with the sessile drops were analyzed with ion scattering spectroscopy (ISS). These analyses were qualitative at best, but did provide some useful insight. In most cases, the interfaces contained larger quantities of sodium than would be expected on the basis of the bulk compositions. This reveals that Na_2O may be active in the interface reaction even though the thermochemical calculations indicated that condensed Na_2O is more stable in the presence of carbon than SiO_2 or B_2O_3. It is possible that Na_2O vaporizes at the interface due to its high vapor pressure at 1250°C, indicated by high vapor pressures of $Na(g)$ according to thermochemical calculations. This suggests that the vaporization processes may be important to the modeling of the interface chemistry in these composites, and points to the possible validity of the model in figure 1b. The ISS analyses also showed that the dopants - Nb and Mo - were present at higher concentrations in the interface than would be expected on the basis of their 1 wt% level in the matrix. These species may segregate there because the oxides Nb_2O_5 and MoO_3 have high thermal segregation coefficients or, alternatively, because they are being consumed in the reaction with the carbon. It is not possible to determine the chemical state of these cations (NbC, Mo_2C vs. NbO_x, MoO_x) using ISS.

More extensive characterization of interfaces was carried out using the fiber reinforced composites. The SEM examination of interlaminar fracture surfaces revealed that debonding of the fiber/matrix interfaces and fiber pull-out were most prevalent (fig. 3a). Nevertheless, regions where glass particles were adherent to one or more fibers could be found. And, there were regions of the debonded interfaces and fiber pull-outs -at least on the Nb and Mo doped composites- where fine particulates or voids could be observed (fig. 3b and c). Clearly, the complimentary use of scanning electron microscopy, scanning Auger microscopy (SAM), and transmission electron microscopy (TEM) are required to effectively characterize these interfaces.

The chemical nature of the interfaces was investigated using Auger microanalysis of the fiber pull-outs and matrix troughs. Due to the ubiquitous presence of carbon, it was necessary to reference the levels of carbon to a control. This was accomplished in each analysis by examining regions of the composite where fracture occurred through the glass matrix. In most cases, there was little or no carbon on these 'bulk' glass fracture surfaces. This indicates that the adsorption of carbon is not prevalent on these fracture surfaces, and that any substantial levels of carbon found in the matrix troughs could be attributed to interactions between the carbon fiber and the glass matrix in the processing of the composite. A similar set of 'control' analyses were used to verify the levels of oxygen on the carbon fiber surfaces. The fiber fracture surfaces, and many as-received fiber surfaces were found to be almost pure carbon; little or no oxide contamination was found.

Figure 4 shows a comparison of Auger spectra for the base glass composite. There is no question that carbon is present in the troughs at a level which is above the background. All of the troughs examined in this composite showed carbon and exposed glass in the troughs (although at various ratios) and no oxide on the carbon fibers. In many cases, these troughs appeared to be enriched in boron. The composites with the MoO_3-doped matrix, on the other hand, exhibited an almost pure carbon surface in the trough. In fact, the Auger spectra for the carbon fiber pull-outs and troughs were almost identical. Figure 5 shows this comparison, where it can also be seen that traces of silicon and oxygen were present on these surfaces. The corresponding SEM micrographs in figure 6 show that the troughs and fibers in the 'base' glass matrix composite are featureless (fig. 6a), whereas in the MoO_3-doped glass matrix, a particulate phase is observed (fig. 6b). On the basis of the Auger analyses, one concludes that these particles are carbon, with trace levels of silica or silicon carbide also present.

The troughs in the Nb_2O_5-doped glass matrix composites were also carbon enriched, but not to the degree observed in the MoO_3-doped materials. In many cases, the glass matrix was exposed, and usually, a weak signal associated with niobium could be identified. Although the fiber pull-outs in these composites also showed particulates on the surfaces (fig. 3c), the Auger analyses showed these fiber surfaces to be pure carbon. The troughs did not show particulates, but rather small voids (fig. 3d). These observations further suggest that the interphase particulates are carbon.

Whereas the SEM and Auger analyses provide an excellent characterization of debonded interfaces, they provide little insight to the nature of adherent interfaces - for example, the regions responsible for adhesion of the glass particles (figure 3b) and carbon particles in the troughs (fig. 3c). Here, it is necessary to examine the adherent interfaces in cross-section. Initially, polished sections were prepared. These were etched in a variety of ways (including chemical and plasma etching) to reveal the presence of interface reaction products and morphology. The only notable features were radial cracks emanating from the interfaces. Any interphases, if present, were below the resolution of the SEM. The transmission electron microscope (TEM), on the other hand,

had sufficient resolution to reveal the presence of microcrystallites (fig. 7). The presence of microcrystallites were most obvious in the MoO_3-doped glass matrix composites. The TEM micrographs in figure 7a show that these microcrystals form in the glass matrix as well as near the interface. Using the previous x-ray diffraction data, energy dispersive spectroscopy, and crystallography, it is believed that the microcrystallites are indeed Mo_2C as predicted by the thermochemical calculations. The Nb-doped composite on the other hand revealed less-localized microcrystals which were also much smaller than those in the Mo-doped sample. Lastly, figure 7c shows a 'clean' yet intimate interface for the standard sodium borosilicate matrix.

Summary

It is a well accepted fact that debonding and fiber pull-out are intrinsic features of the fracture process in these carbon reinforced glass composites. The studies described here revealed that in the absence of variable valence dopants, the debonded surfaces are generally consistent with the model in figure 1b. The fact that carbon is found above the background levels in the trough, suggests that CO or CO_2 transport may occur across the gap and through the glass matrix. The situation, in the absence of dopants, can be represented schematically as in figure 8a. The 'excess' Na_2O observed at these interfaces may be associated with a carbonate. The doped matrix composites show much higher levels of carbon in the trough, and in the case of the MoO_3-doped composite, the trough was almost pure carbon. These surfaces also exhibit a particulate morphology. If the particles are simply carbon microcrystallites 'pulled-out' of the carbon fiber surface, they are quite adherent to the matrix in the trough. This may be due to carbide or oxycarbide formation in the glass matrix near the interface; in the case of the MoO_3-doped composite, this was in fact observed in the TEM. And in the case of the Nb_2O_5-doped composite, crystals were observed in the matrix, although they were not localized at the interface. The schematic in figure 8b describes the situation, at least qualitatively, in these doped composites. It suggests that the weaker, more embrittled, nature of the doped composites were due to a complex interaction zone at the interface. There is a sense of mechanical interlocking due to the particulate morphology which impedes debonding and shear along the glass surface. It is suggested that these interfaces lead to cohesive failure -within the carbon fiber surface- during fracture of the composite. It remains to be shown whether cohesive failure of the carbon, rather than shear failure of the interface in figure 8a, can explain the overall mechanical properties of the composite.

Appendix I

Batch calculations for 'base', MoO_3 doped, and Nb_2O_5 doped glasses.

500 g base 82% SiO_2 14%B_2O_3 4% Na_2O by weight

 410 g SiO_2 from 'Minusil'

 70 g B_2O_3 $\dfrac{\text{mole } B_2O_3 \cdot 2 \text{ moles } H_3BO_3 \cdot 62 \text{ g } H_3BO_3}{70 \text{ g } B_2O_3 \text{ mole } B_2O_3 \qquad \text{mole } H_3BO_3}$
  = 70 · 1.77 = 123.9 g H_3BO_3

 20 g Na_2O $\dfrac{\text{mole } Na_2O \cdot \text{mole } Na_2CO_3 \cdot 106 \text{ g } Na_2CO_3}{62 \text{ g } Na_2O \text{ mole } Na_2O \qquad \text{mole } Na_2CO_3}$
  = 20 · 1.71 = 34.2 g Na_2CO_3

Base plus 1 wt% MoO_3

 5 g MoO_3 $\dfrac{\text{mole } MoO_3 \cdot \text{mole } NaMoO_4 \cdot 2H_2O \cdot 219 \text{ g } NaMoO_4 \cdot 2H_2O}{144 \text{ g } MoO_3 \text{ mole } MoO_3 \qquad \text{mole } NaMoO_4 \cdot 2H_2O}$
  = 5 · 1.52 = 7.60 g mole $NaMoO_4 \cdot 2H_2O$
  less Na_2O from Na_2CO_3

Base plus 1 wt% Nb_2O_5

 5 g Nb_2O_5 $\dfrac{\text{mole } Nb_2O_5 \cdot 2 \text{ moles } NaNbO_2 \cdot 148 \text{ g } NaNbO_2}{234 \text{ g } Nb_2O_5 \quad \text{mole } Nb_2O_5 \quad \text{mole } NaNbO_2}$
  = 5 · 1.27 = 6.32 g $NaNbO_2$
  less Na_2O from Na_2CO_3

Appendix II

 Density calculations were performed using the Archimedes principle. Each measurement was made at least three separate times, and their averages were used to calculate the densities listed in g/cc.

 Base................ 2.25
 Niobium doped....... 2.24
 Molybdenum doped.... 2.23

 Spectroscopic determination of the dopants to the base glass produced at PSU was performed with the following measured in weight percent:

 Niobium doped....... 0.92 wt% Nb_2O_5
 Molybdenum doped.... 0.82 wt% MoO_3

SILICATE GLASS MATRIX ⟋SiC

///CARBON FIBER / / / / /

(a)

SILICATE GLASS MATRIX

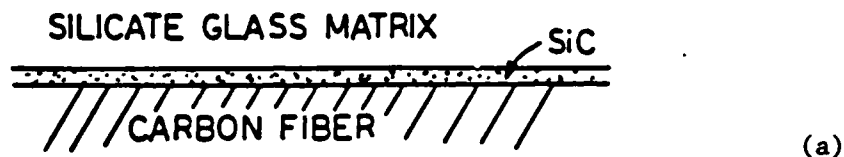⟩SiO   CO⟨

///CARBON FIBER ///////

(b)
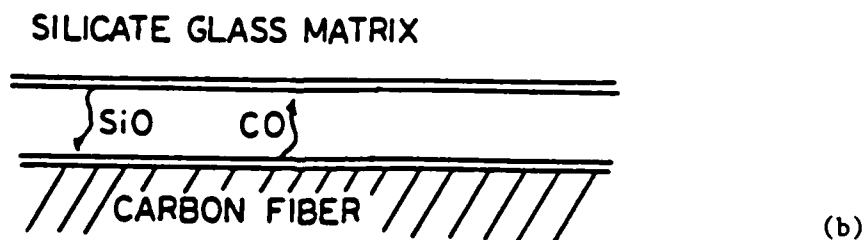
Figure 1.   Schematic diagrams of two possible interface morphologies.
In the upper schematic (a), contact is maintained between the
fiber and matrix; interphase formation is limited by solid-
state transport processes; the interphase may or may not be
continuous (as shown), but an adherent interface is expeccted.
In the lower schematic (b), the gas evolution prevents contact
between fiber and matrix; reactions are limited by gas phase
transport, vaporization and/or solid state transport; interphases
may or may not form on the separated surfaces, but nevertheless,
this situation results in poorly adherent interfaces.
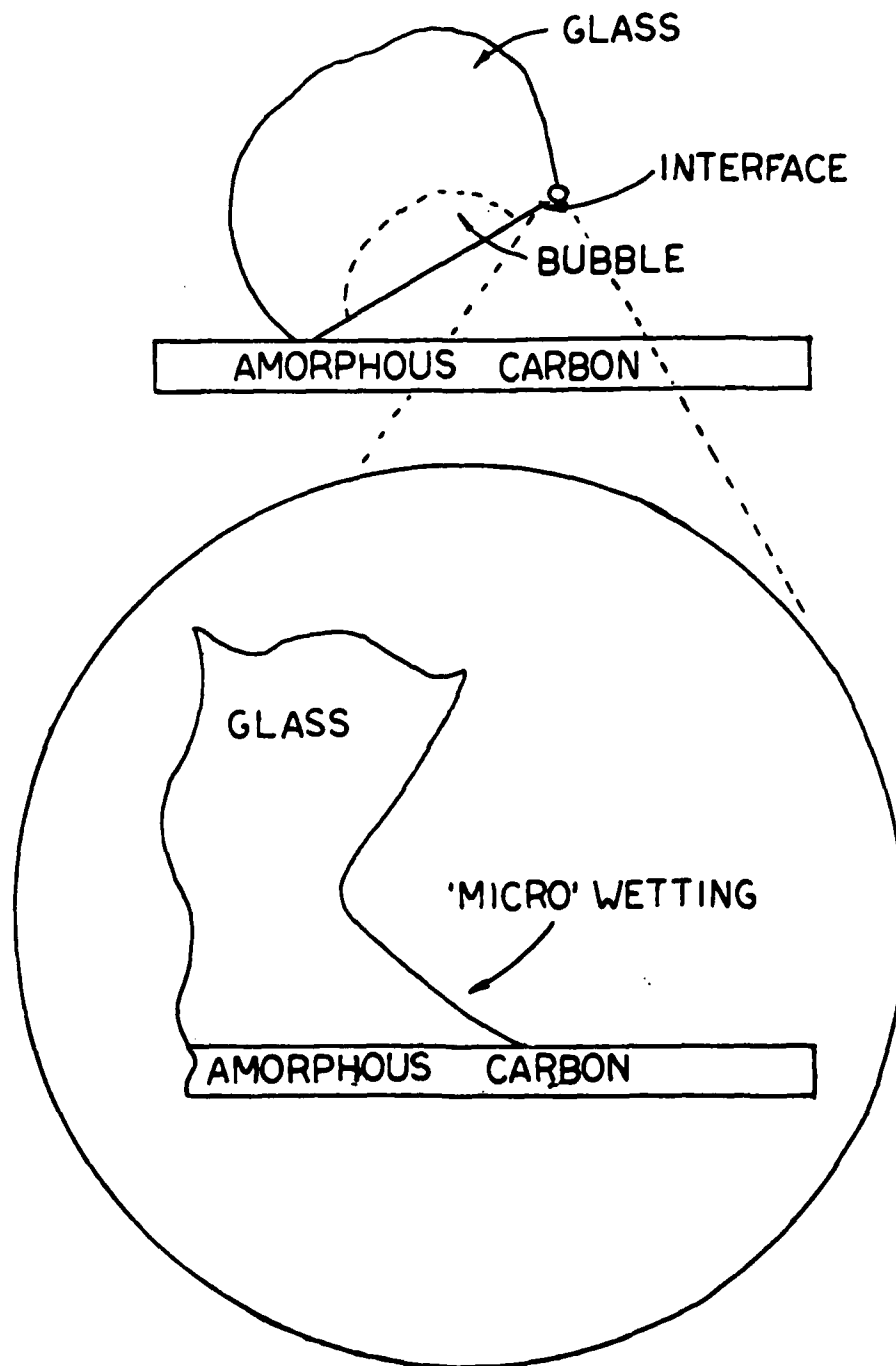
Figure 2. The upper diagram shows the appearance of sessile drops of the glass matrix on a carbon substrate after heating into the softening range. The enlargement (below) reveals that although the drop is macroscopically 'non-wetting', a reaction occurs where the two materials maintain contact, and this reaction alters the wetting behavior.
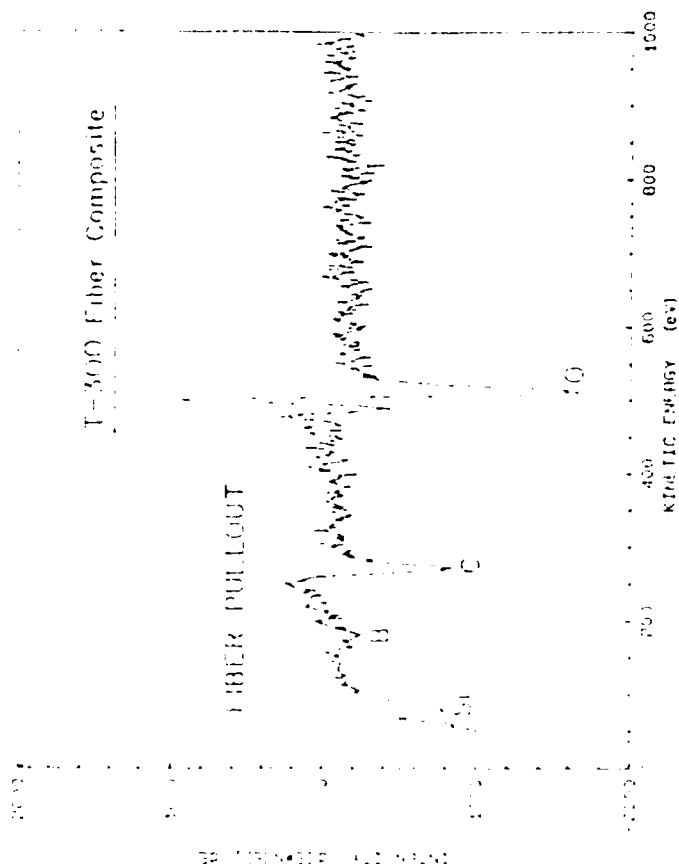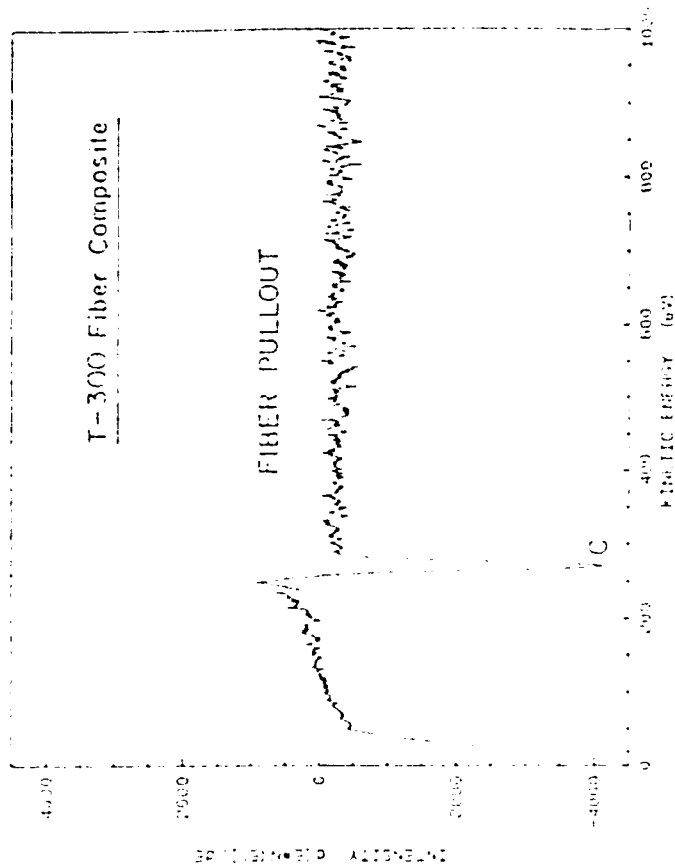
1 μm
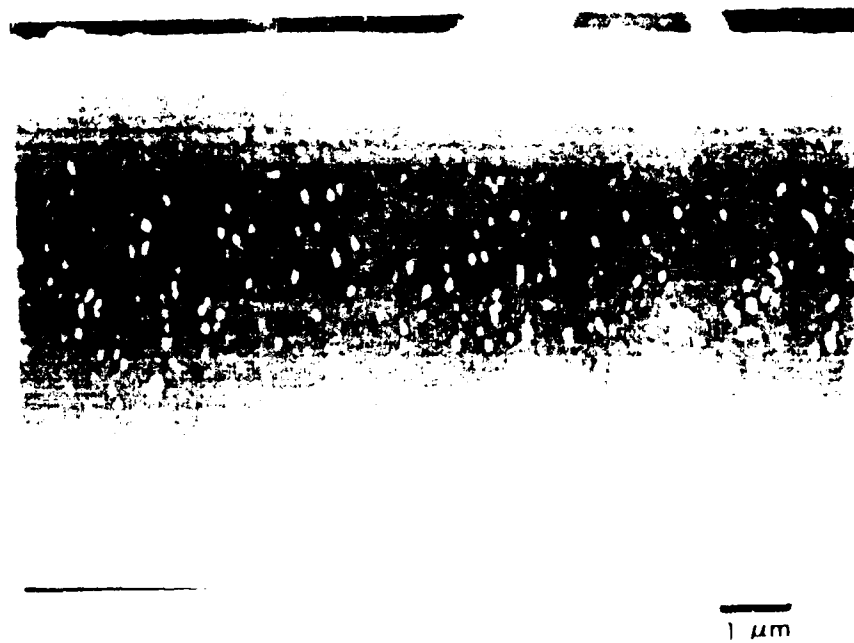
Figure 4. Fiber pullout from a Sb_2O_3-doped glass matrix composite.

1 μm
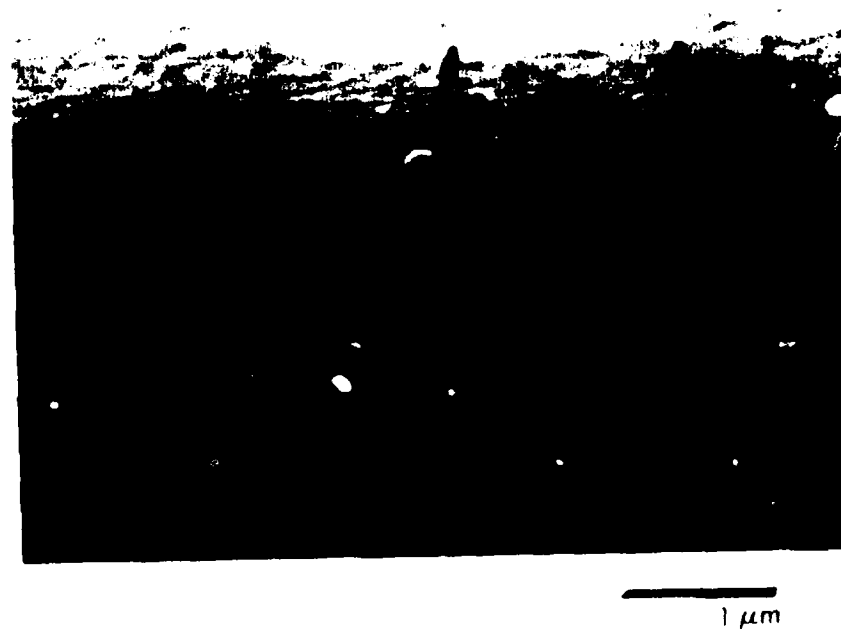
Figure 5. Matrix trough in a Sb_2O_3-doped glass matrix composite.
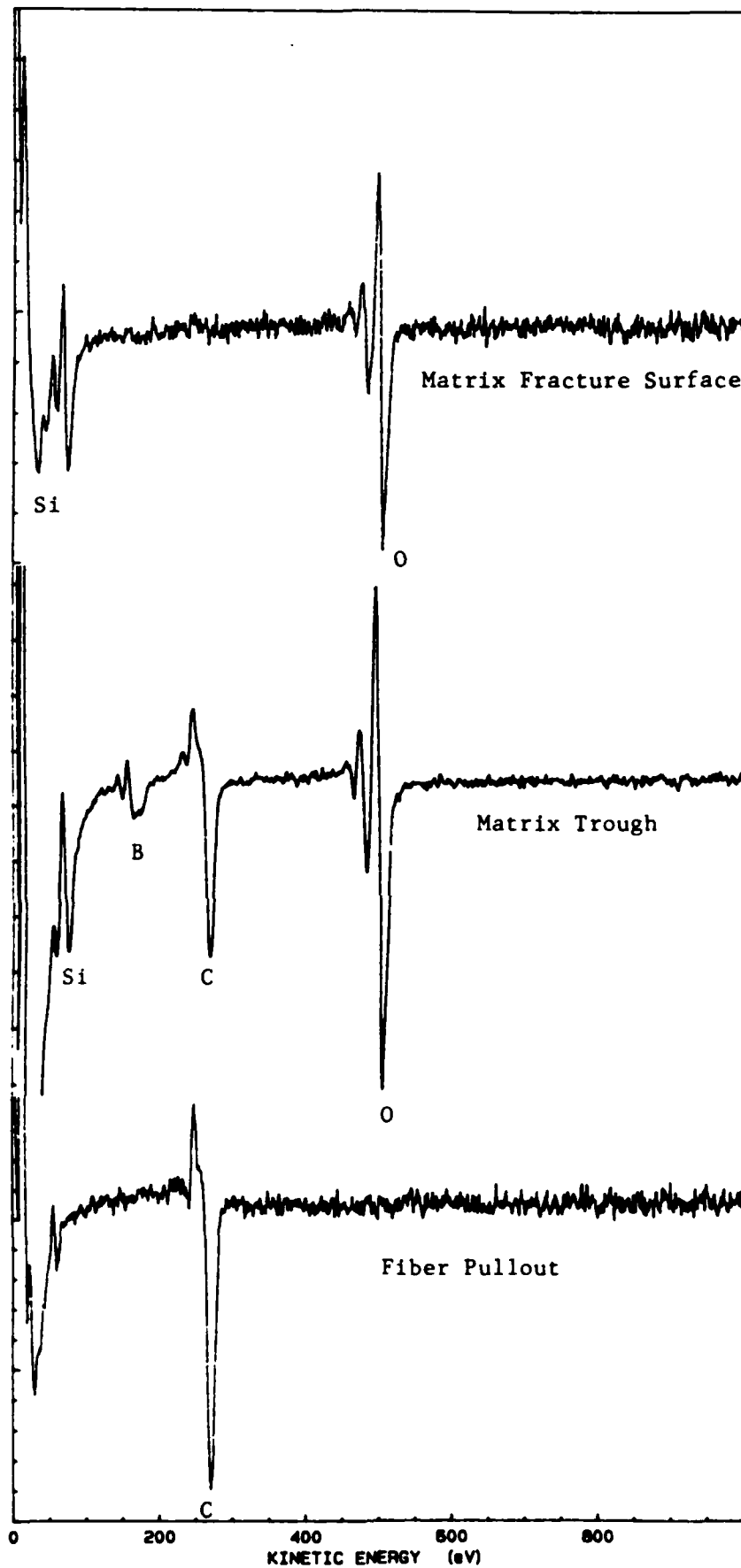
Figure 4.   Auger spectra for a fiber pullout, matrix trough and matrix fracture surface (for reference) in the 'base' glass matrix composite.
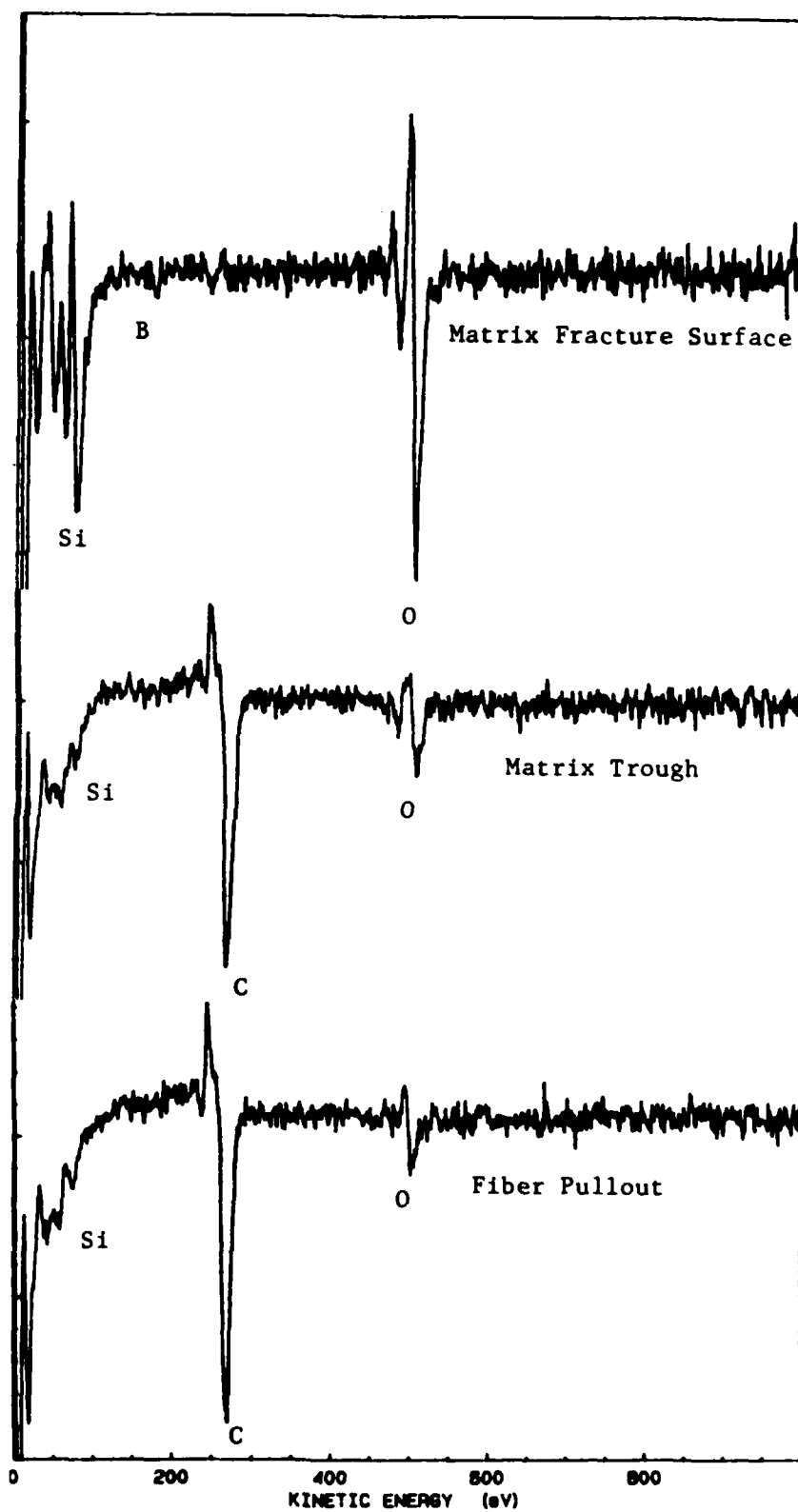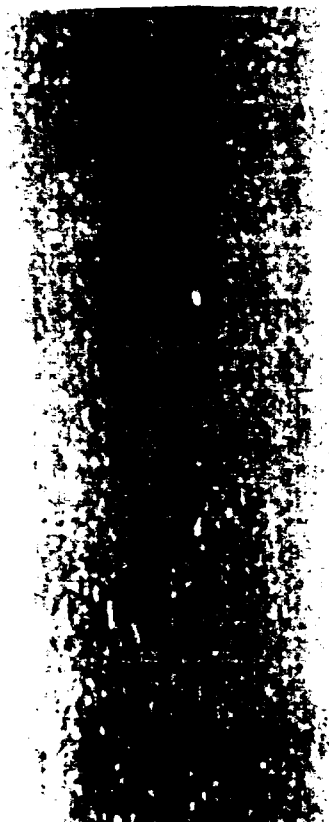
Figure 5. Auger spectra for a fiber pullout, matrix trough and matrix fracture surface (for reference) in the 'MoO$_3$-doped' glass matrix composite.

76

1 μm

(a)

the fibre pullouts (upper and matrix fracture... were observed in (a) the 'base' glass

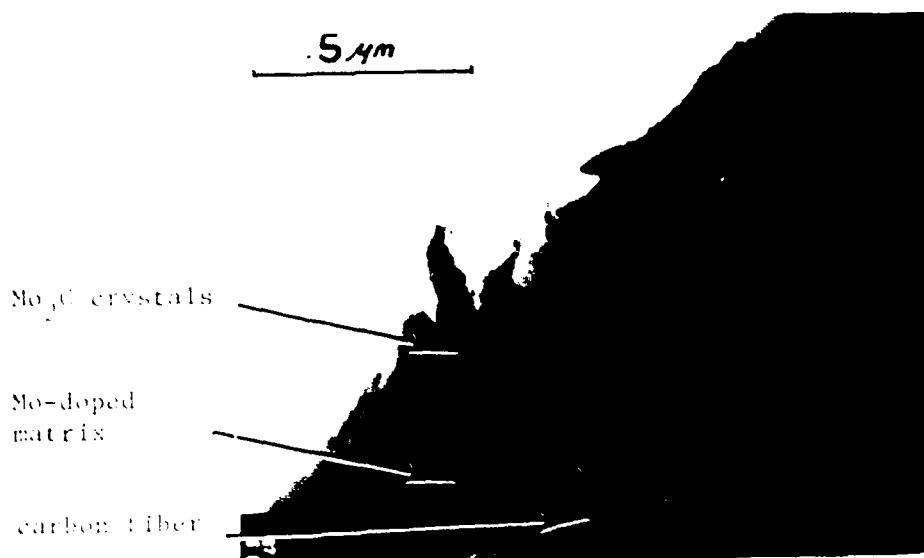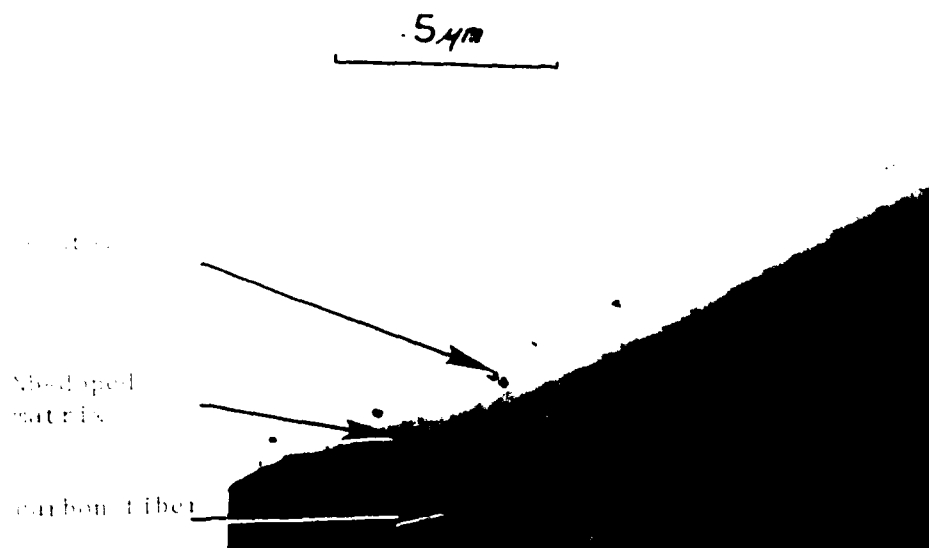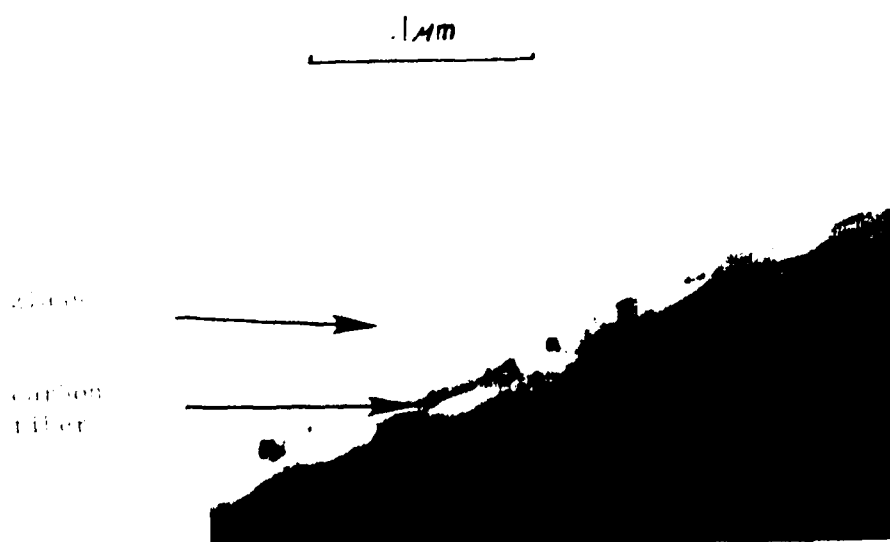82

.5 μm

Mo₃C crystals

Mo-doped matrix

carbon fiber

Figure 7a. TEM micrograph of the interface between carbon fibers and the Mo-doped glass; showing large interfacial crystals believed to be Mo_2C.

.5 μm

Nb-doped matrix

carbon fiber

b. TEM micrograph of the interface between carbon fibers and the Nb-doped glass; showing small de-localized crystals.

.1 μm

carbon fiber

c. TEM micrograph of the 'intimate' interface between the standard sodium borosilicate matrix and carbon fibers.
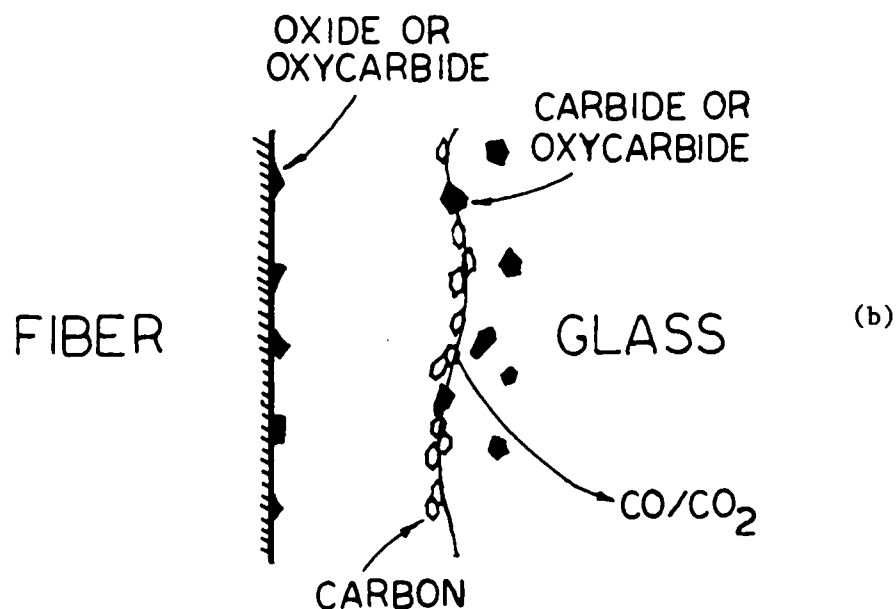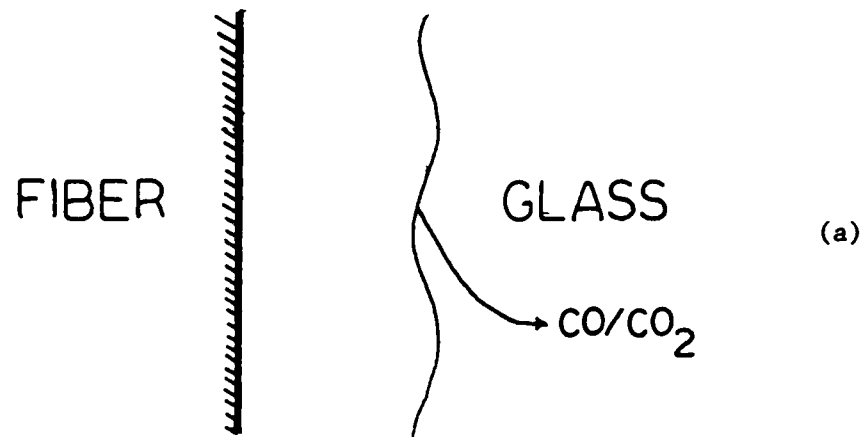
Figure 8. Schematic models of the fractured interfaces in the 'base' (upper) and 'doped' (lower) glass matrix composites. In both cases, the glass does not wet the fiber, and CO/CO_2 transport occurs through the matrix; but in the case of the doped composite, carbon crystallites in the fiber adhere to carbide reaction products in the glass matrix.

VIII. Deliverables

A set of three (3) 10 cm x 7.5 cm plates of unidirectional and 0/90° HMU carbon fiber reinforced glass matrix composites was delivered to the contracting officer on June 8, 1987. A fourth composite plate (10 cm x 7.5 cm) of 0/90° HMU carbon fiber reinforced glass was delivered on August 12, 1987. A portion of each plate (2.5 cm x 10 cm) was retained by UTRC for Charpy impact testing. The first set of three composites contained Corning Code 7740 glass as the matrix, while the fourth plate had a matrix of PS 2 (Nb_2O_5-doped) glass. The composites delivered are listed below.

Specimen #	Fiber Vol. %	Matrix	Orientation
125-87	42	7740	0/90°
126-87	44	7740	0/90°
133-87	43	7740	0°
317-87	41	PS 2 (Nb_2O_5)	0/90°

SUMMARY

Program Importance

This program seeks to develop a fundamental understanding of fiber reinforced glass and glass-ceramics and improve a family of composite materials that are superior to any currently available in their combination of low density, strength, toughness stiffness, and environmental stability. Glass matrices can withstand temperatures and environmental exposure conditions far more severe than possible through the use of more traditional matrices of resins or metals. The carbon fibers reinforce and toughen the glass matrices resulting in a unique high performance composite suited to critical applications. The easy formability of the glass matrix also permits the fabrication of a wide range of engineering shapes and sizes.

Overall Approach

High elastic modulus HMU carbon fibers were combined with several different glass and glass-ceramic matrix compositions. Topics addressed included notch sensitivity of 0/90° reinforced glass matrix composites, the effect of processing conditions on composite stress-strain behavior, preliminary evaluation of carbon fiber reinforced LAS glass-ceramic matrix composites, and the influence of interfacial reactions on composite behavior. The importance of the fiber-matrix interface in the control of composite performance was central to the investigation and was evaluated by correlating mechanical properties with microstructural and microchemical analysis of the interfacial region.

Summary of Significant Progress

• LAS glass-ceramic matrix composites were developed with tensile stress-strain behavior comparable to borosilicate glass matrix composites. Combined with the fibrous nature of fracture, the low CTE behavior of ceramed composites, and the high level of proportional limit strain, this system appears to be very promising for future work. Adjustment of processing parameters should allow for improvement in mechanical behavior, namely UTS and elastic modulus. These composites are anticipated to demonstrate greater resistance to high temperatures than current borosilicate systems.

• Carbon fiber reinforced glass matrix composites of 0/90° orientation were found to be relatively notch insensitive. The presence of holes with diameters ranging from 1.6 to 6.4 mm had no adverse effect on actual ultimate tensile strength. The degree of fiber pullout exhibited by the composites indicated low fiber-matrix interfacial bond strength, in agreement with fracture mechanism theory for notch insensitive composites.

• The processing temperature of 7740/HMU composites was varied to ascertain whether

carbon fiber performance could be enhanced by decreasing fiber-matrix reaction. Composites pressed at 900°C exhibited a fibrous fracture mode, but possessed lower values of UTS, elastic modulus, and failure strain than composites pressed at temperatures above 1100°C. Differences in composite performance were related in large part to the porous microstructure resulting from pressing at 900°C. Highest levels of strength, exhibiting little fiber pull-out, were obtained from composites pressed at 1280°C.

• Based on the results of a detailed thermodynamic analysis, trace amounts of Nb_2O_5 and MoO_3 were added to a borosilicate glass matrix (melted at Penn State University) for the specific purpose of reacting with the carbon fiber to alter the nature of the fiber-matrix interface. These reactions were found to have a profound effect on composite mechanical behavior. Microchemical analysis of fiber-matrix interfacial regions indicated that Mo diffused more rapidly than Nb through the glass to the interface during composite processing. The formation of Mo_2C at the fiber-matrix interface occurred very rapidly and severely degraded composite performance, making the composite weak and brittle. The rate of interfacial reaction in the Nb_2O_5 composite proceeded rather slowly, being controlled by the diffusion rate of Nb to the interface. The formation of a reaction layer at the fiber-matrix interface was found to increase the fiber-matrix interfacial debond strength (τ_{max}), with τ_{max} being the highest for the MoO_3 composite.

Future Plans

The next phase of the program will follow up on some aspects of the previous work while also exploring new methods to improve composite performance. Further work will be conducted in the search for more refractory matrix compositions for carbon fiber reinforced composites. The influence of fiber-matrix reactions on certain aspects of composite behavior will continue to be evaluated. In addition, the incorporation of ultra high modulus pitch based carbon fibers in glass matrix composites will be addressed. An assessment of oxidative stability of carbon fiber reinforced glass and glass-ceramic matrix composites will also be conducted. All of these efforts will be directed towards the goal of reaching the full potential provided by high modulus carbon fibers.

Acknowledgements

REFERENCES

1. I. Crivelli-Visconti and G. A Cooper, "Mechanical Properties of a New Carbon Fiber Material", Nature, 221 [2] 754-55 (1969).

2. R. A. Sambell, D. Bowen, and D. C. Phillips, "Carbon Fiber Composites with Ceramic and Glass Matrices - Part 1, Discontinuous Fibers," J. Mater. Sci., 7, 663 (1972).

3. R. A. Sambell, A. Briggs, D. C. Phillips, and D. H. Bowen, "Carbon Fiber Composites with - Ceramic and Glass Matrices - Part 2, Continuous Fibers," ibid., 7, 676 (1972).

4. D. C. Phillips, R. A. Sambell, and D. H. Bowen, "The Mechanical Properties of Carbon Fiber Reinforced Pyrex," ibid., 7, 1454 (1972).

5. D. C. Phillips, "Interfacial Bonding and Toughness of Carbon Fiber Reinforced Glass and Glass Ceramics," ibid., 9, 1847 (1974).

6. S. R. Levitt, "High Strength Graphite Fibre-LAS", ibid., 8, 793 (1973).

7. R. A. Sambell, D. C. Phillips, and D. H. Bowen, "The Technology of Carbon Fibre Reinforced Glasses and Ceramics", Harwell Report AERE-R-7612, Feb. 1974.

8. M. Sahebkar, J. Schlichting, and P. Schubert, "Possibility of Reinforcing Glass by Carbon Fibers", Berichte de Deutschen Keramischen Gasellschaft, 55 [5] 265-68 (1978).

9. K. M. Prewo and J. F. Bacon, "Glass Matrix Composites - I, Graphite Fiber Reinforced Glass", Proc. Second Intl. Conf. on Composites, edited by B. Noton, AIME, 1978.

10. K. M. Prewo, J. F. Bacon, and E. R. Thompson, "Graphite Fiber Reinforced Glass," Proc. of AIME Conf. on Advanced Fibers and Composites for Elevated Temperatures, edited by I. Ahmad and B. Noton, 1979.

11. K. M. Prewo and E. R. Thompson, "Research on Graphite Reinforced Glass Matrix Composites," NASA Contract Report 165711, May 1981.

12. K. M. Prewo, J. F. Bacon, And D. L. Dicus, "Graphite Fiber Reinforced Glass Matrix Composites," SAMPE Quarterly, 10 [4] 42 (1979).

13. K. M. Prewo, "A Compliant, High Failure Strain Fibre Reinforced Glass Matrix Composite," J. Mater. Sci., 17, 3549 (1982).

14. K. M. Prewo and E. J. Minford, "Graphite Fiber Reinforced Thermoplastic Matrix Composites for Use at 1000°F", SAMPE Jl., 21-22, 26-33, March/April 1985.

15. V. D. Khanna, et. al., "Friction and Wear of Glass Matrix-Graphite Fiber Composite", Proc. Mechanical Behavior of Metal Matrix Composites, edited by J. Hack, AIME, 1983.

16. E. Minford and K. Prewo, "Friction and Wear of Graphite-Fiber-Reinforced Glass Matrix Composites", Wear, 102, 253-64 (1985).

17. K. M. Prewo, "Development of a New Dimensionally and Thermally Stable Composite," Proc. of the Special Topics in Advanced Composites Mtg., El Segundo, California, 1979.

18. K. M. Prewo and E. J. Minford, "Thermally Stable Composites - Graphite Reinforced Glass," Proc. of SPIE - the Intl. Society for Optical Engineers, 505, Aug. 1984.

19. K. M. Prewo and V. C. Nardone, "Carbon Fiber Reinforced Glass Matrix Composites for Space Based Applications", Office of Naval Research Contract N00014-85-C-0332, Report R86-917161-1, September 1986.

20. P. W. McMillan, Glass-Ceramics, Academic Press, New York, 1979.

21. K. M. Prewo, "Advanced Characterization of SiC Fiber Reinforced Glass Ceramics", Office of Naval Research Contract N00014-81-C-0571, Report R83-915939-1, 1983.

22. D. B. Marshall and A. G. Evans, "Failure Mechanisms in Ceramic Fiber - Ceramic Matrix Composites", J. Am. Ceram. Soc., 68 [5] 225-31 (1985).

23. K. M. Prewo, "Tension and Flexural Strength of SiC Fiber Reinforced Glass-Ceramics", J. Mater. Sci., 21, 1986.

24. D. M. Dawson, R. F. Preston, and A. Purser, "High Performance Glass-Matrix Composites", presented at the 11th Annual Conference of the Engineering Ceramics Division of the American Ceramic Society, Cocoa Beach, Florida, January 1987.

25. E. Y. Luh and A. G. Evans, "High-Temperature Mechanical Properties of a Ceramic Matrix Composite", J. Am. Ceram. Soc., 70 [7] 466-69 (1987).

26. V. C. Nardone and K. M. Prewo, "Tensile Performance of Carbon Fiber Reinforced Glass", J. Mater. Sci., accepted for publication, 1987.

27. R. F. Cooper and K. Chyung, "Structure and Chemistry of Fiber-Matrix Interfaces in Silicon Carbide Fiber-Reinforced Glass-Ceramic Composites: An Electron Microscopy Study", J. Mater. Sci., accepted for publication, 1987.

28. J. E. Stanworth, "Oxide Glass Formation from the Melt", J. Am. Ceram. Soc., 54 [1] 61-63 (1971).

29.   D. H. Grande, J. F. Mandell, and K. C. C. Hong, "Fiber/Matrix Bond Strength Studies of Glass, Ceramic, and Metal Matrix Composites", J. Mater. Sci., submitted for publication, March 1987.

END

10-87

DTIC